Photochemical Grafting of Methyl and Ferrocenyl Groups on Si(111) Surface

HERRERA, Marvin Ustaris

Table of Contents

Chapter 1
Introduction

1.1. Self-assembled Monolayer (SAM)

Self-assembled monolayers (Bishop and Nuzzo, 1996; Dubois and Nuzzo, 1992; Duwez, 2004; Smith et. al. 2004; Srisombat et. al., 2011; Ulman, 1991) have become the subject of many researches in recent years. As the word "monolayer" in its name implies, the film is composed of a single layer of organic molecules, thus its thickness could be considered among the thinnest possible molecular assemblies. SAMs possess organized molecular assemblies on a substrate. The process in which these assemblies were organized is "self-assemble", which is the spontaneous ordering of molecules on the top of a substrate. "Self-assemble" has become an important method in producing ordered organic molecular layer. Unlike inorganic materials, organic materials are quite "soft" that it can easily decompose at high temperature and high pressure, thus the traditional ways of preparing well-ordered inorganic films are difficult to be adapted. In this method, the ordering of the molecules is the outcome of the energy configuration of the system rather than mechanical manipulations.

The potential applications of SAMs have remarkably been diversed. They have been eyed for the following: adhesion and friction control (Chaudhury, 1997), corrosion prevention (Jennings and Laibinis, 1996; Whelan et.al. 2003), wetting (Kulinich and Farzaneh, 2004), and resist for pattern transfer (Xia, et.al. 1996). However, its application in electronics (Arya et.al., 2009, Aswal et. al. 2006) can be considered one of the most sought-after. In terms of electronics, some SAMs have potential to function as

dielectric/insulator while others has potential to function as devices such as diodes, transistors, memories devices, sensors, etc. More specifically, SAMs on Si substrate are eyed for molecular electronic application (Aswal et. al, 2006). Molecular electronics utilizes single or small group of molecules to perform electronic function (Carroll and Gorman, 2002). The necessity to study molecular electronics is driven by the fact that the size of the components of integrated circuit is shrinking and would eventually approached the molecular or atomic level. In such, the Si surface could be a circuit board, in which different molecules can be grafted on the Si surface to act as different devices while the spaces left vacant are saturated with molecules functioning as dielectric. Minding with this potential application in the future, this report will focus on two kinds of organic materials, one kind has potential to function as a dielectric (methyl groups) and the other kind has potential to function as a device (ferrocenyl groups). Methyl groups that are grafted on the Si surface have the capability to make the surface chemically inert. Meanwhile, ferrocenyl groups have two stable and reversible oxidation states, which have potential use as memory elements. These two kinds of structures (methyl and ferrocenyl groups) will be discussed in detail in the succeeding chapters.

The formation of SAM is accompanied by the following: (1) bonding of molecules with the substrate and (2) self-assembly process. The molecules (Figure 1.1) that will be bonded with the substrate could be divided into three parts: (1) headgroup, (2) tailgroup, and (3) spacer. The headgroup and the tailgroup are on the opposite ends of the molecule and in between them is the spacer. The headgroups bind on the substrate while the tailgroups become the outer surface of the layer. Meanwhile, the intermolecular forces among the adjacent molecules could serve as a factor that draws the structure into an

organized molecular assembly.

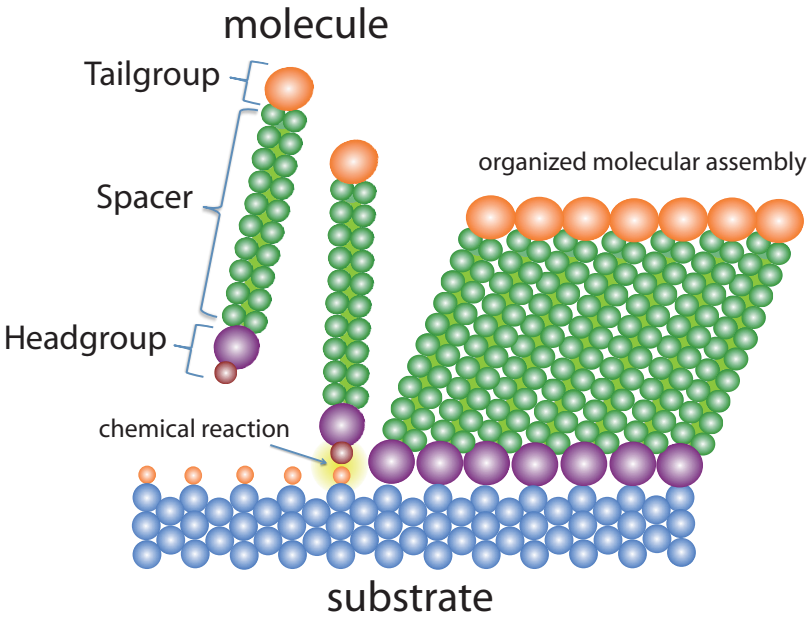

Figure 1.1. Self-assembled monolayer

1.2. Silicon as substrate of SAM

Self-assembled monolayer are not a stand-alone film, rather it needs substrate in which it could anchor. One distinct difference between SAM and Langmuir-Blodgett film is the nature of bonding with the substrate. The former is chemically absorbed in the substrate in which the molecular layer is covalently bonded with the substrate. Meanwhile, the latter is just physically absorbed in the surface, thus is weaker. Different materials have been used as substrate of SAM. These materials ranged from metals (e.g., Ag, Au, Pd, Cu, Pt, and Pd), oxides (e.g., Al_2O_3, ITO, SiO_2,TiO_2), ceramics (e.g., $YBa_2Cu_3O_{7-\delta}$ and TlBaBaCuO), and semiconductors (e.g., GaAs, InP, CdSe, ZnSe, Si).

The choice of substrate might be relevant in two ways. The first is about its

intended application and the second is about its ability to allow the formation of SAM. If the indented application of the SAMs were to integrate it into electronic devices, the use of silicon as substrate would be advantageous. The electronic properties of silicon are tunable and devices based on it can be directly integrated into electronic circuits (Fabre, 2010). The technological processes involving silicon-based technology are also already developed and mature (e.g. removing oxide, patterning), thus these protocols could guide researcher in this field. In addition, crystalline silicon is being mass produced and widely available since it is used in electronics. Silicon (porous silicon and crystalline silicon) is also known to allow the formation of SAM. The sensitivity of silicon's electronic properties with applied voltage and illumination can possibly makes grafting on it with different possible ways.

Silicon can easily reacts with oxygen in atmosphere; thus, it is easily coated with native oxide. There are many molecules that can be are grafted on silicon oxide (e.g., silanes and alcohol); however, silicon oxide may have surface states that may be detrimental if the SAM is intended for electronic device. If it is desired that the molecular layer would be directly connected with the silicon surface, the silicon oxide layer should be removed. Because the silicon surface easily oxidizes, the usual practice is that the removal of native oxide is accompanied by the grafting of another layer (e.g, hydrogen layer). The idea is that this layer is stable enough to prevent oxidation (maybe for a short time) but should be easily displaced by the intended molecule to be grafted. However, for some cases, wherein hydrogen-terminated silicon (Si-H) is difficult to be displaced by the grafting molecules, the Si-H is processed in order for the hydrogen atoms to be replaced by halogen such as chlorine, bromide or iodine. Eves and Lopinski (2005) and Zhou et. al.

(2000) presented some studies about the production of halogen-terminated Si from Si-H.

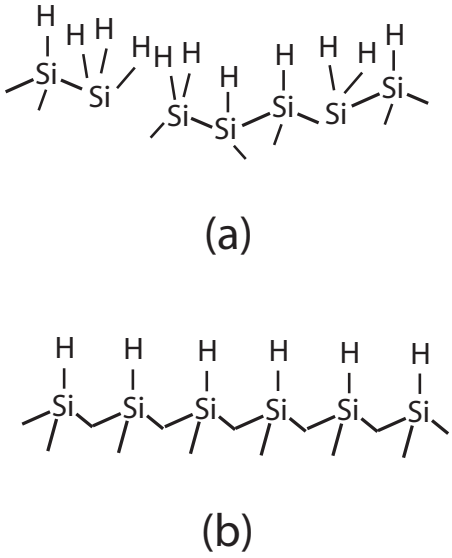

Figure 1.2. (a) Hydrogen-terminated porous Si, (b) crystalline Si with SiO_x on its surface, and Hydrogen-terminated Crystalline Si (Si-H)

The functionalization of Si-H with organic molecules is an active research area (Boukherroub, 2005). The nature of the hydrogenated surface differs for porous Si and for crystalline Si. For porous Si, due to its porous morphology, the outer Si atom is not necessarily bonded with three other Si atoms. Its extra electron(s) could either bond with one, two or three hydrogen atom(s) to form either -SiH, =SiH, or ≡SiH (Figure 1.2a). However, for crystalline Si, ideally, all surface atoms are bonded with three other Si atoms, leaving only one extra atom for binding with other atom. With this configuration, only a monohydride structures (≡SiH) are (ideally) possible to form (Figure 1.2b).

Crystalline silicon is widely used as substrate of self-assembled monolayer. If the intentions were for the Si surface to be circuit board of organic molecules-based

electronic, then a relatively flat crystalline Si would be advantageous rather than the rough porous Si. The common crystallographic orientation of commercially available crystalline silicon is (100) and (111). To note, from this point onward, the term “silicon” would mean “crystalline silicon”.

There are several techniques of producing hydrogen-terminated silicon. The wet-chemical approach using HF and/or NH_4F solutions are commonly done because it is relatively easy to execute and does not require to be done in vacuum. The use of either these chemicals has done the trick of removing the silicon oxide and ending the process with hydrogen atoms attached on the silicon surface.

The use of HF solution in the hydrogenation of the Si surface results to atomically rough surface while that of NH_4F solution yields atomically flat surface (Higashi et. al., 1991). Atomically flat surface is exemplified by the condition wherein the structure of the molecular film, which was formed, copies the structure of the substrate’s surface. In this case, the attached hydrogen atoms are small enough that when it formed a film on the Si surface, it copies the surface’s stair-like structure (Figure 1.3). Figure 1.4 shows an AFM image of a hydrogenated film on Si (111) surface.

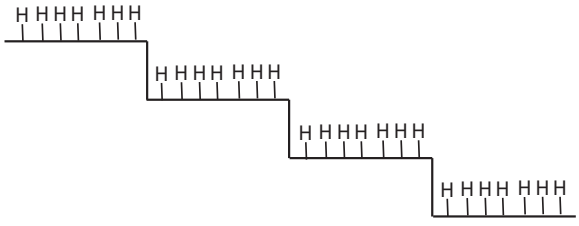

Figure 1.3. Atomically flat structure. The structure of the hydrogen film copies the structure of the substrate’s surface

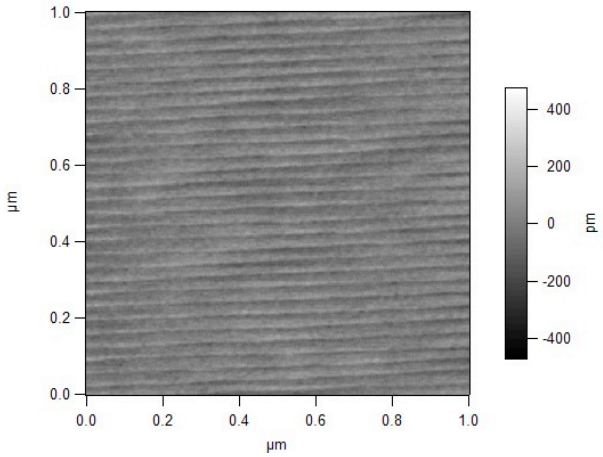

Figure 1.4. Hydrogen-terminated Si(111).

In this report, the hydrogen-termination is done by immersing in HF solution and then in NH_4F solution in an 80°C water bath. HF solution was used to remove the native oxide (although it can also terminated the Si surface with hydrogen molecules) while the use of NH_4F solution is to ensure that the sample has atomically flat surface (Figure 1.4). The NH_4F solution was kept at 80°C to remove oxygen molecules on the silicon surface.

The nature of Si-H would be crucial on its ability to be functionalized with different organic molecules. Because any chemical reactions (e.g., grafting process) requires transfer of charges, analyzing the mechanism on how charges can move in and out the Si surface would be helpful in understanding of how these charge can be used to induce or to control the grafting process.

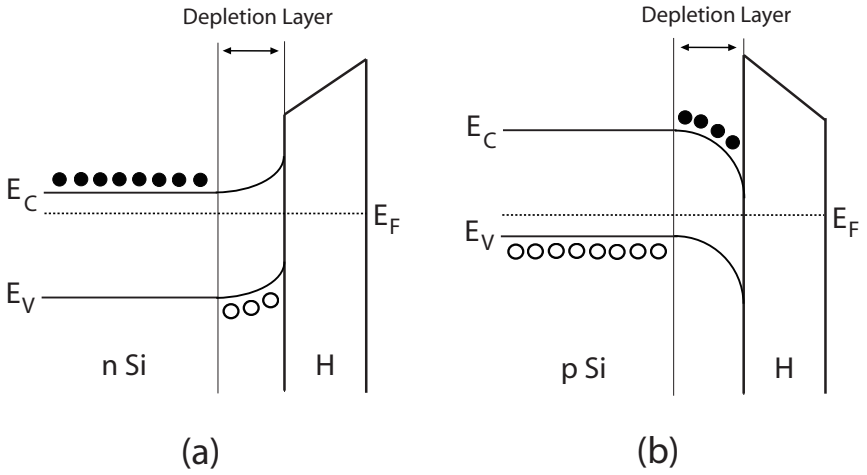

Figure 1.5. Energy band diagram of hydrogen-terminated Si with (a) n-type and (b) p-type substrates, which are placed in the dark and not connected to an external voltage source. The closed circles represent electrons while the open circles are the holes. The terms "E_F", "E_c", and "E_v" denote Fermi energy, conduction band energy , and valence band energy, respectively.

The nature of the energy bands of Si-H can influence the movement of charges from/to the Si substrate to/from its surface. The movement of such charges would be highly important since they can affect the grafting process. Figure 1.5. shows the band diagram of hydrogen-terminated silicon at the dark and not connected to an external voltage source. For Si-H with n-type substrate (n Si-H), the Si energy bands bend upward while for that of p-type (p Si-H), they bend upward. The closed circles represent electrons while the open circles are the holes. The terms "E_F", "E_c", and "E_v" denote Fermi energy, conduction band, and valence band, respectively. Some charges lump on the interface

creating a depletion region and a semiconductor barrier. The width of the depletion region depends on doping concentration of the Si substrate. Substrates with high dopant concentration (or low resistivity) have thinner depletion width while those with low dopant concentration (or high resistivity) have thicker depletion width. Meanwhile, the semiconductor barrier of n Si-H is larger than that of p Si-H counterpart (Table 1.1).

Table 1.1. Barrier Height of n Si-H and p Si-H

Reference	**Barrier Height (eV)**		**Model**
	n Si-H	**p Si-H**	
Faber et. al. 2005	0.461± 0.003	0.695± 0.003	Thermoionic theory
Faber et. al. 2005	0.30 ± 0.03	0.80 ± 0.01	Moth-Schottky
Faber et. al. 2005	0.324 ± 0.001	0.563± 0.003	Current density vs Voltage (J-V) plot
Maldonado et. al., 2007	0.17 ± 0.02	0.82 ± 0.02	J-V plot

Figures 1.6 and 1.7 show the different possible configurations of the energy bands of Si-H. When an external bias is connected to the Si-H, the bond could either maintain the depletion condition or could either change to the following conditions: inversion, flat band and accumulation. At the inversion condition, many of the minority carrier goes to the surface of Si while at the accumulation condition, many majority carries goes to it. The flat band happens when there is no bending of Si energy band.

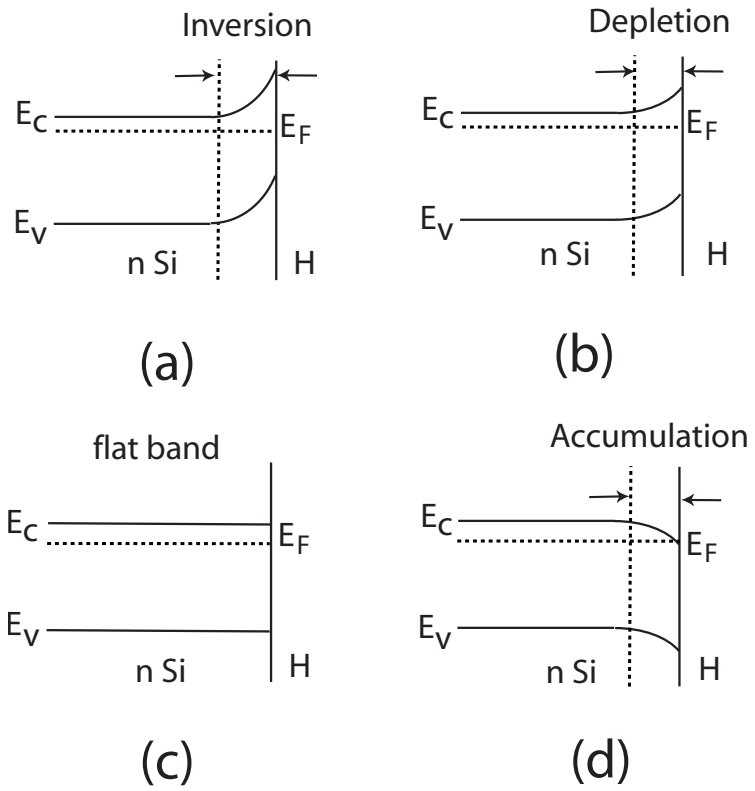

Figure 1.6. Energy band diagram of n Si-H showing (a) Inversion, (b) depletion, (c) flat band and (d) accumulation.

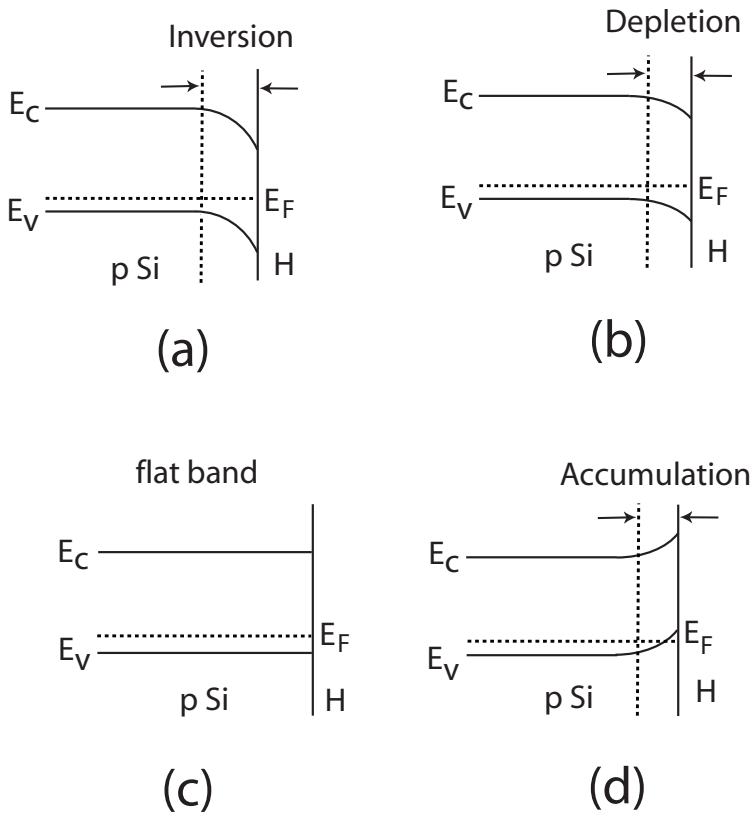

Figure 1.7. Energy band diagram of p Si-H showing (a) Inversion, (b) depletion, (c) flat band and (d) accumulation.

1.3. Precursor Molecules

Some precursor molecules that have been used for grafting molecules on Si surface include those with π bond in one end of the molecules (e.g., 1-alkenes and 1-alkynes) and those that can be decomposed into radical species (e.g. Grignard reagent). For alkenes and alkynes, the π electrons of their C=C bonds are reactive that they can interact with the hydrogenated Si surface. Likewise, molecules can also be decomposed to their radical form, which is very reactive. Example of this is alkyl-based Grignard reagent that can be decomposed to alkyl radical. This section will focus on two types of

precursor molecules, they are (1) Grignard reagent and (2) 1-alkenes molecules.

1.3.1. Grignard Reagent

Grignard reagents or organomagnesium halide (RMgX) are considered as one of the most important synthetic reagents (Tjurina et. al, 2001) and probably the most widely used organomettallic reagents (Seyferth, 2009). Figure 1.8 shows the structure of Methylmagnesium Bromide, an example of a Grignard Reagent. Grignard Reagent is composed of an organic molecule, R (e.g., alkyl), a magnesium atom and a halide atom, X (e.g., Br, Cl, I). Alkyl molecules has been extensively been grafted on semiconductor surfaces using Grignard reagent as precursor (Amy et. al., 2007; Bansal et. al., 2001; Fellah et. al., 2004; Fellah et. al., 2002; Fidelis et. al., 2000; Hunger et. al., 2005; Hunger et. al., 2007; Miyadera et. al., 2003; Okada et. al., 2004; Waluyo et. al., 2010; Webb and Lewis, 2003; Webb et. al., 2006; Yamada, et. al., 2003; Yamada, et. al., 2004; Yu et. al., 2005; Yu et. al., 2006). Grignard reagent is sensitive to many substances. It can be decomposed by water and may react with oxidizing substances. It also reacts vigorously with alcohols, acids and amines and burns spontaneously without solvent. Extreme caution should be done in handling Grignard reagents.

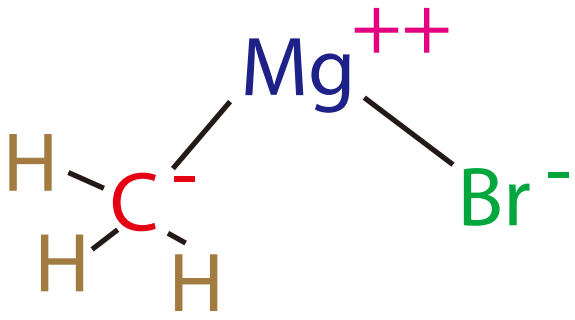

Figure 1.8. Structure of Methylmagnesium Bromide, a Grignard Reagent

Grignard reagent can undergoes oxidative decomposition with the introduction of a positive charge (p^+) (Fellah et.al., 2002):

$$RMgX + p^+ \rightarrow R\bullet + MgX^+ \quad \text{(equation 1.1)}$$

The oxidative decomposition of Grignard reagent allows the release of alkyl radical (R•).

$$\equiv Si\text{-}H + R\bullet \rightarrow \equiv Si\bullet + R\text{-}H \quad \text{(equation 1.2)}$$

$$\equiv Si\bullet + R\bullet \rightarrow \equiv Si\text{-}R \quad \text{(equation 1.3)}$$

The alkyl radicals can extract hydrogen atoms to create Si radicals (Si•) (equation 1.2). Alkyl radicals can also bind with Si radicals to form alkyl-terminated Si (Si-R) (equation 1.3). The reactions show the importance of the oxidative decomposition of Grignard reagent for alkyl molecules to be grafted in the Si surface. Thus, a grafting initiator should have a mechanism to induce the oxidative decomposition of Grignard reagent.

1.3.2. 1-Alkene Molecules

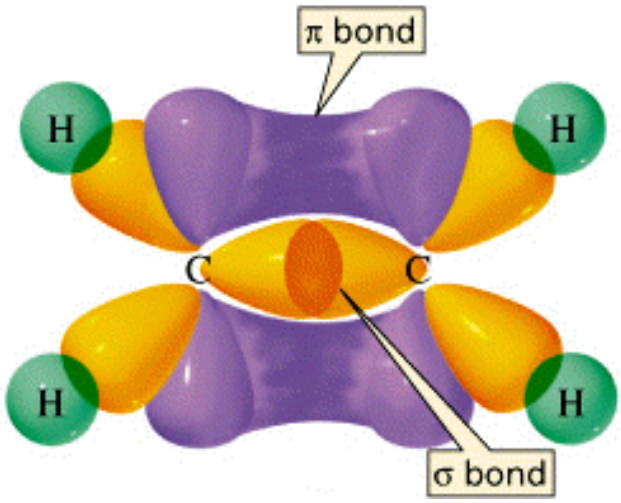

Figure 1.9. Pi (π) and sigma (σ) bonds in an ethylene molecule. (Source: http://www.chem1.com/acad/webtext/chembond/cb07.html)

The preparations of grafted organic molecules on silicon surface using alkenes or olefins as precursor molecules have been cited in literature (Buriak, 2002; Cicero et. al. 2000; Coletti et. al., 2006; Eves et. al. 2004; Kruse, et. al. 2002; Langner, et. al. 2005; Linford et. al. 1995; Lopinsky et. al. 2000; Sano et. al. 2008; Sieval et. al. 1998; Steward and Buriak, 2001; Sun et. al., 2005; Wang et. al. 2010; Zhong and Bernasek, 2011). 1-Alkenes are molecules with carbon double bond at an end of the molecule. Figure 1.9 shows the bonds in an ethylene molecule, which is the simplest among the 1-alkene molecule. To note, the structure of a vinylferrocene molecule is similar that of an ethylene molecule except that a ferrocene molecule substitute one of the hydrogen atoms. The carbon double bonds are composed of pi (π) bond and sigma (σ) bond. The σ bond is the outcome of the overlap of the sp^2 hybridized orbital of the two carbon atoms. Meanwhile,

the π bond is the outcome of the overlap of the unhybridized p_z orbital of the two carbon atoms. Ordinarily, the ethylene molecule is planar, in which the sp^2 hybrids (σ bond) are at the same plane with the molecule. The electron density of the π bond extends above, below and perpendicular to the plane of the molecule. The π electrons are more loosely bounded than the σ electrons, thus could easily break and very reactive.

There are different models on how 1-alkene molecule can interact with the hydrogenated surface and establish Si-C bond. One model is free radical mechanism in which the 1-alkene molecule can (directly) interact with a Si radical to establish Si-C bond (Cicero et. al., 2000; Lopinsky et. al., 2000; Kruse et. al., 2002). In this model, it seems that the chemical potential between the Si radical and grafting molecule is sufficient to drive a chemical reaction to create Si-C bond. Another model is by mean of the production of excitons (Sun et. al. 2005; Steward and Buriak 2001; Zhong and Bernasek, 2011). In this model, the excitons (electron-hole pairs) split, and for n-type substrate, the holes go to the Si surface. The surface holes can facilitate the reaction between the nucleophilic 1-alkene molecules and Si-H bonds to form Si-C bonds. Some models such those presented by Sun et. al. (2005) and Zhong and Bernasek (2011) combined both the radical chain and exciton-based models.

Radical chain mechanism. An example of a model that describes the grafting of alkene molecules on Si surface is radical chain mechanism. In this model (Figures 1.10 and 1.11), an initiator triggers the creation of Si radical, which in turn could react with alkene molecule to established Si-C bond. The establishment of Si-C bond is accompanied by the formation of carbon radical, which can extract hydrogen atom from the nearby Si atom, to create a new Si radical. The Si radical can trigger grafting of another alkene molecule, thus

the grafting process propagates. The radical initiator such as diacyl peroxide (Linford et. al. 1995), high temperature (Buriak, 2002), or UV light (Cicero et. al., 2000) can be used to create Si radical. Lopinsky et. al. (2000) (Figure 1.12) and Kruse et. al. (2002) (Figure 1.13) used this type of model to explain the grafting of styrene and of vinylferrocene on silicon surface, respectively.

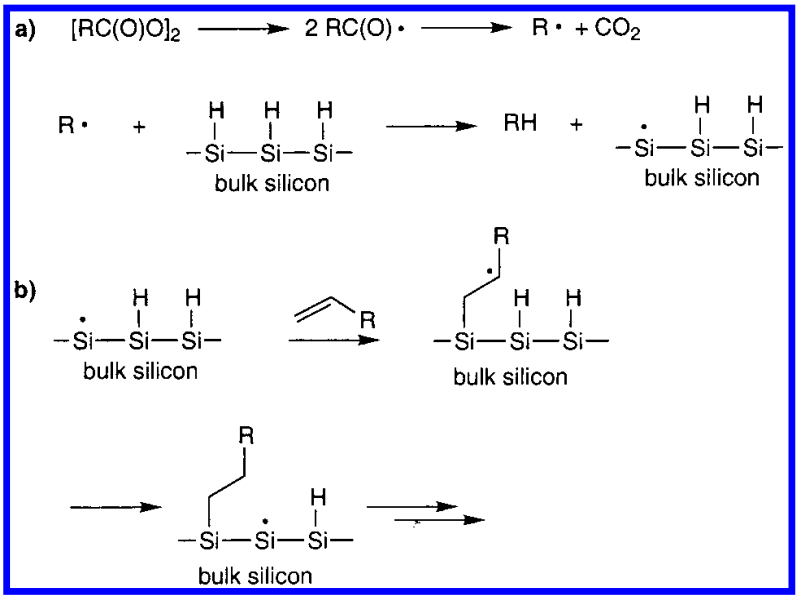

Figure 1.10. Use of diacyl peroxide to initiate grafting of alkene molecule on Si surface (Illustration taken from Buriak, 2002)

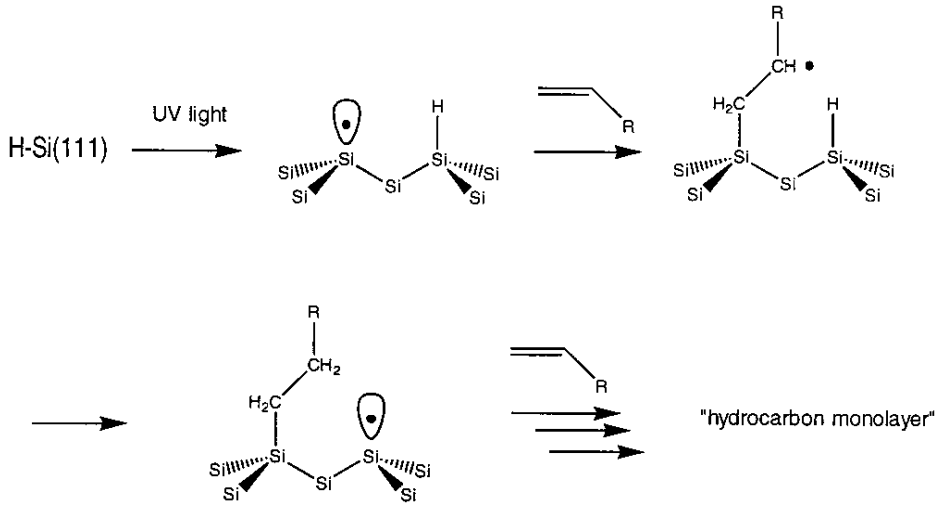

Figure 1.11. Use of UV to initiate grafting of alkene molecule on Si surface (Illustration taken from Cicero, et. al. 2000)

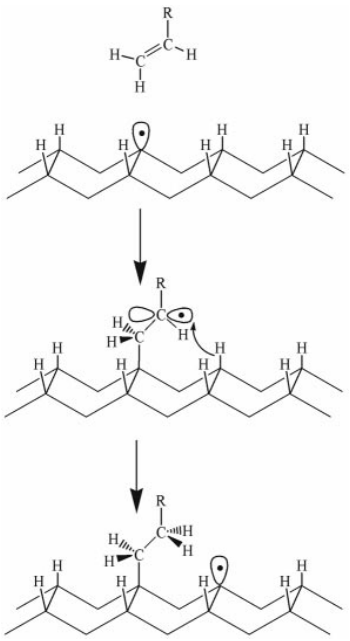

Figure 1.12. Radical chain reaction mechanism involving alkene molecule on Si surface (Illustration taken from Lopinsky et. al., 2000)

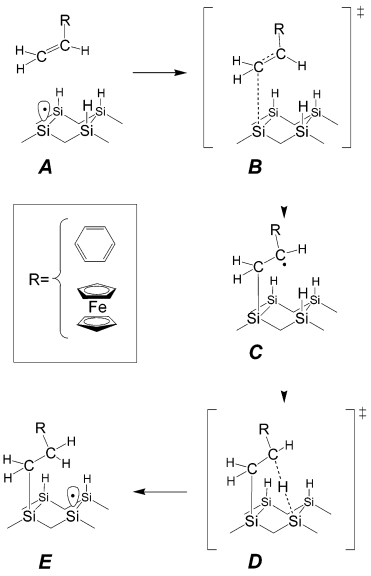

Figure 1.13. Radical chain reaction mechanism involving vinylferrocene molecule on Si surface (Illustration taken from Kruse et. al., 2002)

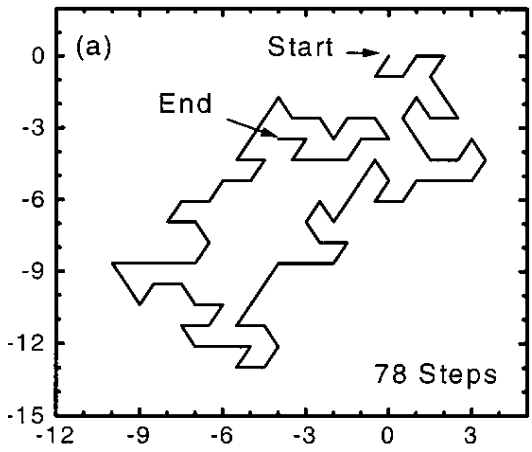

Figure 1.14. Result of Monte Carlo simulation of self-avoiding random walk on triangular lattice model (Illustration taken from Cicero, et. al. 2000)

Radical chain mechanism predicts that alkene grafting on Si(111) substrate would yield an island-like structure during the initial stage of grafting process. This structure is expected since the succeeding grafting process would occur at nearby Si atom. Figure 1.14 shows the possible arrangement of the grafted structure on Si(111) surface (Cicero et. al., 2000). The configuration was the outcome using Monte Carlo simulation of self-avoiding random walk on triangular lattice model and such configuration resembled an island-like structure.

Exciton-based mechanism. Both the illumination of UV and of visible light can trigger the formation of electron-hole pairs on Si. However, unlike the ultraviolet radiation, the energy of visible light is less than the bond strength of weakest Si-H bond (3.5 eV), thus its energy is insufficient to promote the dissociation of Si-H bonds. Stewart and Buriak (2001) proposed a mechanism for visible light-induced hydrosilylation reaction based from exciton-mediated mechanism (Figure 1.15). In this model, visible light induces the formation of localized positive charge on the porous silicon surface. A positive charge can interact with an alkene molecule, establishing a Si-C bond and a carbocation. The carbocation can extract the hydrogen atom that is still connected on the Si atom. Sun et. al. (2005) proposed almost similar mechanism involving crystalline silicon (Figure 1.16). In their mechanism, the carbon radical that was formed during the establishment of Si-C bond, extract hydrogen atom from neighboring silicon atom, instead on itself. This extraction of hydrogen atom led to the formation of Si radical that can trigger the grafting of another alkene molecule, similar to that of radical chain mechanism.

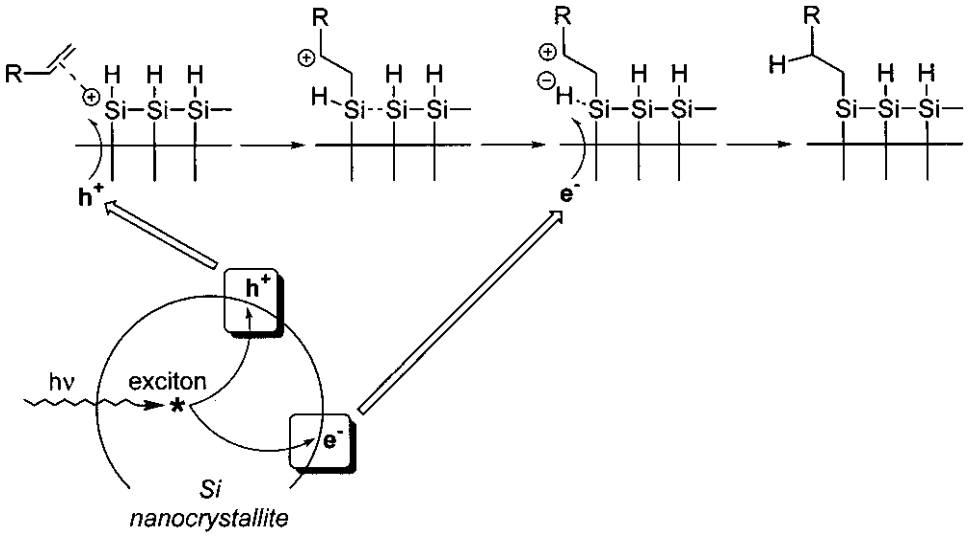

Figure 1.15. Use of visible light to initiate grafting of alkene molecule on porous Si surface (Illustration taken from Stewart and Buriak, 2001)

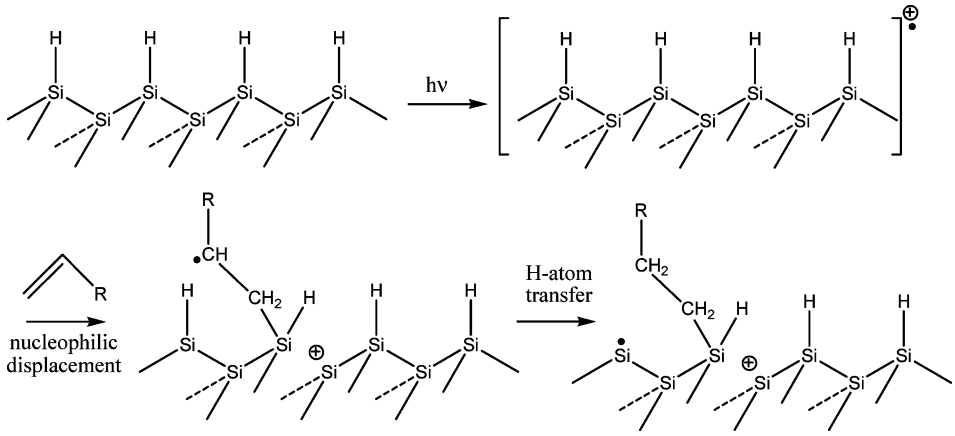

Figure 1.16. Use of visible light to initiate grafting of alkene molecule on Si surface (Illustration taken from Sun et.al., 2005)

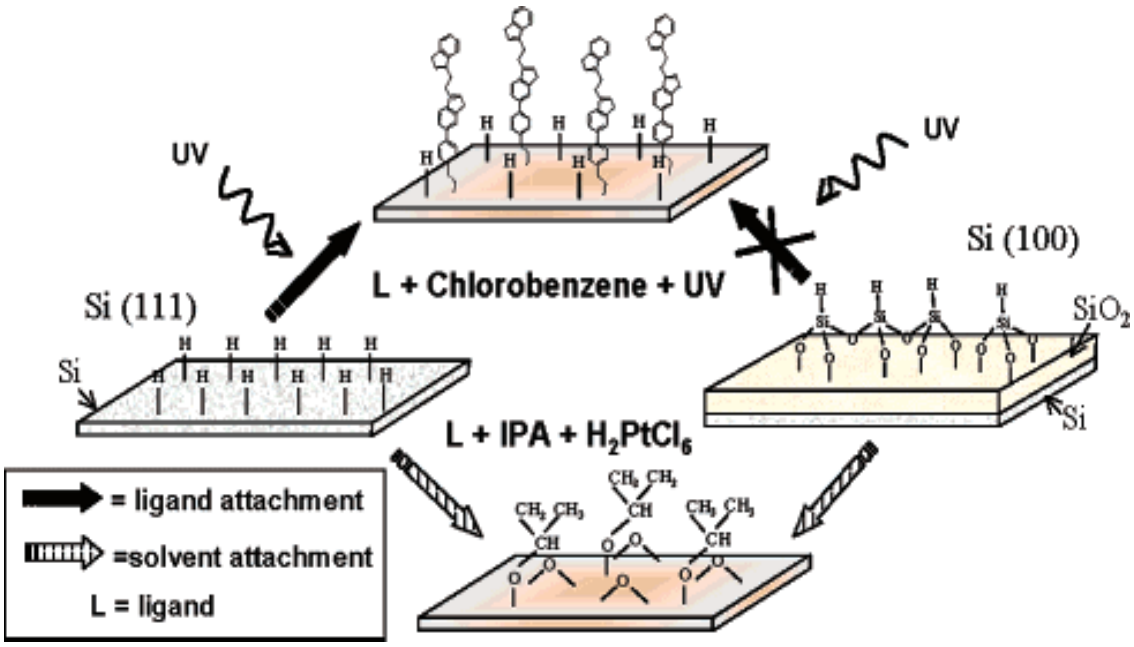

Figure 1.17. Attaching ligand molecule on Si-H surface and hydrogenated oxidized silicon surface (Illustration taken from Langner et. al. 2005)

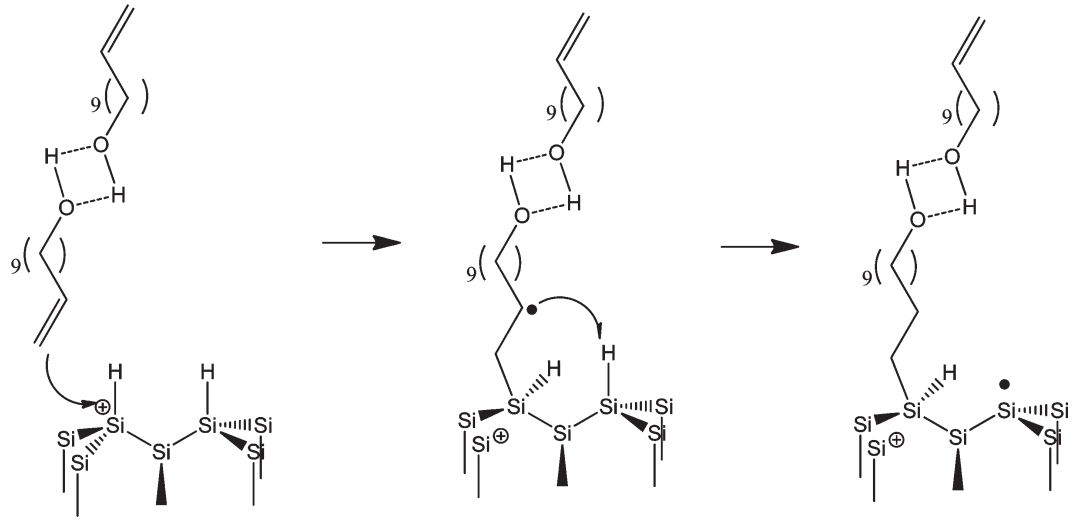

Figure 1.18. Use of UV to initiate grafting of alkene molecule on Si surface (Illustration taken from Zhong and Bernasek, 2011)

The paper of Langner et .al. (2005) seems to suggest that the grafting of organic molecules onto the Si atoms using UV illumination is also induced by excitons (Figure 1.17), instead of the by Si-H bond breaking mechanism (Figure 1.11) (Cicero, et. al. 2000). Langner et. al (2005) shows that UV treatment did not result to grafting of molecules when an intermediated oxide layer is in between the bulk silicon and hydrogenated surface (Figure 1.17). In their experiment, they attributed the said failure to graft molecules to the failure to transfer photogenerated holes from the bulk silicon to the hydrogenated surface because of the intermediated oxide barrier. The results suggest the necessity of photogenerated charges to be at the hydrogenated surface for grafting to occur.

Citing the work of Langner et .al., (2005), paper published by Zhong and Bernasek (2011) used the exciton-based mechanism, similar to that of Sun et. al. (2005) Figure 1.16, to explain the grafting of alkene onto the Si(111) surface using UV illumination (Figure 1.18). However, they also use the radical propagation in their model about alkene molecule grafting.

1.4. Objectives of the study

This study will explore two different processes in which alkyl structures could be grafted on the Si surface using visible light illumination. One process involves the use of organomagnesium halide (Grignard reagent) while the other involves the use of 1-alkene (vinylferrocene) molecules. With this, the general objectives of this study are the following (the specific objectives will be presented on per chapter basis):

(1) to photochemically graft methyl groups on Si(111) surface using Grignard

reagent, and,

(2) to photochemically graft ferrocenyl groups on Si(111) surface.

The two kinds of self-assembled monolayers that are intended to achieve in this study are (1) Si-CH_3 and (2) Si-C_2H_4Fc molecular assemblies. Both molecular assemblies are composed of alkyl-like molecules that are covalently bounded on Si(111) surface. Such establishment of bonding is achieved with the aid of illumination of visible light.

This manuscript will focus on the use visible light as initiator for grafting. Unlike the use of ultraviolet illumination and thermal method, the use of visible light illumination is a mild process, thus it can avoid inducing potential damage to organic molecules. Compare to electrochemical method, the use of visible light illumination avoids the tedious method of establishing ohmic contact between the Si substrate and an electrode, which may induce permanent damage to the Si substrate. Unlike in the use of radical initiator, the use of visible light illumination avoids the use of additional chemical reagents that may leave impurities to the grafted molecules.

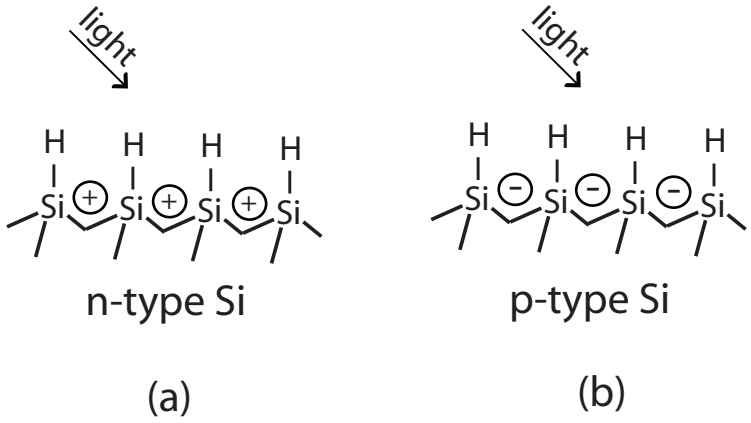

Figure 1.19. Creation of photogenerated charges on (a) n-type and (b) p-type Si surfaces

The illumination of visible light onto the Si-H surface induces the creation of electron-hole pairs. The electric field in the depletion region splits these electron-hole pairs. For n-type Si, holes go onto the Si surface (Figure 1.19a) while for p-type Si; electrons go onto the surface (Figure 1.19b). The role of these photogenerated charges onto the grafting process may differ depending on the grafting condition. Its role on the grafting of methyl group and vinylferrocene group will be described on the succeeding chapters.

1.5. Outline

Chapter 1 is the introduction of this manuscript. This chapter presents the basic concepts of self-assembled monolayer (SAM). This chapter gives an overview about the use of Si as substrate of SAM, and basic information on the use of Grignard reagent and 1-alkene in grafting.

Chapter 2 discusses about the photochemical grafting of methyl groups on Si(111) surface using Grignard reagent. This chapter discusses the different factors that can affect the grafting of methyl groups on the Si surface. It also presented the different characteristics of the methyl-terminated silicon.

Chapter 3 tackles the effect of grafting medium on the preparation of ferrocenyl groups on Si(111) surface. The three grafting medium that were used were (1) tetrahydrofuran, (2) diethyl ether and (3) dibutyl ether.

Chapter 4 gives a new insight on the role of surface charges on the grafting of vinylferrocene molecules on the Si substrate. This chapter analyzes the effect of the characteristics of Si substrate on the availability of charges on the Si surface and its effect on grafting rate.

Chapter 5 presents a model that explains the effect of illumination intensity on the electrochemical characteristics of immobilized ferrocene moieties on n-type Si substrate.

Chapter 6 summarizes this manuscript and present conclusions.

References

1. S. R. Amy, D.J. Michalak, Y.J. Chabal, L. Wielunski, P.T. Hurley, N.S. Lewis: *J. Phys. Chem. C*. **2007.** 111. 13053.

2. S.K. Arya, P.R. Solanki, M. Datta, B. D. Malhotra: *Biosensors and Bioelectronics*. **2009.** 24. 2810.

3. D.K. Aswal, S. Lenfant, D. Guerin J.V. Yakhmi, D. Vuillaume: *Analytica Chimica Acta*. **2006.** 568. 84.

4. A. Bansal, X. Li, S.I. Yi, W.H. Weinberg, N.S. Lewis: *J. Phys. Chem. B*. **2001.** 105. 10266.

5. A.R. Bishop, R.G. Nuzzo: *Current Opinion in Colloid & Interface Science*. **1996.** 1. 127.

6. R. Boukherroub: *Current Opinion in Solid State and Materials Science*. **2005.** 9. 66.

7. J.M. Buriak: *Chemical Reviews*. **2002.** 102. 1271.

8. R.L. Cicero, M.R. Linford, C. E. D. Chidsey: *Langmuir.* **2000.** 16. 5688.

9. C. Coletti, A. Marrone, G. Giorgi, A. Sgamellotti, G. Cerofolini, N. Re: *Langmuir.* **2006.** 22. 9949.

10. L. Carroll, C.B. Gorman: *Angew. Chem. Int. Ed*. **2002.** 41. 4378.

11. M.K. Chaudhury: *Current Opinion in Colloid & Interface Science*. **1997.** 2. 65.

12. C. H. de Villeneuve, J. Pinson, M. C. Bernard, P. Allongue: *J. Phys. Chem. B*. 1997. 101, 2415.

13. L.H. Dubois, R.G.Nuzzo: *Annu. Rev. Phys Chem*. **1992.** 43. 437.

14. A.-S. Duwez: *Journal of Electron Spectroscopy and Related Phenomena*. **2004.** 134. 97.

15. B.J. Eves, G.P. Lopinski: *Surface Science*. **2005.** 579. L89.

16. B.J. Eves, Q.-Y. Sun, G.P. Lopinski, H. Zuilhof: *J. Am. Chem. Soc*. **2004**. 126. 14318.

17. E.J. Faber, L.C.P.M. de Smet, W. Olthuis, H. Zuilhof, E.J.R. Sudholter, P. Bergveld, A. van den Berg. *ChemPhysChem*. **2005.** 6. 2153.

18. S. Fellah, A. Teyssot, F. Ozanam, J.-N. Chazalviel, J. Vigneron, A. Etcheberry: *Langmuir.* **2002.** 18. 5851.

19. S. Fellah, R. Boukherroub, F. Ozanam, J.-N. Chazalviel: *Langmuir.* **2004.** 20. 6359.

20. A. Fidelis, F. Ozanam, J.-N. Chazalviel: *Surface Science*. **2000.** 444. L7.

21. B. Fabre: *Accounts of Chemical Research*. **2010.** 43. 1509.

22. G.S. Higashi, R.S. Becker, Y.J. Chabal, A.J. Becker: *Appl. Phys. Lett*. **1991.** 58. 1656.

23. R. Hunger, R. Fritsche, B. Jaeckel, W. Jaegermann, L.J. Webb, N.S. Lewis: *Phys. Rev. B*. **2005.** 72. 045317.

24. R. Hunger, R. Fritsche, B. Jaeckel, L.J. Webb, W. Jaegermann, N.S. Lewis: *Surface Science*. **2007.** 601. 2896.

25. G.K. Jennings, P.E. Laibinis: *Colloids and Surfaces A: Physicochemical and Engineering Aspects*. **1996.** 116. 105.

26. P. Kruse, E.R. Johnson, G.A. DiLabio, R. A. Wolkow: Nanoletters. **2002.** 2. 807.

27. S.A. Kulinich, M. Farzaneh: *Applied Surface Science*. **2004.** 230, 232.

28. A. Langner, A. Panarello, S. Rivillon, O. Vassylyev, J.G. Khinast, Y. J. Chabal: *J. Am. Chem Soc*. **2005.** 127. 12798.

29. G. P. Lopinski, D. D. M. Wayner, R. A. Wolkow: *Nature*. **2000.** 406. 48.

30. M.R. Linford, P. Fenter, P.M. Eisenberger, C.E.D. Chidsey: *J. Am. Chem Soc*. **1995.** 117, 3145.

31. S. Maldonado, K.E. Plass, D. Knapp, N.S. Lewis: J. Phys. Chem. C. **2007.** 111. 17690.

32. T. Miyadera, A. Koma, T. Shimada: *Surface Science*. **2003.** 526. 177.

33. R. Okada, T. Miyadera, T. Shimada, A. Koma, K. Ueno, K. Saiki: *Surface Science*. **2004.** 552. 46.

34. H. Sano, H. Maeda, S. Matsuoka, K.-H. Lee, K. Murase, H. Sugimura: *Japanese Journal of Applied Physics*. **2008.** 47. 5659.

35. D. Seyferth: *Organometallics*. **2009.** 28, 1598.

36. A. B. Sieval, A. L. Demirel, J. W. M. Nissink, M. R. Linford, J. H. van der Maas, W. H. de Jeu, H. Zuilhof, and E. J. R. Sudholyer: *Langmuir.* **1998.** 14. 1759.

37. R.K. Smith, P.A. Lewis, P.S. Weiss: *Progress in Surface Science*. **2004.** 75. 1.

38. L. Srisombat, A.C. Jamison, T.R. Lee: *Colloids and Surfaces A: Physicochem. Eng. Aspects*. **2011.** 390. 1.

39. M.P. Stewart, J.M. Buriak: *J. Am. Chem. Soc*. **2001.** 123. 7821.

40. Q.-Y. Sun, L.C. P. M. de Smet, B. van Lagen, M. Giesbers, P. C. Thune, J. van Engelenburg, F. A. de Wolf, H. Zuilhof, E. J. R. Sudholter: *J. Am. Chem. Soc*. **2005.** 127. 2514.

41. L.A. Tjurina, V.V. Smirnov, G.B. Barkovskii, E.N. Nikolaev, S.E. Esipov, I.P. Beletskaya: *Organomettalics*. **2001.** 20. 2449.

42. A. Ulman: *Introduction to Ultrathin Organic Films from Langmuir-Blodgett to Self-Assembly*, Academic Press, **1991**.

43. I. Waluyo, H. Ogasawara, M. Kawai, A. Nilsson, T. Yamada: *J. Phys. Chem. C*. **2010.** 114. 19004.

44. X. Wang, R.E. Ruther, J.A. Streifer, R. J. Hamers: *J. Am. Chem. Soc*. **2010.** 132. 4048.

45. L.J. Webb, N.S. Lewis: *J. Phys. Chem. B*. **2003.** 107. 5404.

46. L. J. Webb, S. Rivillon, D.J. Michalak, Y.J. Chabal, N.S. Lewis: *J. Phys. Chem. B*. **2006.** 110. 7349.

47. C.M. Whelan, M. Kinsella, L. Carbonell, H.M. Ho, K. Maex: *Microelectronic Engineering*. **2003.** 70. 551.

48. Y. Xia, X.-M. Zhao, G.M. Whitesides: *Microelectronic Engineering*. **1996.** 32. 255.

49. T. Yamada, T. Inoue, K. Yamada, N. Takano, T. Osaka, H. Harada, K. Nishiyama, I. Taniguchi: *J. Am. Chem. Soc*. **2003.** 125. 8039.

50. T. Yamada, M. Kawai, A. Wawro, S. Suto, A. Kasuya, *A. J. of Chem. Phys*. **2004.** 121. 10660.

51. H. Yu, L.J. Webb, J.R. Heath, N.S. Lewis: *Appl. Phys. Lett*. **2006.** 88. 252111.

52. H. Yu, L.J. Webb, R.S. Ries, S.D. Solares, W.A. Goddard, J.R. Heath, N.S. Lewis: *J. Phys. Chem. B*. **2005.** 109. 671.

53. Y. L. Zhong, S.L. Bernasek: *Langmuir.* **2011.** 27. 1796.

54. X. Zhou, M. Ishida, A. Imanishi, Y. Nakato: *Electrochimica Acta*. **2000.** 45. 4655.

Chapter 2
Photochemical Grafting of Methyl Groups on Si(111) Surface using Grignard Reagent

2.1. Introduction

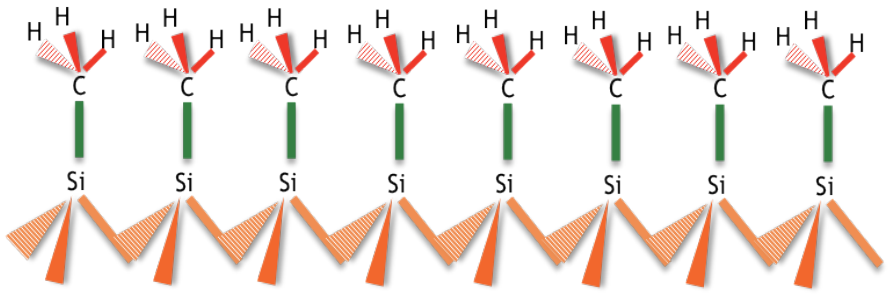

Figure 2.1. Methyl-terminated Si(111)

Methylated silicon (Si-CH_3) surfaces have been topic of many researches (Fellah et. al., 2002; Fidelis et. al. 2000; Hunger et. al., 2005; Hunger et. al., 2007; Miyadera et. al., 2003; Okada et al., 2004; Waluyo et. al., 2010; Webb et. al., 2006; Yamada et. al.; 2004, Yu et. al., 2005, Yu et. al., 2006). Methyl groups are the smallest among the alkyl groups and can form stable Si-C bonds with the Si surface. The combination of these qualities marks its unique advantage among other molecules. Methyl (–CH_3) is the simplest and the smallest among the alkyl groups (C_nH_{2n+1}). Its van der Waals radius is small enough to fit in between the spacing of Si(111) surface. Thus, compare with other alkyl groups that can also form Si-C bonds, methyl groups has the ability to completely cover (Fidelis et. al, 2000; Yamada et. al., 2004; Nemanick 2006) the entire the Si(111) surface (Figure 2.1). In such, it is desired to completely saturate all the atoms on the Si surface with Si-C bonds to

prevent unwanted oxidation. The presence of silicon oxide can introduce additional surface states that could be detrimental if the intended function of the SAM is for electronic application. Meanwhile, unlike hydrogen and halogen (X) atoms that could also completely terminated every atoms on the Si surface, methyl groups can establish Si-C bonds, which is more stable than Si-H and Si-X bonds.

Organic molecules on silicon surfaces (Amy et. al., 2007; Bansal et. al., 2001; Boukherroub et. al., 1999; Boukherroub, 2005; Buriak, 2002; Cicero, et. al. 2000; Fellah, et. al., 2004; Linford and Chidsey, 1993; Linford et. al., 1995; Sieval et. al., 1998; Sieval et. al., 2000; Sun et. al., 2005; Takakusagi et. al., 2007; Touahir et. al., 2010; Webb and Lewis, 2003) have been cited in different researches. Different techniques were done to attach organic molecules on the Si surface. For attaching alkyl groups on semiconductor surfaces in particular, the following methods have been done using Grignard reagent as precursor: (1) chlorination-alkylation method (Bansal et. al., 2001; Hunger et. al., 2005; Hunger et. al., 2007; Waluyo et. al., 2010; Webb et. al., 2006; Webb and Lewis, 2003; Yamada et. al., 2004; Yu et. al., 2005; Yu et. al., 2006), (2) electrochemical method (Fellah et. al., 2002; Fidelis et. al., 2000; Miyadera et. al., 2003; Okada et. al., 2004; Webb and Lewis, 2003), (3) thermal grafting (Fellah et. al., 2004) and (4) photoanodic method (Takakusagi et. al., 2007).

In the chlorination-alkylation technique, a chlorine-terminated Si (Si-Cl) acts as the substrate for the methylation process. In such process, the Si-H sample was initially processed to become Si-Cl. The production of Cl-terminated surface can be done either by placing PCl_5 in chlorobenzene at an elevated temperature (Hunger et. al., 2005; Hunger et. al., 2007; Webb et. al., 2006; Yu et. al., 2006; Yu et. al. 2005) or by using Cl_2 gas diluted in

argon atmosphere (Yamada et. al. 2004; Waluyo et. al., 2010). Si-Cl bonds are more reactive and less stable than Si-H bonds, thus it could easily react with the Grignard reagent to produce a methylated surface. In the electrochemical technique (Fellah et. al., 2002; Miyadera et. al., 2003; Okada et. al. 2004; Fidelis et. al., 2000), external bias is used to trigger methylation. In thermal grafting (Fellah et. al., 2004), the alkylation process is at elevated temperature (e.g., 90°C) to promote grafting. In the photoanodic method (Takakusagi et. al. 2007), the grafting process was promoted both by the use of external bias and the presence of illumination. However, for advance electronic applications, which would need the designing of circuit patterns on the Si surface, a light-based technique would be advantageous so that it could be adaptable with photopatterning technique. Thus, this chapter will present a light-based technique to graft methyl groups onto the Si surface without the aid of an external bias. The placement of external bias onto the Si substrate, similar to that of electrochemical method and of photoanodic method, would require the placement of ohmic contact between the Si substrate and electrode, which could introduce potential and/or irreparable damage to the substrate. Our method is advantageous compare to that of chlorination-alkylation process since our method utilizes hydrogen-terminated Si only, instead of further processing it to chlorine-terminated Si. With this, our method avoids the difficulty of using gas-based chlorination process in an inert atmosphere or the hazardous thermal chlorination process.

Patterned from the model presented by Fellah, et. al. (2002, 2004), the grafting of methyl groups onto the Si substrate is visualized as follows:

$$CH_3MgBr + p^+ \rightarrow CH_3\cdot + MgBr^+ \qquad (2.1)$$

$$\equiv Si\text{-}H + CH_3\cdot \rightarrow \equiv Si\cdot + CH_4 \qquad (2.2)$$

$$\equiv Si\cdot + CH_3\cdot \rightarrow \equiv Si\text{-}CH_3 \qquad (2.3)$$

Equations 2.1-2.3 are similar to equations 1.1-1.3 (Chapter 1), in which the alkyl (R) is taken to be methyl. Equation 2.1 shows the decomposition of Grignard reagent into methyl radical ($CH_3\cdot$) by the introduction of positive charge. The presence of methyl radical initiates the formation of Si radical ($\equiv Si\cdot$) (Equation 2.2), which is needed in order for the surface Si atom to have one free electron for possible binding with a molecule. The Si radical and methyl radical could interact with each other to establish Si-C bond (Equation 2.3).

The decomposition of the Grignard reagent, which is needed to promote the methyl grafting process, could be triggered by (1) electron capture by the reduction of alkyl halide (Fellah et. al., 2004), (2) by anodization (Fellah et. al, 2002), or (3) by phototanodization (Takakusagi et. al, 2007). In the case of reduction of alkyl halide, the charges that are needed for the decomposition of Grignard reagent can come within the grafting solution while in the cases of anodization and photoanodization, the charges comes within the Si substrate. It is our aim to look on the possibility of using illumination to generated surface holes in order to trigger the decomposition of Grignard reagent and promote the grafting of methyl groups.

The main objective this research is to photochemically graft methyl groups on Si(111) using Grignard reagent. The specific objectives of this research are as follows:

(1) to obtain the O 1s, C 1s, and Si 2p spectra of the samples using XPS,

(2) to measure the water contact angle of the sample using water contact angle meter,

(3) to observe the surface topography of the sample using AFM,

(4) to measure the infrared spectra using ATR-FTIR,

(5) to measure the surface dipole of the sample using photoemission yield spectroscopy,

(6) to compare the grafting process on n-type and on p-type substrates,

(7) to determine the effect of grafting time,

(8) to determine the effect of illumination intensity,

(9) to determine the effect of substrate's dopant concentration.

2.2. Methodology

2.2.1. Hydrogen-termination process

The following kinds of substrates were used in this experiment: (1) Phosphorus-doped Si with resistivity of 1-10 Ω cm (n low Si), (2) Phosphorus-doped Si with resistivity of 0.001-0.004 Ω cm (n high Si) and (3) Boron-doped Si with resistivity of 1-30 Ω cm (p low Si). The terms "n" and "p" indicate n-type and p-type, respectively. The terms "low" and "high" in the notations indicates low and high dopant concentrations, respectively. Si substrates with low dopant concentration have high resistivity while those with high dopant concentration have low resistivity.

Figure 2.2 shows the schematic diagram of the hydrogen-termination process. The wafer was cut into size that can fit inside the optical cell (Figure 2.2a). The cut wafer was cleaned ultrasonically with ethanol (Figure 2.2b) and with ultrapure water (UPW) (Figure 2.2c) for 20 min each, respectively. The sample was then photochemically cleaned using vacuum ultraviolet (VUV) for 20 min (Figure 2.2d). The VUV was used to remove organic contaminants. The UV radiation that was used came from a xenon excimer lamp

that has wavelength of 172 nm and intensity of 10 $mW \cdot cm^{-2}$. The cleaned sample was then immersed in 5%HF solution (Figure 2.2e). The immersion time depends on the dopant concentration. The immersing time of samples with low dopant concentration is 5 min while for the samples with high dopant concentration is 30 s. Afterwards, the samples were immersed in 40%NH_4F solution (Figure 2.2f). The immersing time of samples with low dopant concentration is 30 s while for the samples with high dopant concentration is 1 min. The Si-H sample (Figure 2.2g) was dried using streams of nitrogen.

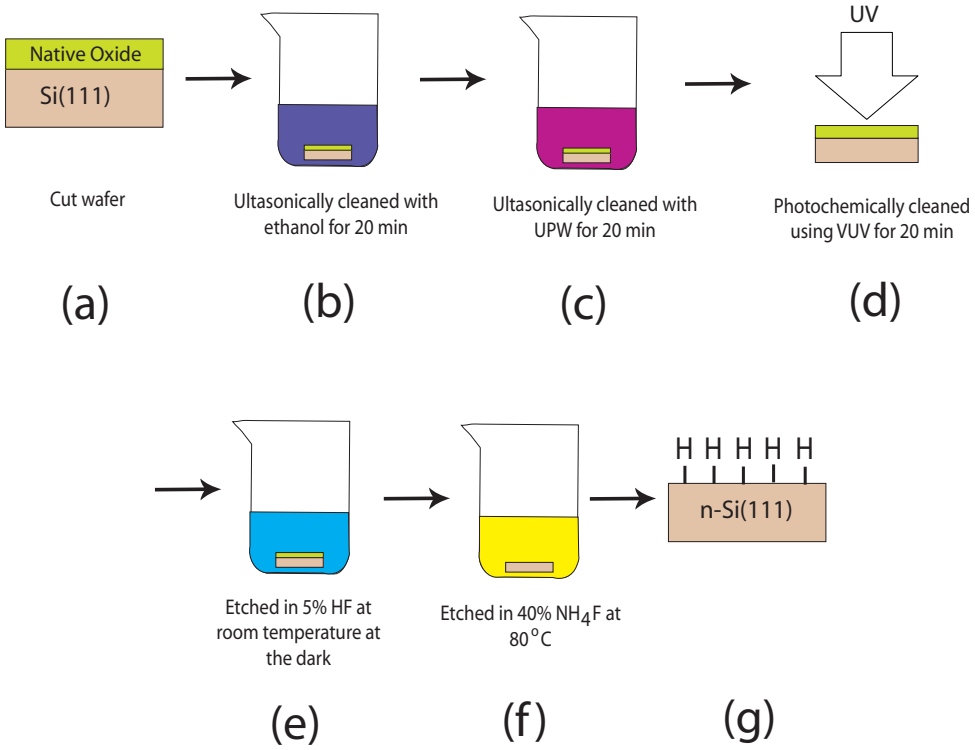

Figure 2.2. Hydrogen-termination Process

2.2.2. Photochemical grafting

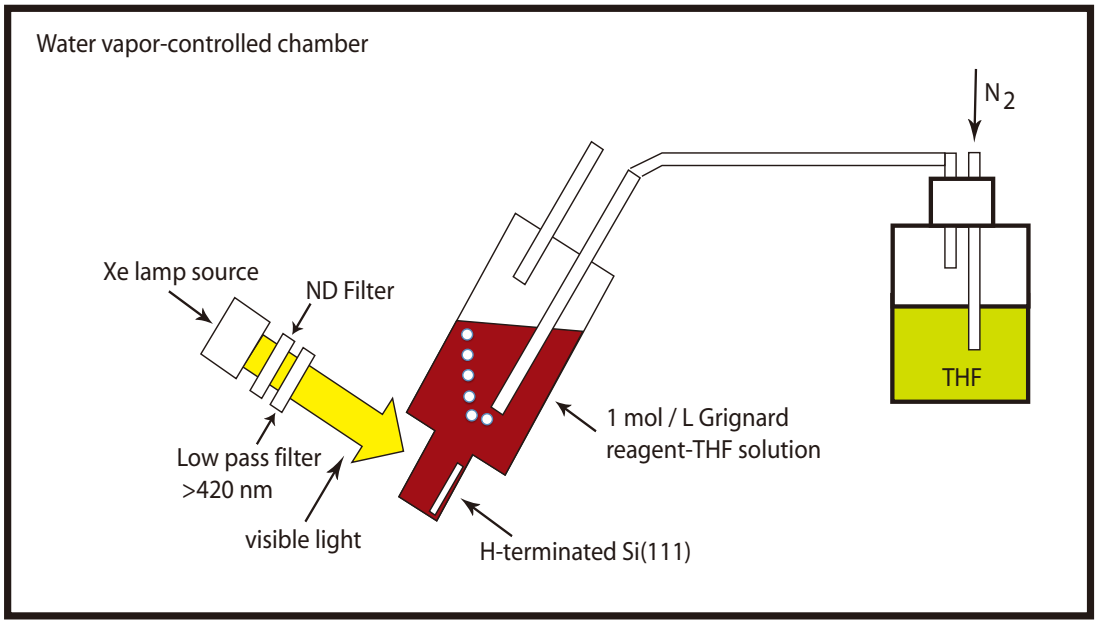

Figure 2.3. Experimental set-up of the photochemical grafting process

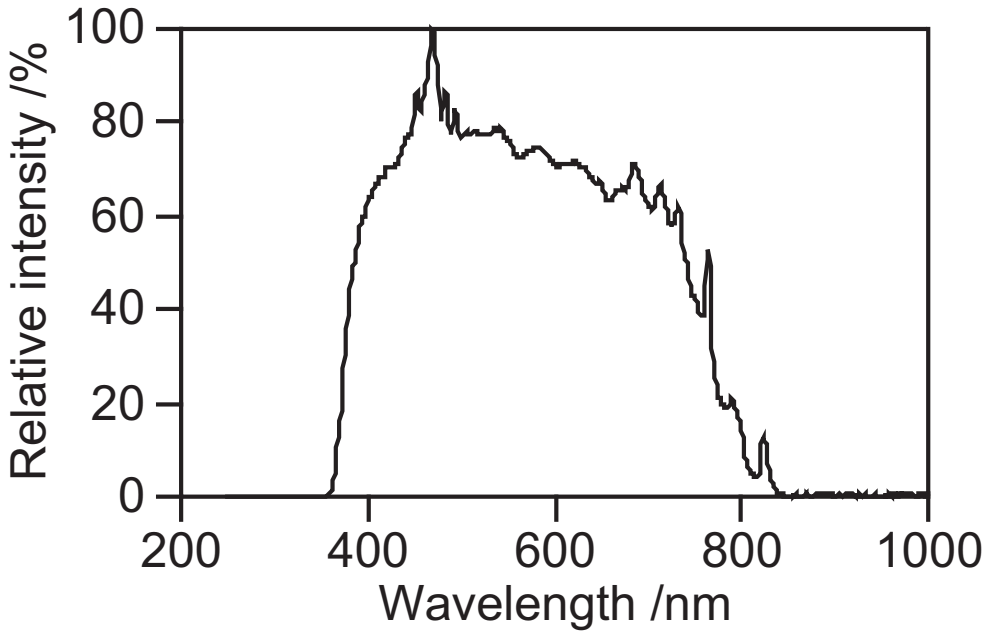

Figure 2.4. Spectrum of visible light that was used in the grafting process (Taken from Sano, et . al. 2011)

Figure 2.3 shows the experimental set-up that was used during the photochemical grafting process. The grafting was done by illuminating the Si-H, which was immersed in the Grignard Reagent-tetrahydrofuran solution (CH_3MgBr-THF) at room temperature, with visible light. The spectrum of the visible light that was used is presented in Figure 2.4. The visible light comes from a xenon lamp device (Asahi Spectra Co., Ltd., Max 1000) with has detachable optical filters and controllable light intensity. A quartz vessel with a cylindrical upper body and a rectangular-shaped bottom was used as the optical cell. The quartz optical cell was covered with a silicone stopper with an inlet and an outlet for nitrogen gas bubbling. One mol/l (12 %) CH_3MgBr-THF was placed inside the cell and serve as the grafting medium. The grafting solution was purged with nitrogen gas, prior to and during the grafting process. To compensate for the THF that would be lost in the grafting solution because of its volatility, a reservoir bottle with THF was placed along the nitrogen line as seen in Figure 2.3.

CAUTION: As stated in Chapter 1.3.1, Grignard reagent reacts vigorously with water, acids, alcohols and amines, thus extreme caution should be done in handling it. The grafting process, as well as the opening and storage of Grignard solution, were done inside a water vapor controlled chamber for safety reason. All the materials that will be in contact with Grignard reagent, including the hydrogen-terminated Si, were kept dry. Because Grignard reagent is extremely sensitive with many reagents, waste Grignard reagents were made first to react with acetone. Afterwards, their by-product pH was made to be near neutral before placing in the chemical waste container to ensure safe disposal.

2.2.3. Post-cleaning treatment

After the photochemical grafting process, the sample was rinsed with THF to remove excess Grignard reagent in the sample's surface. After which, the sample was ultrasonically cleaned in ethanol and in UPW for 20 mins, respectively. The cleaned sample was then dried using streams of nitrogen.

2.2.4. Characterizations

X-ray photoelectron spectroscopy (XPS) was done using an XPS system (Kratos Analytical Ltd., ESCA-3400). Using the XPS system, the O 1s, the C 1s and the Si 2p spectra of the sample was measured. The source of the X-ray was MgKα. The X-ray source is working at an emission current of 10 mA and an acceleration voltage of 10 kV. Step size of 0.1 eV was used for the XPS scan and was repeated for 10 times. XPS quantitative analysis was done using the built-in software to determine the oxygen atomic percent (O at%), the carbon atomic percent (C at%) and the silicon atomic percent (Si at%).

A Digilab FTIR spectrometer (Excalibur FTS 3000) sample chamber with a GATR™ single reflection horizontal ATR accessory was used to determine the ATR-FTIR spectrum of the samples. The ATR accessory uses Ge ATR crystal and has a 65° angle of incidence. Digilab Resolutions Pro 4.0 software package was used to record the IR spectrum.

The static water contact angle of the samples was measure using a water contact angle meter (Kyowa Interface Science Co., Ltd., DM 500). The volume of the water droplets that were used in the measurements was 1.8 μl.

The surface topographical images of the sample were obtained using an atomic force microscope (Asylum Research, MFP-3D-SA AFM) in AC mode using an aluminum-backside coated Si (SII NanoTechnology Inc., SI-DF20) as probe.

A photoemission yield spectroscopy (PYS) system (Riken-Keiki Co., Ltd., Surface Analyzer AC-2) was used to determine the ionization potential of the methyl-terminated Si sample. During the measurement, the sample was illuminated with 3 nW ultraviolet light, scanned from 4.20 to 6.00 eV in 0.05 eV steps.

2.3. Results and Discussion

We are successful in producing methyl-terminated Si(111) on an n-type substrate, however, we were not successful in producing a methyl-terminated surface on a p-type substrate using photochemical preparation.

2.3.1. Photochemical Grafting Process

Table 2.1. Different samples that were prepared

Acronym	Description
(a) Light and Grignard Reagent	n-low Si-H sample, which was irradiated with 35 mW cm^{-2} visible light for 2 h in the Grignard reagent-THF solution
(b) Si-H	n-low Si-H sample, which has undergone post cleaning treatment
(c) No light but with Grignard reagent	n-low Si-H sample that was immersed in the Grignard reagent-THF solution for 2 h in the dark

(d) With light but with no Grignard reagent	n-low Si-H sample that was irradiate with 35 mW cm^{-2} visible light in THF for 2 h without Grignard reagent

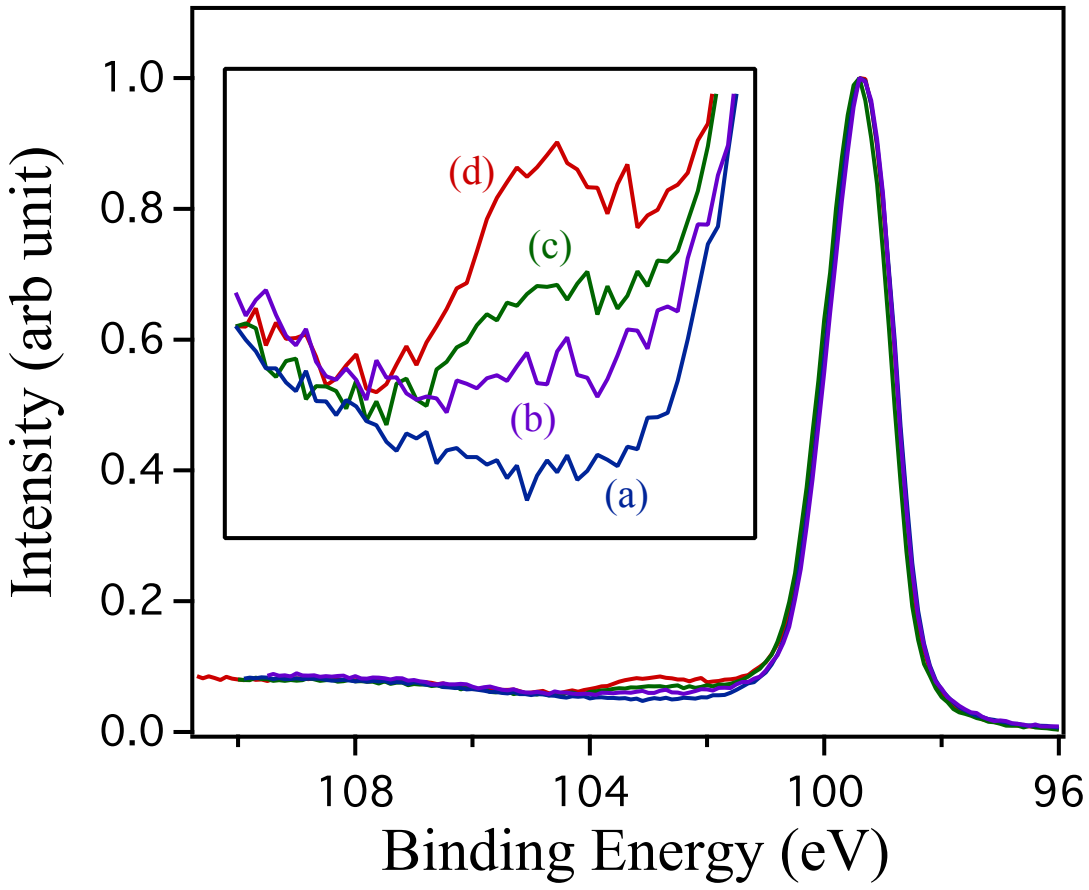

Figure 2.4. Si 2p spectra of the different samples specified in Table 2.1. The inset highlights the portion of the spectra, which is associated with the formation of silicon oxide.

Table 2.1 shows the different samples that were prepared. Figure 2.4 shows their Si 2p spectra. The two possible peaks in Si 2p spectra can be associated with the existence of the following: (1) crystalline silicon (large peak at around 99.4 eV) and (2) silicon oxide (small peak at higher binding energy and highlighted in the inset of the graph). Among the different samples that were prepared, the Si-H sample that undergone photochemical grafting process shows no apparent silicon oxide peak (Figure 2.4a). This indicates that

methyl groups are grafted on the silicon surface, thus prevents the formation of silicon oxide. Meanwhile, the Si-H sample shows small silicon oxide peak (Figure 2.4b), which may have developed during its post-cleaning treatment. Its higher silicon oxide level, compare to the Si-CH_3 sample (Figure 2.4a), shows that Si-C bonds are more effective in preventing the growth of silicon oxide than Si-H bonds. Likewise, the sample that was immersed in Grignard reagent-THF solution for 2 h in the dark shows the presence of silicon oxide, in which its level is larger than that of Si-H (Figure 2.4c). The presence of silicon oxide is attributed to the absence (or very low amount) of grafted methyl groups. This signifies that the procedure, which we have implemented, does not promote methyl grafting in the dark (or has very slow methylation process in the dark). On the other hand, the sample that was illuminated for 2 h without Grignard reagent shows the largest silicon oxide content among the different samples (Figure 2.4d). Since there were no Grignard reagent molecules in the grafting solution, no methyl group would be grafted to protect the surface from oxidization. The illumination of visible light induces the formation of photogenerated charges that further accelerate the oxidation of the silicon surface.

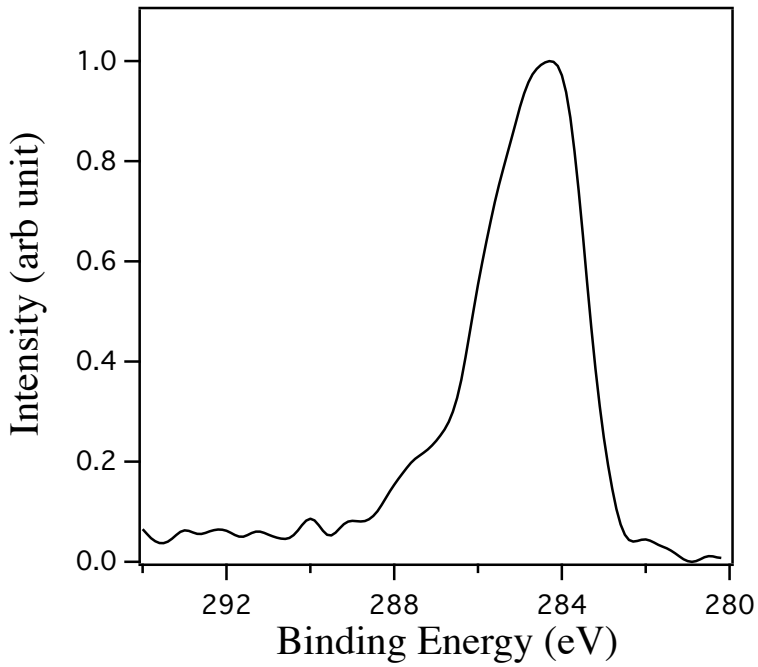

Figure 2.5. C 1s spectra of the methyl-terminated sample

Figure 2.5 shows C 1s spectrum of the methyl-terminated Si sample. The spectrum shows the existence of a "shoulder" at the higher binding energy. This "shoulder" could be due to carbon-based contaminations that may have cling on the surface during the photochemical grafting process and during the post-cleaning treatment.

The energy band diagram of hydrogen-terminated Si is presented in Figure 1.5 (Chapter 1). In the dark and in absence of external voltage, the depletion layer of the Si-H sample hinders the transport of charges from/to Si substrate to/from the hydrogenated surface. Some possible ways in order for positive charges to go at the Si surface, includes the following: (1) by placing external voltage and (2) by illumination of the surface.

The placement of sufficient external bias on the Si-H sample can make positive charges available on the Si surface. Connecting a positive bias on n Si-H sample creates an

inversion layer (Figure 1.6a in Chapter 1). At this condition, the Si surface would be rich in positive charges, which are the minority carrier of n-type Si. Meanwhile, connecting a positive bias on p Si-H sample creates an accumulation layer (Figure 1.7d in Chapter 1). At this condition, the Si surface would be rich in positive charges, which is the majority carrier of p-type Si. To note, the connection of an external bias on an n-type (Miyadera et. al., 2003, Okada et. al., 2004) or a p-type (Fellah et. al., 2002, Fidelis et. al., 2000) substrate has resulted to the production of methyl-terminated silicon.

The success of our photochemical grafting process in producing methyl-terminated Si(111) indicates that it is also possible to use the photogenerated holes in triggering the methyl grafting process.

2.3.2. Effect of the type of substrate (n-type vs. p-type)

Table 2.2. n-type and p-type samples

Acronym	Description
(a) n Si-H	n-low Si-H sample, which has undergone post cleaning treatment
(b) n Si-H (Light)	n-low Si-H sample, which was irradiated with 35 mW cm^{-2} visible light for 2 h in the Grignard reagent-THF solution
(c) p Si-H	p-low Si-H sample, which has undergone post cleaning treatment
(d) p Si-H (Light)	p-low Si-H sample, which was irradiated with 35 mW cm^{-2} visible light for 2 h in the Grignard reagent-THF solution

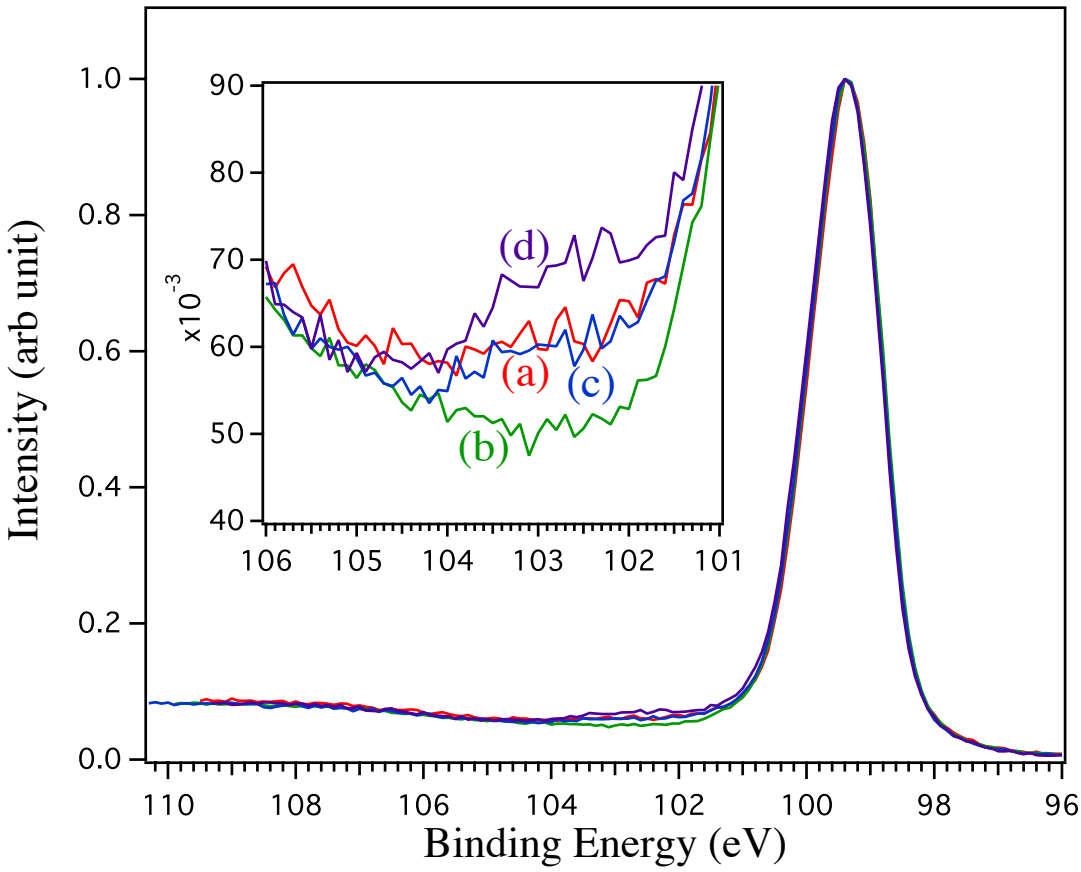

Figure 2.6. Si 2p spectra of the different samples specified in Table 2.2. The inset highlights the portion of the spectra, which is associated with the formation of silicon oxide.

Figure 2.6 shows the Si 2p spectra of the samples that were specified in Table 2.2. The inset highlights the portion of the spectra, which is associated with the formation of silicon oxide. Photochemical preparation using n-type substrate (Figure 2.6b) yields a low silicon oxide level compare with its p-type counterpart (Figure 2.6d), and the two Si-H samples (Figures 2.6a, 2.6c). The low level of its silicon oxide is attributed with the

presence of grafted methyl groups while the high oxide level of the p-type sample was attributed in its absence (or very low amount). The nature of charges that goes on the Si surface during illumination depends on the type of substrate (whether n-type or p-type) (Figure 1.19 Chapter 1). For n-type Si, holes go on the Si surface. Meanwhile for p-type, electrons go on the Si surface. The presence of photogenerated positive charges on the Si surface induces the oxidative decomposition of Grignard reagents that led to methyl grafting. On the other hand, the illumination of p-type Si with visible light results to the presence of photogenerated electrons, which do not promote the oxidative decomposition of Grignard reagents rather they enhances the oxidation process.

2.3.3. Rate of methyl grafting

Figure 2.7 shows the plot of the oxygen atomic percent of the samples with grafting time. Note that the "0 hr sample" is an n low Si-H sample, which underwent post cleaning treatment. The graph shows that the oxygen atomic percent decreases with grafting time. This decrease indicates the improvement of the coverage of the methylated surface with respect to grafting time. The rate at which the O at% decrease is faster on lower grafting time (0 to 2 h) compared with that of longer grafting time (2 to 4 h). The faster grafting rate at lower grafting time can be attributed to the larger number of available grafting site at the start of the grafting process. As the surface is being methylated, the number of available grafting site decreases, thus the rate of methylation becomes slower.

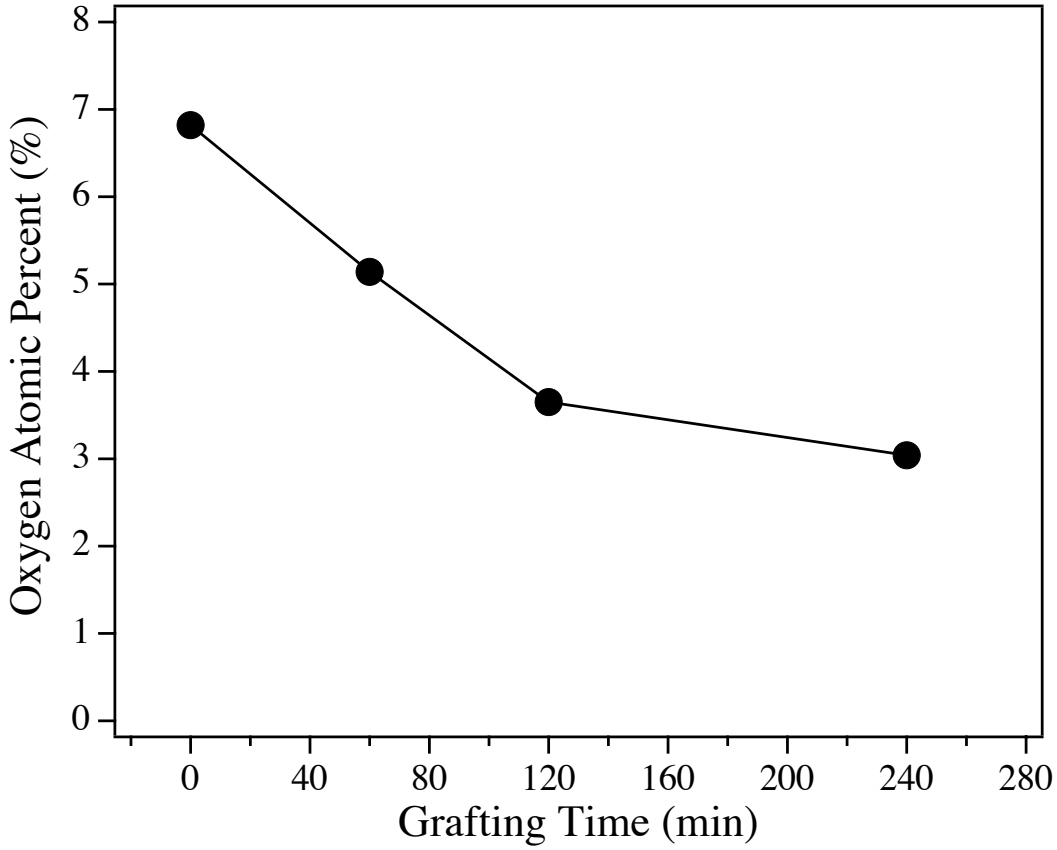

Figure 2.7. Grafting time vs. oxygen atomic percent of n low Si-H with resistivity of 1-10 Ω cm that underwent photochemical preparation using 200 mW・cm^{-2} illumination.

The rate at which positive charges accumulate on the silicon surface can affect the rate of methyl grafting process. The absorption of light on the Si surface induces the creation of electron-hole pair. The splitting of the electron-hole pair primarily happens in the depletion region due to the electric field in it. (Let us neglect the effect of possible splitting of electron-hole pairs outside the depletion region.) As stated earlier, for n Si, the holes went onto the Si surface. The rate in which holes accumulates on the Si surface can be influenced by (1) by the rate of the electron-hole pair generation and (2) by the width of the depletion region.

Table 2.3. XPS quantitative analytical data and water contact angle of n low Si-H that underwent photochemical preparation for 2 hr.

Illumination Intensity ($mW \cdot cm^{-2}$)	O (at. %)	C (at. %)	Si (at. %)
35	5.28	4.97	89.75
70	5.09	5.24	89.67
145	5.08	6.85	88.07
200	3.65	6.61	89.74
400	3.52	5.52	90.96
600	2.46	7.65	89.89

The rate of electron-hole pair generation (or optical generation rate) depends on the effective flux of photon hitting the surface of the sample. The effective photon flux is in turn affected by (1) the sample's quantum efficiency, (2) the transmittance of the grafting medium and (3) the intensity of visible light illumination that was used during the grafting process. The effect of the rate of electron-hole pair generation on the rate of the methyl grafting process was investigated by varying the intensity of visible light that was used during the grafting process. Other factors such as the nature of the Si-H sample (which may affect the quantum efficiency of the sample), concentration of Grignard reagent on the grafting solution (which may affect the transmittance of the grafting solution) were kept or assumed to be constant.

Table 2.3 shows the O at%, the C at%, the Si at% and the water contact angle of

samples that were prepared under different illumination intensities. The table shows that as the illumination intensity increases, the O at% of the sample decreases. The decrease in O at% signifies that the coverage of the methylated surface improves with the increase in illumination intensity. High illumination intensity increases the rate of positive charge production on the Si surface, which in turn triggers a faster grafting process. Table 2.3 also shows that the water contact angle of the sample increases with illumination intensity. The increase in water contact angle reflects the increase in coverage of the methylated surface. To note, it would be difficult to drive conclusions based from the carbon atomic percent because sufficiently large signals from carbon-based impurities are superimposed on the C 1s spectra as shown in Figure 2.5.

The thickness of depletion region can be affected by the dopant concentration of the substrate. Samples with low dopant concentration (or high resistivity) have thicker depletion region while those with higher dopant concentration (or low resistivity) has thinner depletion region. Samples with thinner depletion region have fewer regions where the electron-hole pair splitting occurs, thus this could translate to lower density of photogenerated holes on the Si surface, which in turn could translate to a slower methylation process.

Table 2.4 shows the O at%, the C at%, the Si at% and the water contact angle of samples that used substrate with different dopant concentrations. The sample that used substrate with high dopant concentration had higher O at% than that of sample that used substrate with low-dopant concentration. This suggests that the rate of methyl grafting process on low-doped substrate is faster than on high-doped substrate. Likewise, the water contact angle of the sample that used substrate with low dopant concentration is higher

than the sample that used substrate with high dopant concentration. This supports that the rate of methylation on low-doped substrate are faster than that high-doped substrate.

Table 2.4. XPS quantitative analytical data of n Si-H that underwent photochemical preparation for 60 min using 200 mW・cm^{-2} illumination.

Doping level	Resistivity (Ω cm)	O (at. %)	C (at. %)	Si (at. %)	Water contact angle (°)
n-low Si	1-10	5.14	7.18	87.69	84.6 ± 1.5
n-high Si	0.001-004	6.98	11.15	81.87	75.5 ± 1.4

2.3.4. Characteristics of the methyl-terminated Si surface

The methylated Si surface that was produced using photochemical preparation has atomically flat and hydrophobic surface. The surface also has lower electron affinity compare with that of the Si substrate.

The Si-CH_3 sample has surface potential step (δ) of -0.31 eV as depicted in Figure 2.8. Surface potential step is the contribution of the surface dipole, which is caused by the grafting of molecules on a substrate, to the electron affinity. The value of surface potential step is calculated from the value of the different parameters of bulk silicon and the sample's ionization potential, which was determined from the Photoemission Yield Spectroscopy (PYS). The sample's ionization potential (I_p = 4.86 eV) was estimated as the energy threshold of the graph of the photon energy hitting the surface of the sample vs. square root of yield (Figure 2.9). The energy threshold is taken as the crossing point of

the yield line (with gradient of 25.95 $cps^{1/2}$/eV) and of the background (1.7 $cps^{1/2}$). Specifically, the value of the surface potential step is the difference between the calculated value of electron affinity of the methylated surface (χ = 3.74 eV) and the electron affinity of the bulk silicon ($\chi_{bulk\ Si}$ = 4.05 eV) (He, et. al. 2008). The value of the sample's electron affinity was the difference between sample's ionization potential (I_p = 4.86 eV) and the band gap of silicon (E_g = 1.12 eV).

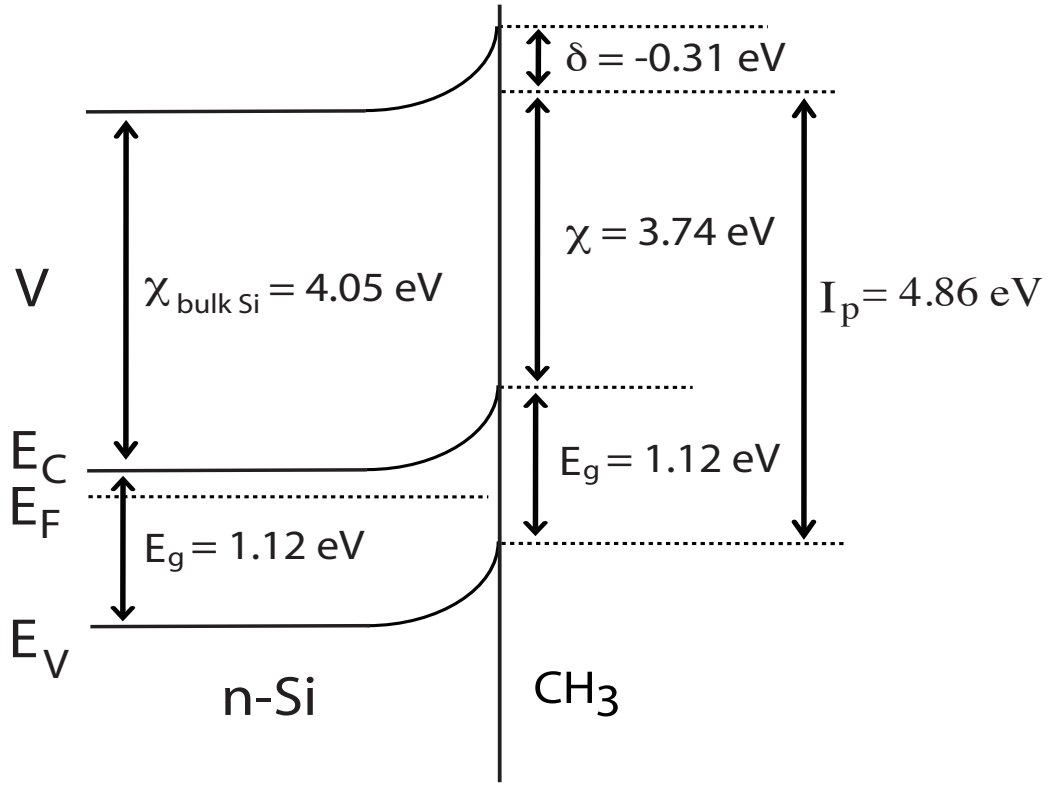

Figure 2.8. Band diagram of methyl-terminated Si(111) on n-type substrate. V, E_c, E_v and E_F denote vacuum level, conduction band, valence band and Fermi energies, respectively. The terms I_p, δ and χ are the ionization potential, surface potential step and electron affinity of the grafted surface, respectively.

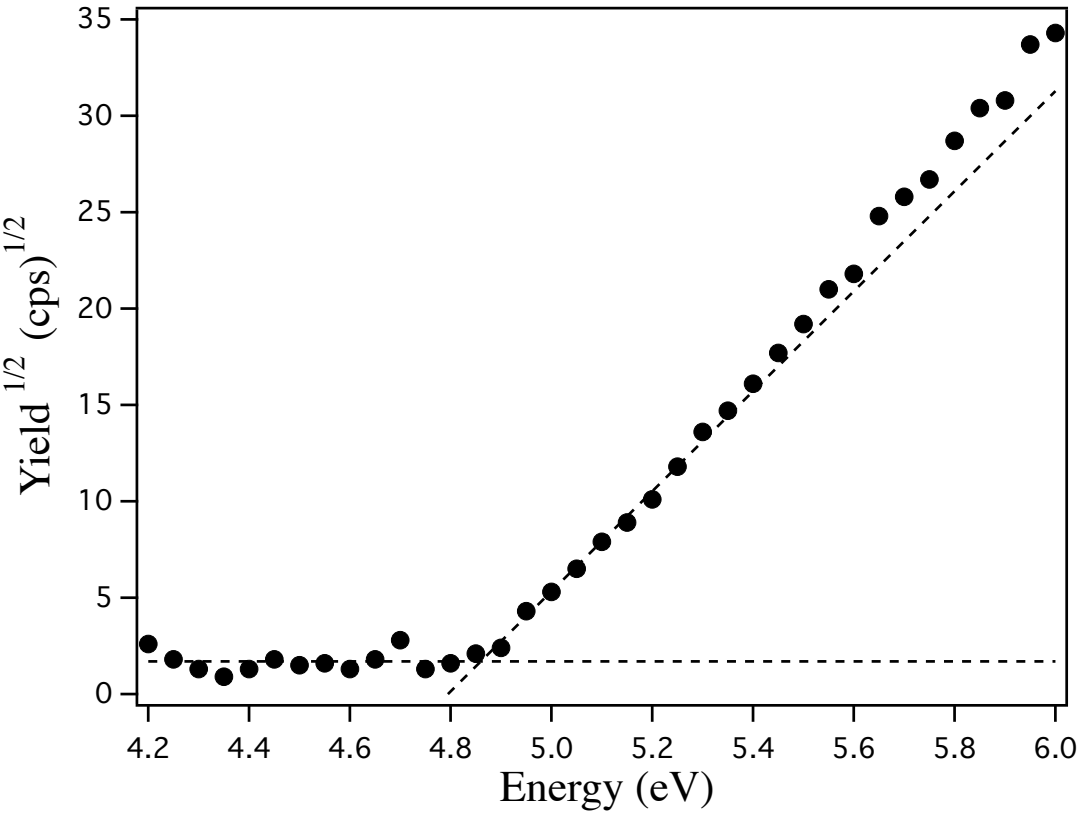

Figure 2.9. Graph of square root of photoemission yield vs. photon energy of a methyl-terminated Si(111) sample

Figure 2.10 shows the AFM topographical images of the methyl-terminated Si sample. The images show stair-like structure, which is similar that of a Si-H (Figure 1.4 Chapter 1). The stair-like structure of Si-H was preserved even after grafting. This indicates that the methylated silicon surface also has an atomically flat structure, similar to that of a Si-H surface. The atomically flat structure of the methylated surface can be the consequence of the perpendicular orientation of the methyl group with respect to the Si(111) plane and it having a van der Waal radius that is smaller than the Si(111) spacing. With these characteristics, the overlapping of methyl groups on the Si(111) surface is avoided, thus the methyl film could copy the surface topology of the Si(111) surface. To

note, the Si-C bonds, which are sp^3-hybridized, should position the methyl groups perpendicular to the Si(111) plane (Webb et. al., 2006).

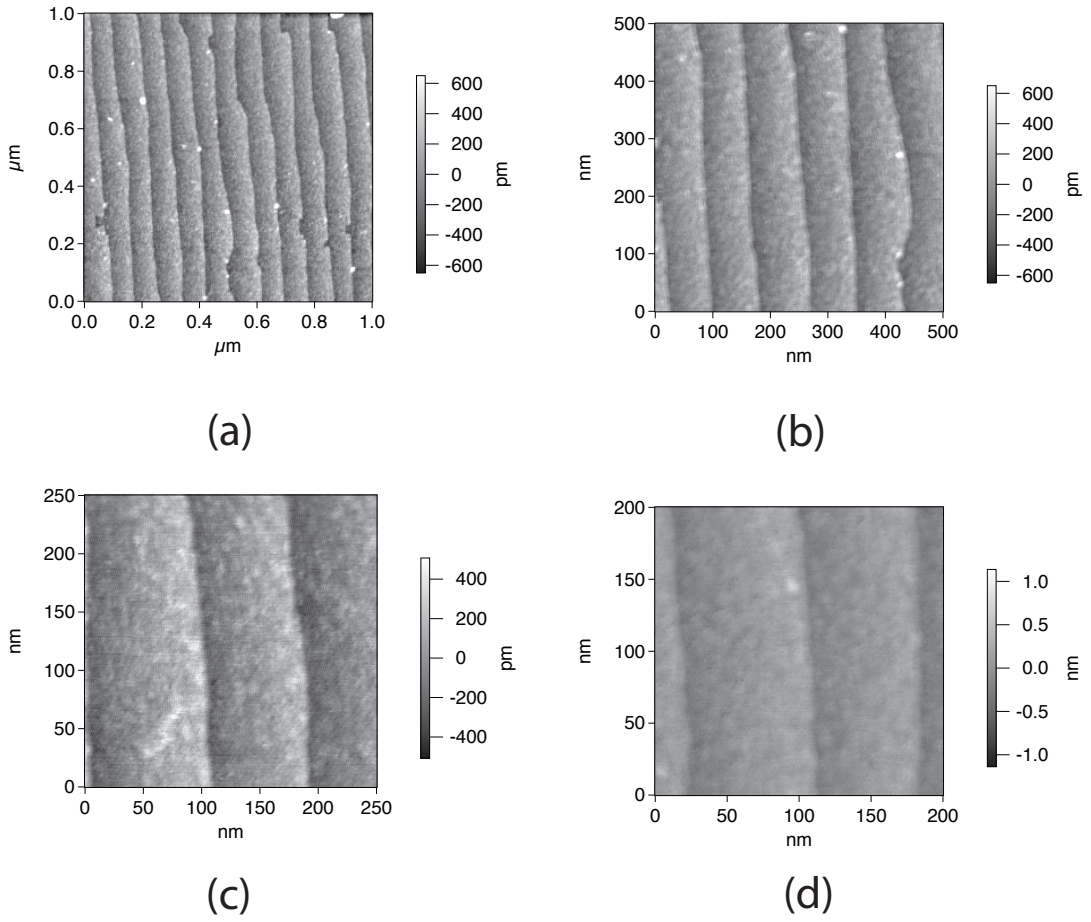

Figure 2.10. AFM images of the methyl-terminated Si(111) showing different scan sizes: (a) 1 μm x μm, (b) 500 nm x 500 nm, (c) 250 nm x 250 nm and (d) 200 nm x 200 nm.

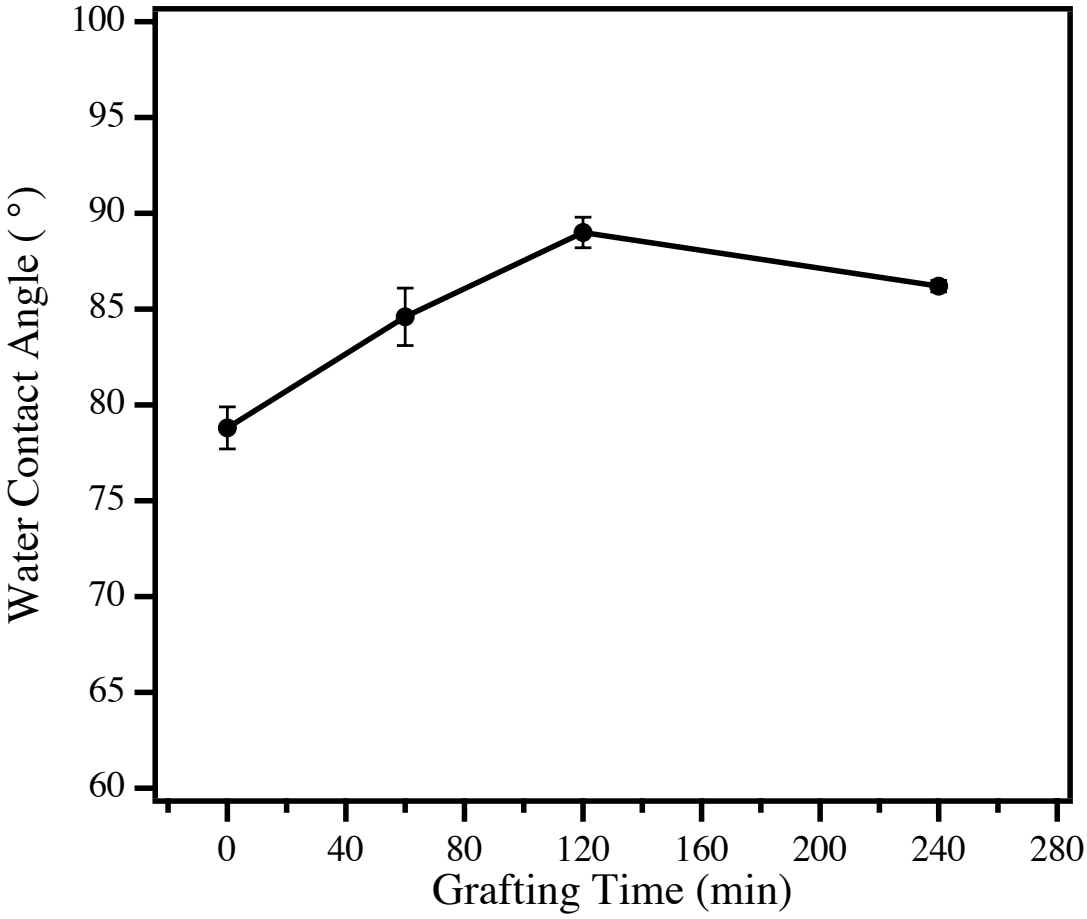

Figure 2.11. Grafting time vs. water contact angle of n low Si-H that underwent photochemical preparation using 200 mW · cm^{-2} illuminations.

A methyl-terminated silicon surface is hydrophobic. Its hydrophobic nature is seen in its high water contact angle. Figure 2.11 shows the graph of water contact angle as function of grafting time. As grafting time increases to 120 min, the water contact angle increases to 89.0 ± 0.8°. This increase is attributed to the increase in surface coverage of grafted methyl groups. However, when the grafting time is further increase to 240 min, the value of water contact angle fell to 86.2 ± 0.3°. The long time of exposing the sample with visible light may have degrading effect to the hydrophobicity of the grafted methyl groups.

2.3.5. Infrared Spectroscopy profile of the methyl-terminated Si samples

Figure 2.12 shows the ATR-FTIR of a hydrogen-terminated Si with n-type substrate that underwent photochemical grafting process under 600 mW · cm^{-2} illumination for 210 min. The graph's vertical axis is in ΔI/I, where "I" is the ATR signal of a Si-H sample that served as the reference. For presentation purposes, the graph is divided into three regions: (1) 700-1800 cm^{-1} (Figure 2.12a), 1800-2700 cm^{-1} (Figure 2.12b), and 2700-3050 cm^{-1} (Figure 2.12c). The symbols "||" (parallel) and "⊥" (perpendicular) in the graph signify the IR vibration direction, in which the reference position is the Si surface. Table 2.5 summarizes the different peaks of the ATR-FTIR profile.

The high peak of the ATR-FTIR profile at around 1255 cm^{-1} (Figure 2.12a), is attributed to the presence of C-H symmetric bending/deformation mode ($\delta_s(CH_3)$) or Si-CH_3 umbrella mode (Amy et. al., 2007; Fidelis et. al., 2000; Ferguson and Raghavachari, 2006; Webb et. al., 2006). This mode is perpendicular to the Si surface. Meanwhile, the FTIR signal from CH_3 rocking mode ($\rho(CH_3)$) (which is located at 751 cm^{-1}) is very weak. This mode is parallel to the Si surface. The peaks located at around 2958 and 2908 cm^{-1} in Figure 2.12c are associated with the asymmetric ($\nu_a(CH_3)$) and symmetric ($\nu_s(CH_3)$) stretching of CH_3, respectively. On the other hand, the peaks at 2928 and 2854 cm^{-1} are attributed with the CH_2 asymmetric ($\nu_a(CH_2)$) and symmetric ($\nu_s(CH_2)$) stretching modes, respectively. The presence of these peaks could be due organic contaminations that cling on the surface during the photochemical preparation. These impurities are suspected to cause the asymmetry in the C 1s spectra (Figure 2.5). These CH_2 infrared peaks are also presence in other methyl-terminated surfaces (Amy et. al., 2007; Webb et. al., 2006). The

stretching mode of the Si-H bonds (ν(Si-H)) is manifested as a negative peak at around 2082 cm^{-1} (Figure 2.12c). The "negative" signifies that this peak is initially present in the hydrogen-terminated Si but diminished during the photochemical grafting process.

Table 2.5. ATR-FTIR spectra peaks of the methyl-terminated Si(111)

Symbol	Mode	Wavenumber (cm^{-1})	∥ or ⊥ to the Si surface
$\nu_a(CH_3)$	Asymmetric stretching (CH_3)	2958	∥
$\nu_a(CH_2)$	Asymmetric stretching (CH_2)	2928	
$\nu_s(CH_3)$	Symmetric stretching (CH_3)	2908	⊥
$\nu_s(CH_2)$	Symmetric stretching (CH_2)	2854	
ν(Si-H)	Stretching (Si-H)	2082	⊥
$\delta_s(CH_3)$	Symmetric bending (CH_3)	1255	⊥
ρ (CH_3)	Rocking (CH_3)	751	∥

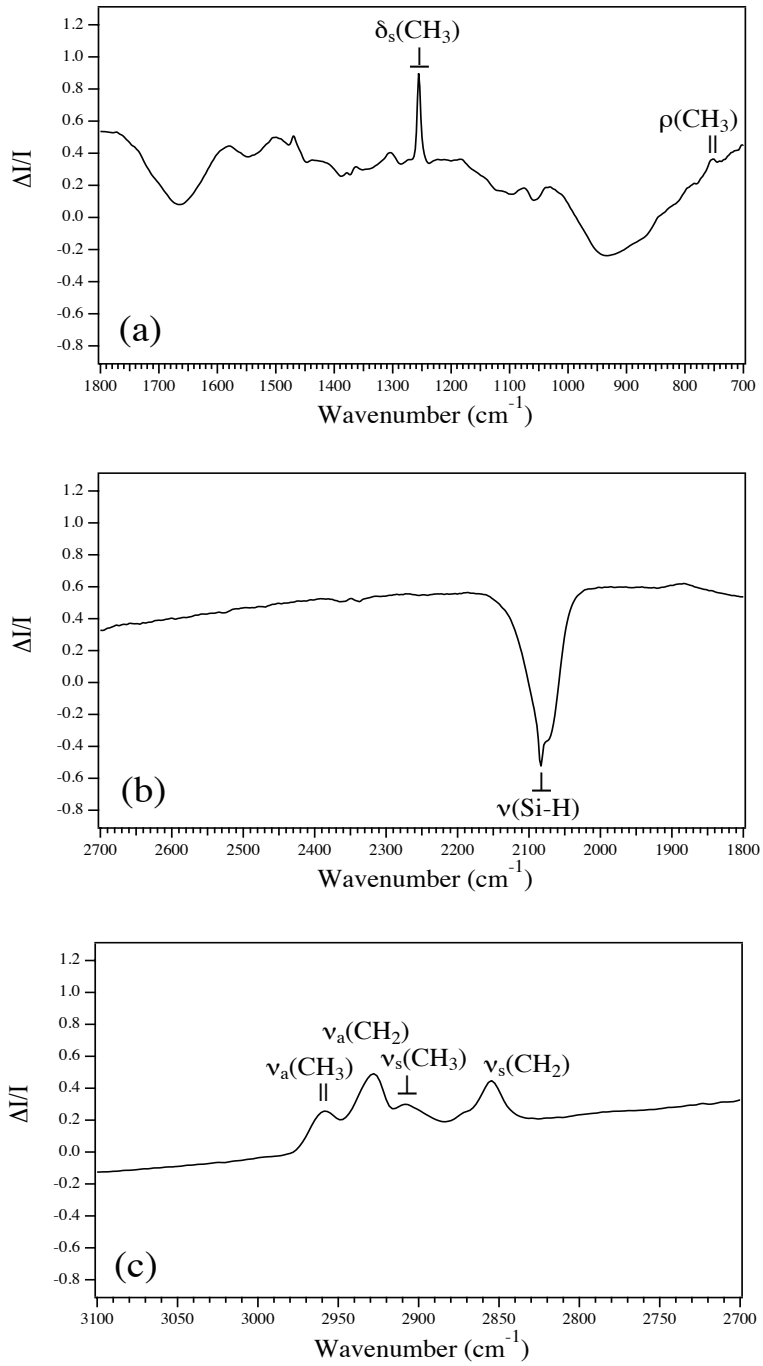

Figure 2.12. ATR-FTIR of a methyl-terminated Si(111) that was prepared using photochemical grafting technique

2.4. Summary and Conclusion

Photochemical preparation of methyl-terminated Si(111) was successfully done on an n-type substrate using Grignard reagent. ATR-FTIR spectrum confirms the presence of a methylated Si surface. It shows the presence of high intensity peak at around 1255 cm^{-1}, which is attributed to the presence of Si-CH_3 umbrella mode. The success of producing methylated Si surface on n-type substrate shows the ability of photogenerated holes to trigger the oxidative decomposition of Grignard reagent, which promotes the methyl grafting process. The dependence of the methylation process on illumination-induced holes makes the grafting process highly influenced by illumination intensity and by the doping concentration of the substrate. In such, the rate of methyl grafting increases with the use of high illumination intensity and the use of substrate with low dopant concentration. The Si surface that is terminated with methyl groups had atomically flat structure and is hydrophobic. The methylated surface also has lower electron affinity compare to the bulk Si.

References

1. S. R. Amy, D.J. Michalak, Y.J. Chabal, L. Wielunski, P.T. Hurley, N.S. Lewis: *J. Phys. Chem. C*. **2007.** 111. 13053.
2. A. Bansal, X. Li, S.I. Yi, W.H. Weinberg, N.S. Lewis: *J. Phys. Chem. B*. **2001.** 105. 10266.
3. R. Boukherroub, S. Morin, F. Bensebaa, D.D.M. Wayner: *Langmuir*. **1999.** 15. 3831.
4. R. Boukherroub: *Current Opinion in Solid State and Materials Science*. **2005.** 9. 66.
5. J.M. Buriak: *Chemical Reviews*. **2002.** 102. 1271.
6. R.L. Cicero, M.R. Linford, C.E.D. Chidsey: *Langmuir.* **2000.** 16. 5688.
7. S. Fellah, R. Boukherroub, F. Ozanam, J.-N. Chazalviel: *Langmuir.* **2004.** 20. 6359.
8. S. Fellah, A. Teyssot, F. Ozanam, J.-N. Chazalviel, J. Vigneron, A. Etcheberry: *Langmuir.* **2002.** 18. 5851.
9. A. Fidelis, F. Ozanam, J.-N. Chazalviel: *Surface Science*. **2000.** 444. L7.
10. G.A. Ferguson, K. Raghavachari: *The Journal of Chemical Physics*. **2006.** 125. 154708.
11. T. He, H. Ding, N. Peor, M. Lu, D.A. Corley, B. Chen, Y. Ofir, Y. Gao, S. Yitzchaik, J.M. Tour: *J. Am. Chem. Soc*. **2008.** 130. 1699.
12. R. Hunger, R. Fritsche, B. Jaeckel, W. Jaegermann, L.J. Webb, N.S. Lewis: *Phys. Rev. B*. **2005.** 72. 045317.
13. R. Hunger, R. Fritsche, B. Jaeckel, L.J. Webb, W. Jaegermann, N.S. Lewis: *Surface*

Science. **2007.** 601. 2896.

14. M. R. Linford, C.E.D. Chidsey: *J. Am. Chem. Soc*. **1993.** 115. 12631.

15. M.R. Linford, P. Fenter, P.M. Eisenberger, C.E.D. Chidsey: *J. Am. Chem. Soc*. **1995.** 117. 3145.

16. T. Miyadera, A. Koma, T. Shimada: *Surface Science*. **2003.** 526. 177.

17. E. J. Nemanick, S. D. Solares, W. A. Goddard III, N. S. Lewis: *J. Phys. Chem. B*. **2006.** 110. 14842

18. R. Okada, T. Miyadera, T. Shimada, A. Koma, K. Ueno, K. Saiki: *Surface Science*. **2004.** 552. 46.

19. H. Sano, M. Zhao, D. Kasahara, K. Murase, T. Ichii, H. Sugimura: *Journal of Colloid and Interface Science*. **2011.** 361. 259.

20. A. B. Sieval, A.L. Demirel, J.W.M. Nissink, M.R. Linford, J.H. van der Maas, W.H. de Jeu, H. Zuilhof, E.J.R. Sudholter: *Langmuir.* **1998.** 14. 1759.

21. A.B. Sieval, R. Opitz, H.P.A. Maas, M.G. Schoeman, G. Meijer, F.J. Vergeldt, H. Zuilhof, E.J.R. Sudholter: *Langmuir.* **2000.** 16. 10359.

22. Q.-Y. Sun, L.C.P.M. de Smet, B. van Lagen, M. Giesbers, P.C. Thune, J. van Engelenburg, F.A. de Wolf, H. Zuilhof, E.J.R. Sudholter: *J. Am. Chem. Soc*. **2005.** 127. 2514.

23. S.M. Sze, K.K. Ng: *Physics of Semiconductor Devices, 3rd ed*. John Wiley & Sons: New Jersey, **2007.**

24. S. Takakusagi, T. Miyasaka, K. Uosaki: *J. of Electroanalytical Chemistry*. **2007.** 599. 344.

25. L. Touahir, P. Allongue, D. Aureau, R. Boukherroub, J.-N. Chazalviel, E. Galopin, A.C. Gouget-Laemmel, C.H. de Villeneuve, A. Moraillon, J. Niedziolka-Jonsson, F. Ozanam, J.S. Andresa, S. Sam, I. Solomon, S. Szunerits: *Bioelectrochemistry*. **2010.** 80. 17.

26. I. Waluyo, H. Ogasawara, M. Kawai, A. Nilsson, T. Yamada: *J. Phys. Chem. C*. **2010.** 114. 19004.

27. L.J. Webb, N.S. Lewis: *J. Phys. Chem. B*. **2003.** 107. 5404

28. L. J. Webb, S. Rivillon, D.J. Michalak, Y.J. Chabal, N.S. Lewis: *J. Phys. Chem. B*. **2006.** 110. 7349.

29. T. Yamada, M. Kawai, A. Wawro, S. Suto, A. Kasuya, *A. J. of Chem. Phys*. **2004.** 121. 10660.

30. H. Yu, L.J. Webb, R.S. Ries, S.D. Solares, W.A. Goddard, J.R. Heath, N.S. Lewis: *J. Phys. Chem. B*. **2005.** 109. 671.

31. H. Yu, L.J. Webb, J.R. Heath, N.S. Lewis: *Appl. Phys. Lett*. **2006.** 88. 252111.

Chapter 3
Effect of Grafting Medium on the Photochemical Grafting of Ferrocenyl groups on Si(111) Surface

3.1. Introduction

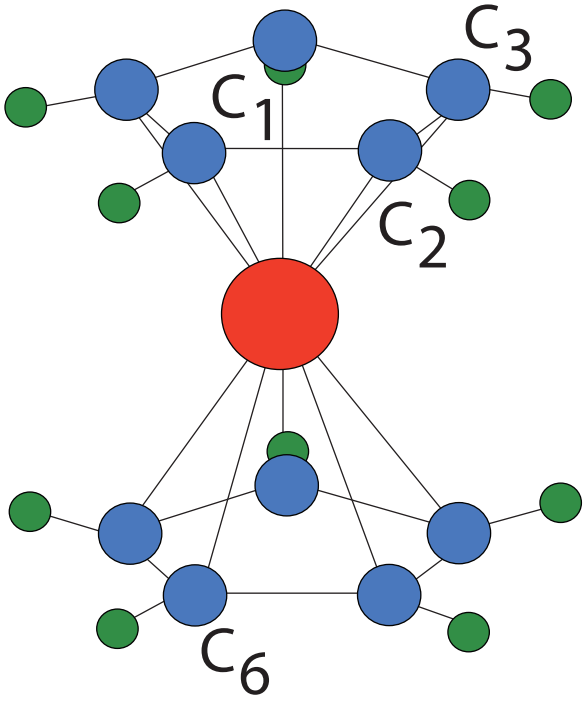

Figure 3.1. Molecular structure of ferrocene (Based from the illustration of Bohn and Haaland, 1966). (Blue circles : carbon, green circles : hydrogen, red circle : iron)

Figure 3.1 shows a ferrocene or bis(cyclopentadienyl)iron(II) or $Fe(C_5H_5)_2$. Ferrocene (Fc) is an organometallic compound with two cyclopentadienyl anions rings sandwiching one Fe(II) cation. The blue circles in the figure represent carbon atoms, the green circles represent hydrogen atoms and the one red circle represents an iron atom. The distance between C_1 to C_6 is 3.3 Å (Bohn and Haaland, 1966). The C-C (C_1 to C_2) bond

distance within the rings is 1.40 Å while the Fe-C bond is 2.04 Å (Eckermann, et. al, 2010). The iron in the ferrocene has two stable and reversible oxidation states. It can change from +2 (neutral ferrocenyl) to +3 (charged ferrocenyl) upon the introduction of positive potential and vice-versa when grounded. A neutral ferrocene measures (4.1x 3.3) Å and is orange in color and it expands to (4.1 x 3.5) Å and changes its color to blue when oxidized (Eckermann, et. al, 2010).

Ferrocenyl layers on silicon or silicon oxide have been eyed for the construction of memory devices (Fabre, 2010; Li et. al., 2002; Li et. al., 2003; Roth et. al., 2003). Fc can act as memory elements, in which the two reversible and stable oxidation states of its Fe atom can correspond to the memory bit "0" and "1".

Several linkers have been used to connect the ferrocene groups with either the Si surface or silicon oxide (Fabre, 2010; Li et. al., 2002; Li et. al., 2003; Roth et. al., 2003; Ciampi, et. al., 2009; Ciampi et. al., 2008; Cossi et. al., 2006; Dalchiele et. al., 2005; Lu, et. al. 2008; Marrani et. al. 2009). However, if the thinnest possible monolayer is desired, the use of vinylferrocene (VFc), as a precursor, is advantageous because it can connect the Si surface and the Fc with just one ethyl unit.

The grafting of VFc molecules to the Si surface may involve some challenges. Grafting may induced damage on the Fc or may produce unwanted by-products. The unwanted by-product may even distort the electrochemical characteristics of the grafted ferrocenyl groups. Thus, the careful choice of grafting method and its parameters are very important.

The attachments of molecules on semiconductor surface have been topic of different researches (Amy et. al., 2007; Bansal et. al., 2001; Boukherroub et. al., 1999;

Boukherroub, 2005; Buriak, 2002; Cicero, et. al. 2000; Fellah et. al., 2002; Fellah, et. al., 2004; Fidelis et. al. 2000; Hunger et. al., 2005; Hunger et. al., 2007; Linford and Chidsey, 1993; Linford et. al., 1995; Miyadera et. al., 2003; Okada et al., 2004; Sieval et. al., 1998; Sieval et. al., 2000; Sun et. al., 2005; Takakusagi et. al., 2007; Touahir et. al., 2010; Waluyo et. al., 2010; Webb and Lewis, 2003; Webb et. al., 2006; Yamada et. al.; 2004, Yu et. al., 2005, Yu et. al., 2006). Several methods have been employed in grafting molecules onto the silicon surface. Each method has its own advantages and disadvantages. One technique used in grafting is the use of visible light. Grafting using visible light is a mild method, compared with the use of UV and the use of high thermal energy that could possibly induced damage on the grafted organic molecules (e.g. vinylferrocene). With this, it is our aim to attach ferrocenyl groups on Si(111) surface at room temperature using visible light as grafting initiator.

The photochemical technique employed by Sano, et. al. (2011) used a simple one-step self-assembled monolayer formation process involving the use of n-decane as grafting medium. In terms of the physical and electrochemical characteristics of the resulted products, they have shown that the use of visible light is advantageous than the use of thermal method.

Many technical challenges face the construction of an electronic device from SAM. In such, the properties of SAM (e.g., electrical, physical) should be attuned to the processes in which it may undergo to become a device (e.g., its surface adheres with other surfaces, Si surface inhibits oxidation during the subsequent processes of constructing a device). Making a mixed monolayer (Bain, 1989; Chen, 2002; Folkers, 1992; Frederix, 2003; Hobara, 2002; Laibinis, 1992; Offord, 1994; Ostuni, 2003, Shimazu, 2002; Stranick,

1994; Tamada, 1997; Tong, 2011) by grafting other substance is a possible technique to tune its properties. However, the creation of mixed monolayer using a technique that involves mixed reaction must use a grafting medium that would allow the immobilization of all intended substances on the substrate's surface. The identification of other grafting media (besides n-decane) for the Fc immobilization process would be advantageous because this would make the process more flexible and more adaptable to different situations.

The choice of grafting medium may influence the nature of the grafted substance. It is the reservoir of the precursor molecules and passageway of light from the light source to the sample. The interface between the grafting solution and the hydrogenated Si sample would be filled with photogenerated charges when illuminated. This condition may trigger reactions that could affect the quality of the final product.

The success in identifying grafting media that would be compatible in accommodating Grignard reagent will widens the numbers of possible substance that can be immobilized with the ferrocenyl moiety in a mixed monolayer. Grignard reagents are precursor molecules in grafting alkyl group on Si (Bansal 2001, Fellah, 2002, Fellah, 2004, Fidelis, 2000, Hunger, 2005, Hunger, 2007, Miyadera, 2003, Okada, 2004, Takakusagi, 2007, Waluyo, 2010, Webb, 2006, Yamada, 2004, Yu, 2005, Yu, 2006). Some of the solvents of Grignard reagents are (1) tetrahydrofuran (THF), (2) diethyl ether, and (3) dibuyl ether. The success of using these solvents in grafting VFc molecules on Si surface opens the possibility of immobilizing alkyl groups with the ferrocenyl moiety. The insulating nature of immobilized alkyl group on Si makes them candidate materials for tuning the properties of Fc-terminated Si, without distorting much its electrochemical

properties. Alkyl could also form Si-C bonds with the Si surface that can minimize the formation of silicon oxide. It can also function as insulating barrier between ferrocenyl moieties (or clusters of ferrocenyl moities). The building of dielectric barrier between a ferrocenyl moiety (or its cluster) from other moities (or from other clusters) is crucial in building memory cell on the Si surface.

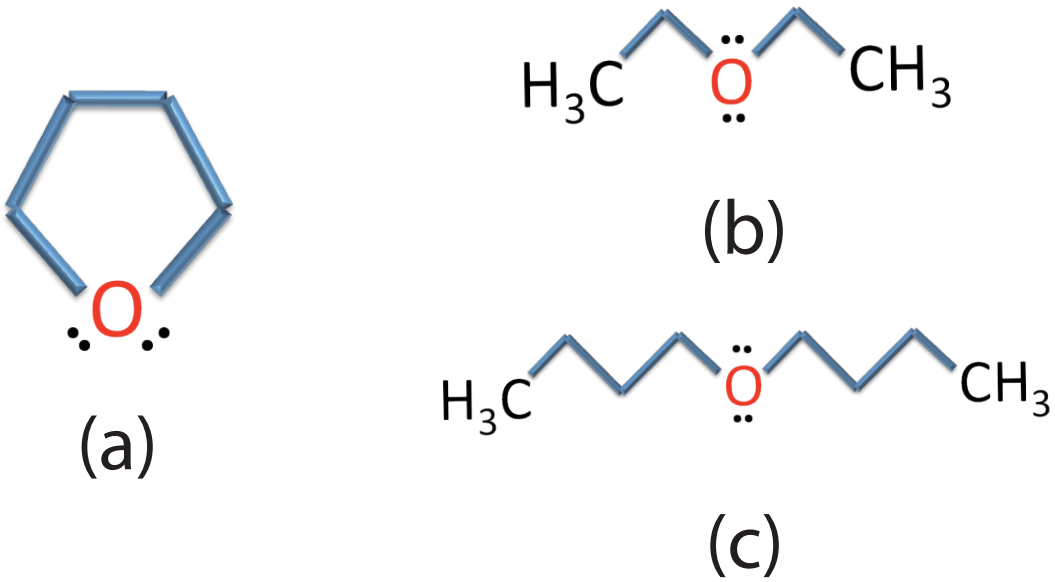

Figure 3.2. Grafting media that were used in the experiment

Table 3.1. Characteristics of grafting media that were used in the experiment

Parameter	THF	Diethyl ether	Dibutyl ether
Molecular Formula	C_4H_8O	$C_4H_{10}O$	$C_8H_{18}O$
Boiling point (°C)	65°C (volatile)	34°C (volatile)	140.84°C (less volatile)
Polarity	Polar	Less polar	Less polar

We will use three media for grafting ferrocenyl groups on Si(111) surface (Figure 3.2), they are (1) tetrahydrofuran (THF), (2) diethyl ether, and (3) dibuyl ether. All of these media are solvent of Grignard reagent. Table 3.1 shows some of their characteristics. Both tetrahydrofuran and diethyl ether are volatile; their boiling point is 65°C and 34°C, respectively. The use of these media would require additional procedure to compensate for the solvent, which would have been lost during the grafting process, because of their volatility. On the other hand, dibutyl ether is less volatile, thus, the use of this medium would be less difficult (in terms of procedure) compare to use of THF or of diethyl ether.

The main objective of this research is the determine the effects of grafting media (tetrahydrofuran, diethyl ether, and dibuyl ether) on the photochemical grafting of ferrocenyl groups on Si(111) surface.

3.2. Methodology

3.2.1. Hydrogen-termination process

The following kinds of substrates were used in this experiment: (1) Phosphorus-doped Si with resistivity of 1-10 Ω cm (n Si), and (2) Boron-doped Si with

resistivity of 1-30 Ω cm (p Si). The terms "n" and "p" indicate n-type and p-type, respectively.

A cut wafer was cleaned ultrasonically with ethanol and with ultrapure water, respectively, for 20 min each. It was then cleaned electrochemically by exposing it to vacuum ultraviolet from a xenon excimer lamp (172 nm, 10 $mW \cdot cm^{-2}$) for 20 min to remove the organic contaminants. The removal of native silicon oxide and H-termination process was done by immersing the cleaned Si(111) in a 5%-HF solution at room temperature for 1 min. It was also immersed in a 40%-NH_4F solution in an 80 °C water bath for 30 s to removed the dissolved oxygen. However, for the samples that would be grafted in diethyl ether or dibutyl ether, the immersion time was increased to 1 min. The hydrogen-terminated sample was dried using stream of nitrogen.

3.2.2. Photochemical grafting

The photochemical preparations were done by irradiating a hydrogen-terminated Si(111), which is immersed in a solvent-vinylferrocene solution, with visible light. The solvent (tetrahydrofuran, diethyl ether or dibutyl ether) serves as the grafting medium. The visible light comes from a xenon lamp device (Asahi Spectra Co., Ltd., Max 1000) with detachable optical filters and controllable light intensity. The spectrum of the visible light that was used is shown in Figure 2.4 (Chapter 2). The solvent-vinylferrocene solution was prepared by mixing vinylferrocene precursor powder with the solvent so that the concentration was 10 mM. The initial volume that was used for both the tetrahydrofuran-vinylferrocene and the dibutyl ether-vinylferrocene solutions were 40 mL while the initial volume for diethyl ether-vinylferrocene solution was 80 mL. The solution

was placed inside a quartz optical cell and undergone nitrogen bubbling before and during the grafting process. For the tetrahydrofuran-vinylferrocene solution, a reservoir bottle filled with tetrahydrofuran was placed along the nitrogen line to compensate for the liquid that would be lost during the nitrogen bubbling process due to the volatility of the liquid. For the diethyl ether-vinylferrocene solution, aside from placing a reservoir bottle filled with diethyl ether, the addition of extra diethyl ether was done to prevent the grafting solution from drying. However, since dibutyl ether was less volatile, no additional method or set-up was done.

3.2.3. Post-cleaning treatment

After the photochemical grafting process, the sample was rinsed with the solvent (e.g. for the sample that was immersed in THF-vinylferrocene solution, it was rinsed with THF). After which, it was cleaned ultrasonically with ethanol and with ultrapure water, respectively for 10 min each. The sample was dried using streams of nitrogen.

3.2.4. Characterizations

X-ray photoelectron spectroscopy (XPS) was done using an XPS system (Kratos Analytical Ltd., ESCA-3400). Using the XPS system, the Fe 2p, the O 1s, the C 1s and the Si 2p spectra of the samples were measured. The source of the X-ray was MgKα. The X-ray source is working at an emission current of 10 mA and an acceleration voltage of 10 kV. Step size of 0.1 eV was used for the XPS scan. For the Fe 2p spectra, the scan was repeated 30 times while for the other spectra, they were repeated 10 times. Based from the spectra that were obtained, XPS quantitative analysis was done using the built-in software

to determine the iron atomic percent (Fe at%), the oxygen atomic percent (O at%), the carbon atomic percent (C at%) and the silicon atomic percent (Si at%).

The thicknesses of the deposited film were measured using a spectroscopic ellipsometer. The "air-VFc film-Si" model was used in the analysis of thickness. However, in the absence of the true value of the VFc film's refractive index, the refractive index of silicon oxide was used as substitute. With this, the measured film thicknesses were not absolute values.

The surface topographical images of the sample were obtained using an atomic force microscope (Asylum Research, MFP-3D-SA AFM) in AC mode using an aluminum-backside coated Si (SII NanoTechnology Inc., SI-DF20) as probe.

The cyclic voltammetry measurements were done using a three-electrode setup that is connected to an electrochemical analyzer at room temperature. A 0.1 M $HClO_4$ solution serves as the electrolyte. The sample serves as the working electrode while a platimum coil serves as the counter electrode. An Ag/AgCl electrode, which was immersed in 3.0 M NaCl, serves as the reference electrode.

3.3. Results and Discussion

Table 3.2 shows the three types of sample that were prepared. For simplicity the term "THF-prepared sample", "Diethyl ether-prepared sample" and "Dibutyl ethyl-prepared sample" will be used to refer the samples as indicated in Table 3.2.

Table 3.2. Different samples that were prepared

Term	Description
(a) THF-prepared sample	Sample that was prepared using tetrahydrofuran as grafting medium
(b) Diethyl ether-prepared sample	Sample that was prepared using diethyl ether as grafting medium
(c) Dibutyl ether-prepared sample	Sample that was prepared using dibutyl ether as grafting medium

3.3. 1. Tetrahydrofuran-prepared samples

The samples that was photochemically prepared in tetrahydrofuran-vinylferrocene solution yielded degraded, oxidized and polymerized grafted structures on the Si(111) surface.

Table 3.3. XPS Quantitative analysis, ellipsometric thickness and C/Fe

Grafting time	Fe at%	O at%	C at%	Si at%	Thickness (nm)	C/Fe
0	0	6.8	5.7	87.4	--	--
2	0.4	12.2	17.1	70.4	1.84	42.8
4	2.6	21.4	20.4	55.6	4.48	7.8
8	8.4	42.5	34.1	15	16.05	4.1

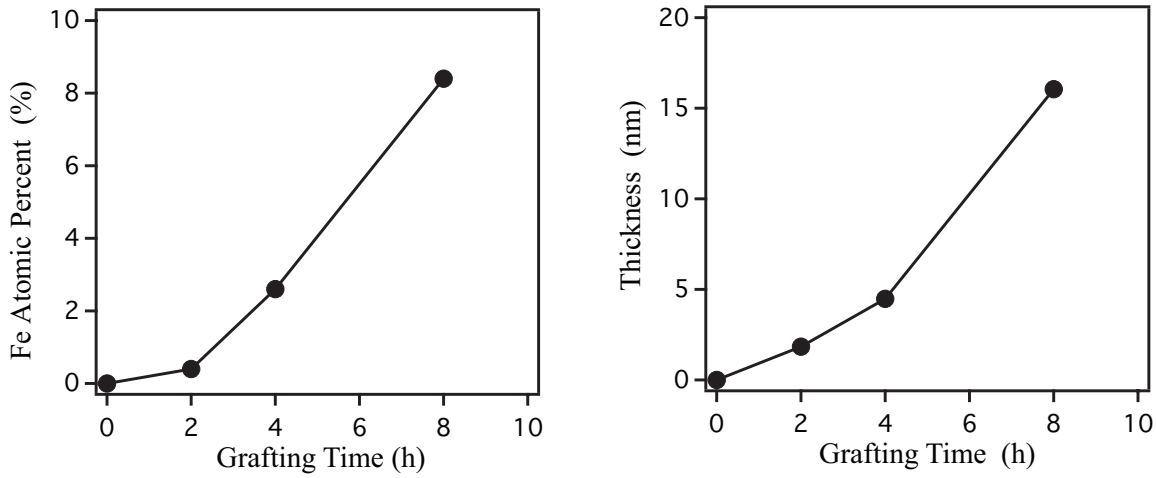

Figure 3.3. Graphs of (a) Fe atomic percent Fe and (b) ellipsometric thickness as a function of grafting time. The samples were n-type H-terminated Si(111) that were irradiated with 200 mW cm^{-2} visible light at different grafting time in THF-vinylferrocene solution.

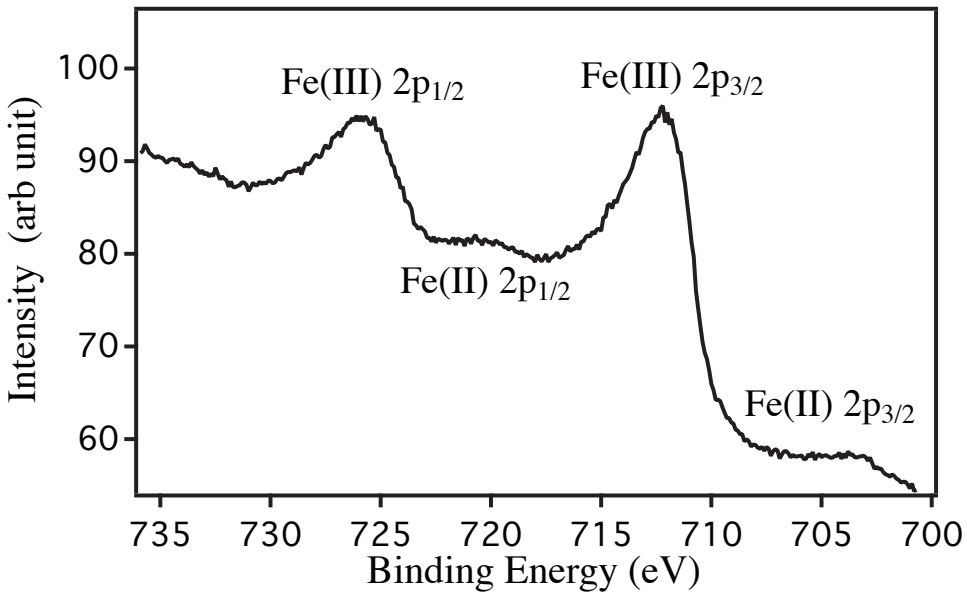

Figure 3.4. Fe 2p spectrum of sample that was irradiated with 200 mW cm^{-2} visible light in THF-vinylferrocene solution.

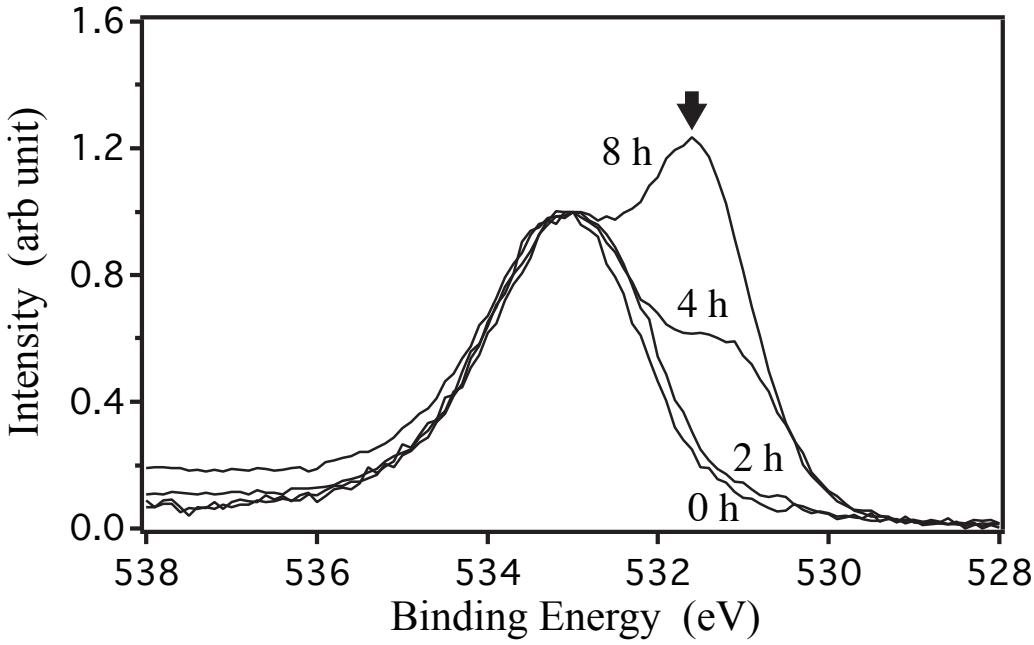

Figure 3.5. O 1s spectra of samples that were irradiated with 200 mW cm^{-2} visible light in THF-vinylferrocene solution at different grafting time.

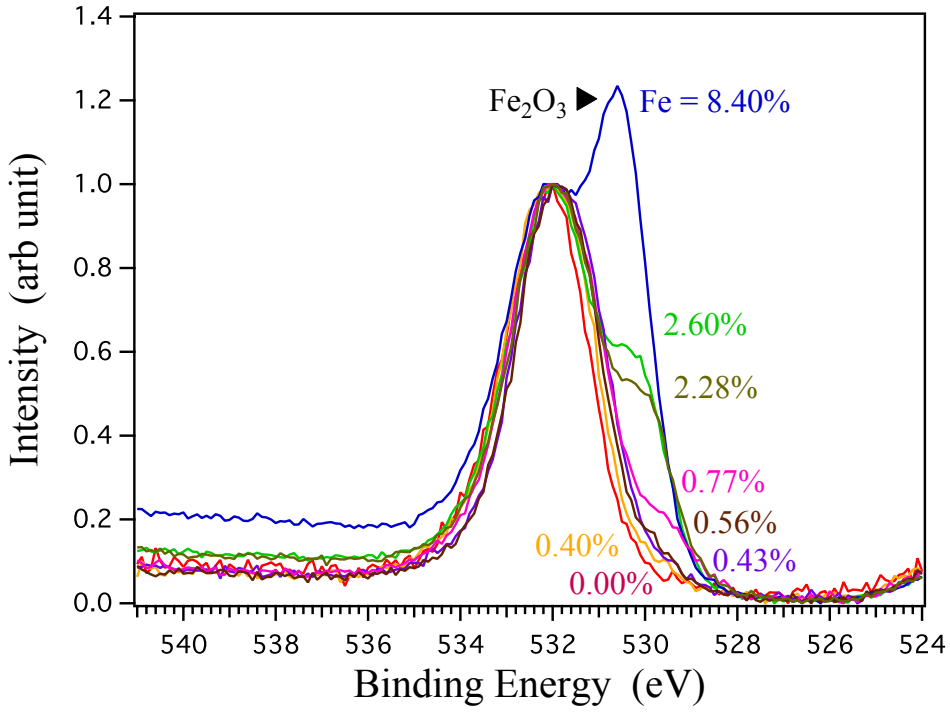

Figure 3.6. Fe atomic percent and O 1s spectra of THF-prepared samples

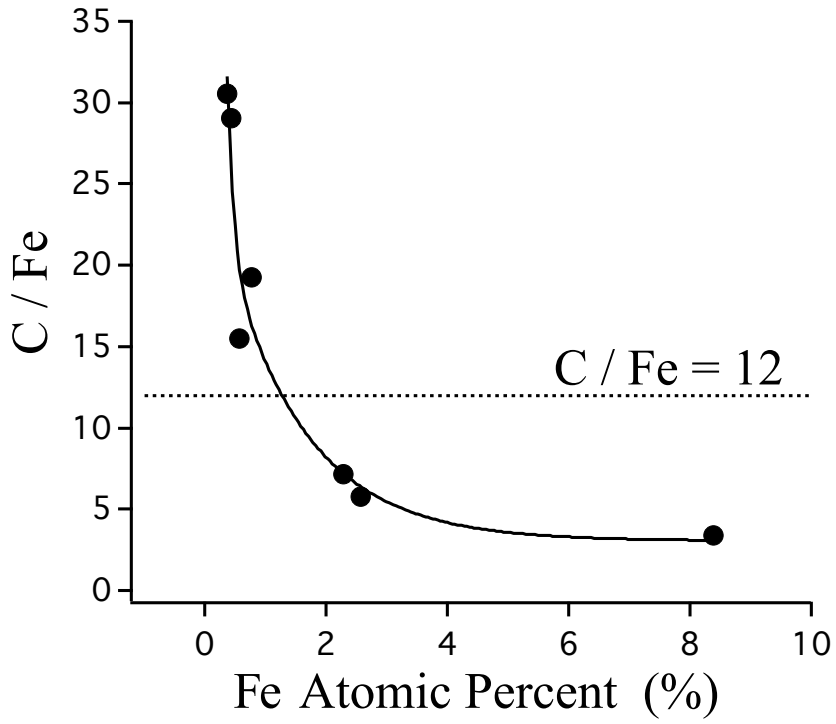

Figure 3.7. Plot of Fe at% vs. C/Fe of THF-prepared samples

The use of THF resulted to the polymerization of the grafted structure on the Si surface. Table 3.3 shows the Fe at%, the O at%, the C at%, the Si at%, the ellipsometric thickness and the C/Fe of the THF-prepared sample. The value of Fe at% is proportional with the amount of grafted ferrocenyl groups on the silicon surface. As shown in Figure 3.3, both the Fe atomic percent and the ellipsometric thickness increase with grafting time. These increases suggest that the grafted structures were polymerized during the photochemical preparation. The values of the Fe at% and the ellipsometric thickness reached as high as 8.4% and 16.05 nm, respectively. These values are too high to be characteristics of ethyl-linked Fc monolayer. The typical values of its Fe at% as result of XPS analysis usually are less than 2% while its ellipsometric thickness is around 2 nm.

The use of THF resulted to the oxidation of the grafted structure. The Fe 2p

spectrum (Figure 3.4) of the sample shows peak at around 725.5 and 712.2 eV, which correspond to Fe(III) $2p_{1/2}$ and Fe(III) $2p_{1/2}$ respectively. The spectrum shows that the Fe oxidation state of the grafted molecules is +3. This is compatible with result of O 1s spectra (Figure 3.5), which reveals the presence of iron oxide (Fe_2O_3). The peak corresponding to the presence of iron oxide increases with grafting time (Figure 3.5) and Fe at% (Figure 3.6).

The grafted polymerized structures were also degraded. The detachment of some carbon atoms from the grafted structures might be a possible reason for low C/Fe ratio. The C/Fe ratio decreases with the increase in grafting time (Table 3.3) and with the increase in Fe at% (Figure 3.7). For ethyl-linked ferrocene-terminated Si, the ideal C/Fe ratio is 12. The higher-than-twelve values of C/Fe ratio at earlier grafting time (lower Fe at%) maybe are due to the presence of carbon-based impurities that adhere on the sample due to absence of grafted organic molecules.

Tetrahydrofuran is a medium that is commonly used for polymerization. The photoinduced charges that were generated during the illumination of light may have served as initiator for the grafting of vinylferrocene monomer onto the silicon surface. However, the tetrahydrofuran might have also facilitated the transfer of charges from the silicon surface to medium itself and to the free end of the grafted monomers to promote reaction with other monomers that leads to its polymerization.

3.3.2. Diethyl ethyl-prepared samples

Table 3.4. XPS quantitative analytical data, ellipsometric thickness and C/Fe of diethyl ether-prepared samples with n-type substrate

Grafting Time (h)	Fe (at%)	O (at%)	C (at%)	Si (at%)	Thickness (nm)	C/Fe
0	0.00	5.61	4.73	89.67	---	---
2	1.05	10.62	26.60	61.73	2.31	25.3
4	1.34	9.57	23.83	65.26	2.64	17.8

Table 3.5. XPS quantitative analytical data, ellipsometric thickness and C/Fe of diethyl ether-prepared samples with p-type substrate

Grafting Time (h)	Fe (at%)	O (at%)	C (at%)	Si (at%)	Thickness (nm)	C/Fe
0	0.00	4.26	4.57	91.17	---	---
2	1.04	11.70	24.27	62.99	2.48	23.3
4	1.37	13.77	19.89	64.97	2.47	14.5

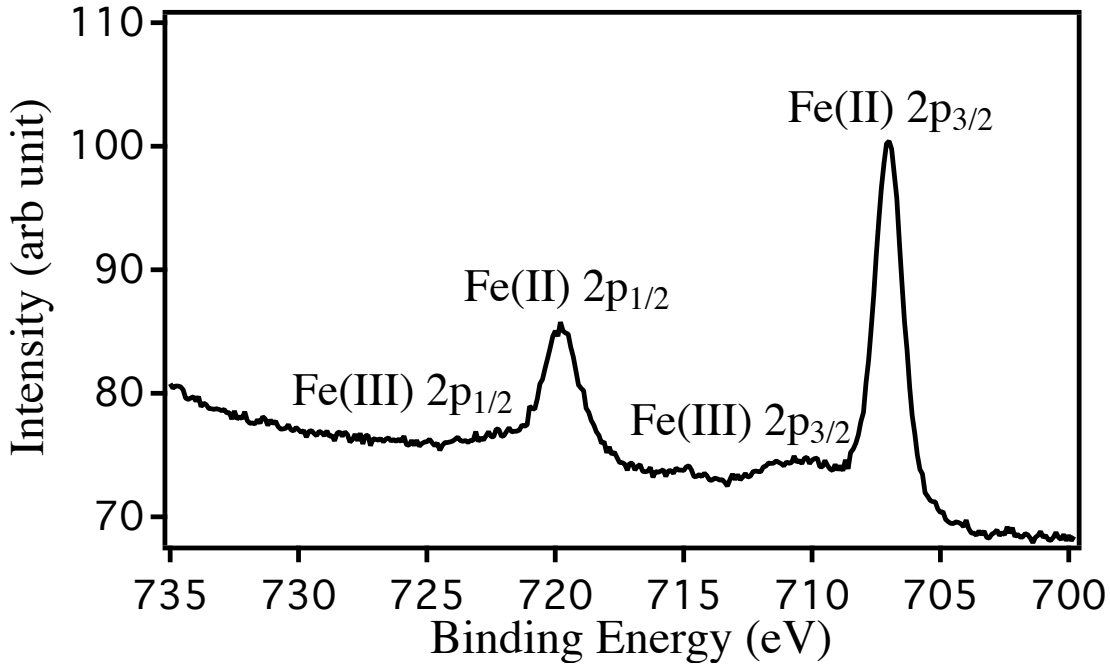

Figure 3.8. Fe 2p spectra of samples irradiated with 400 mW·cm^{-2} visible light in diethyl ether-vinylferrocene solution.

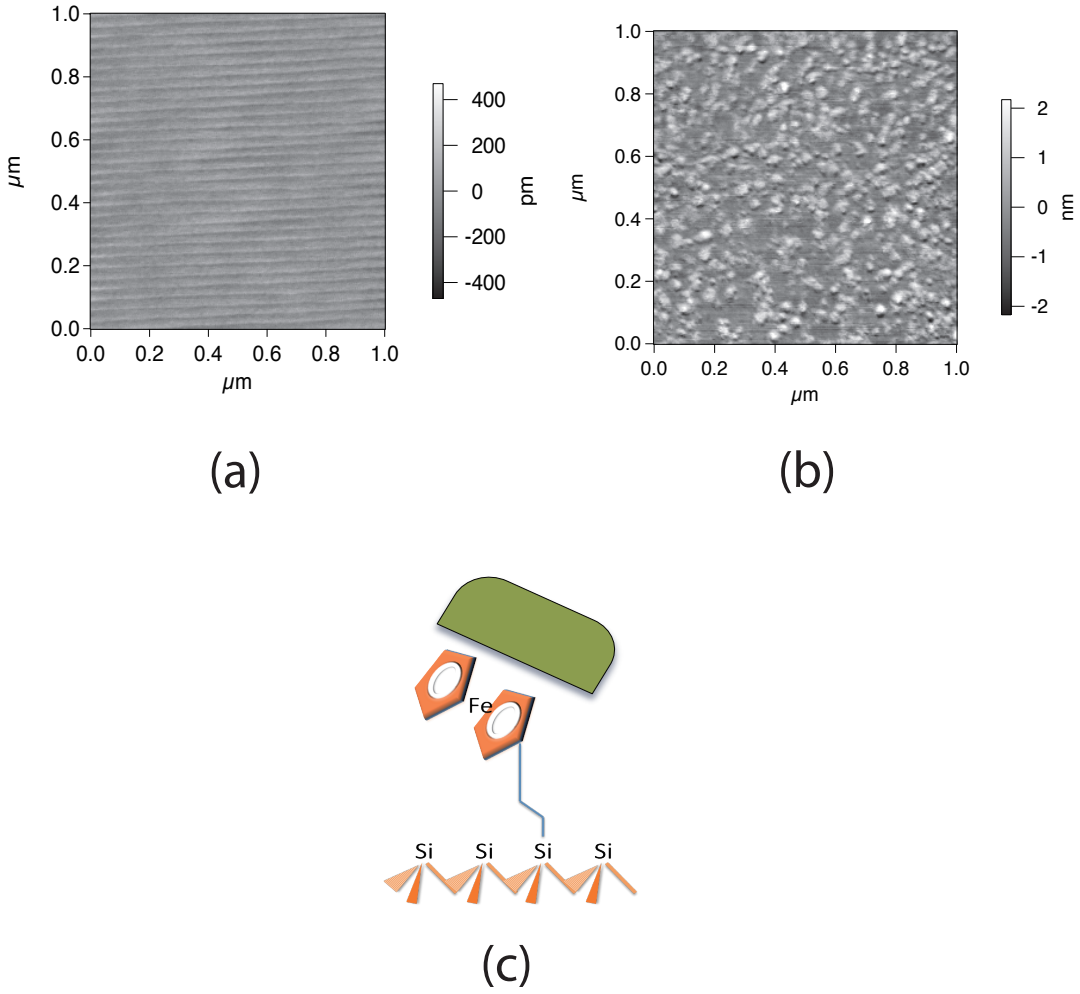

Figure 3.9. AFM topographical images of (a) Hydrogen-terminated Si(111), (b) Si-H sample that was irradiate with 400 mW·cm^{-2} visible light in diethyl ether-vinylferrocene molecules for 4 hrs, and (c) interpretation of the AFM image in Fig 3.9b.

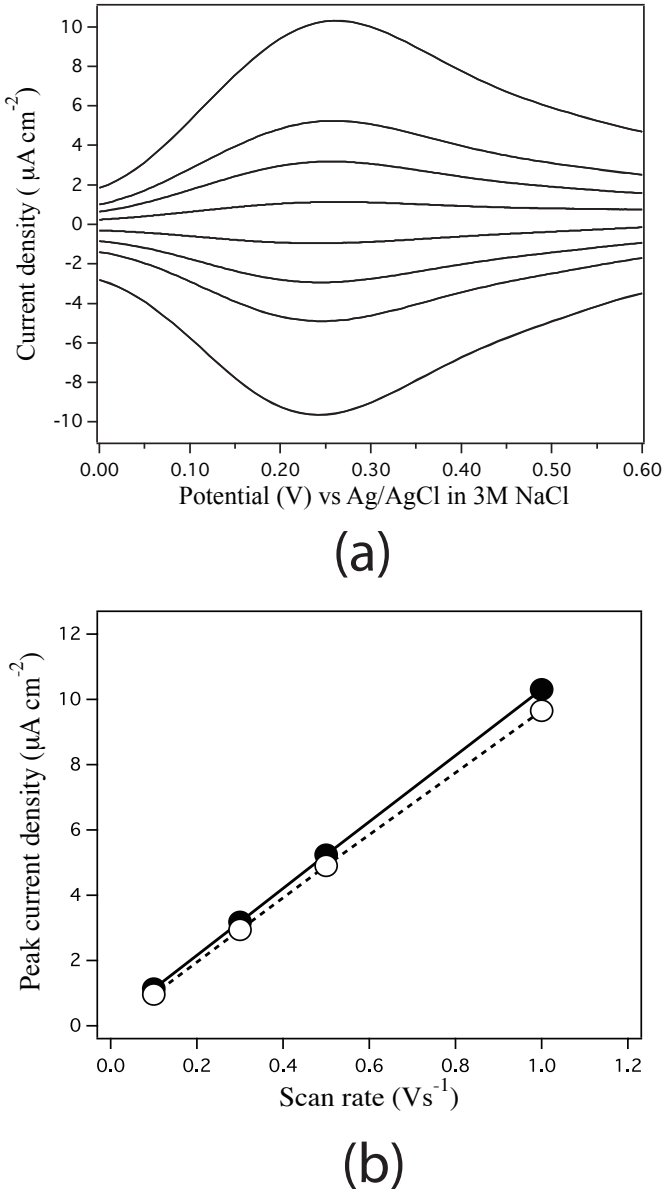

Figure 3.10. (a) Cyclic Voltammmograms of diethyl ether- prepared vinylferrocene-terminated Si(111) on p-type substrate (scan rates are 1, 0.5, 0.3, and 0.1 V/s) and (b) its corresponding graph of scan rate vs. peak current density (anodic current density: closed circle and solid line, anodic current density: open circle and dashed line).

Table 3.6. Parameters of cyclic voltammmograms of diethyl ether- prepared vinylferrocene- terminated Si(111) on p-type substrate. (I_{pa} = anodic peak current density, E_{pa} = anodic peak potential, I_{pc} = cathodic peak current density, E_{pc} = cathodic peak potential)

Scan rate (V/s)	I_{pa} ($\mu A /cm^2$)	E_{pa} (V)	I_{pc} ($\mu A /cm^2$)	E_{pc} (V)
1	10.3	0.259	9.65	0.241
0.5	5.24	0.260	4.90	0.246
0.3	3.18	0.257	2.94	0.242
0.1	1.14	0.257	0.96	0.236

Scan rate (V/s)	$\lvert E_{pa}-E_{pc} \rvert$ (V)
1	0.018
0.5	0.014
0.3	0.014
0.1	0.021

The samples that were photochemically prepared in diethyl ether- vinylferrocene solution yielded a monolayer of neutral ferrocenyl film that is electrically attached with the silicon surface. However, lumps of deposited materials are adhered on its surface.

Tables 3.4 and 3.5 show the Fe at%, the O at%, the C at%, the Si at%, the ellipsometric thickness and the C/Fe ratio of the diethyl ether-prepared samples with n-type

and p-type substrates, respectively. (The "zero grafting time" samples are Si-H samples, which have undergone the same post-cleaning treatment as the diethyl ether-prepared sample.) The Fe at%, for both the n-type and the p-type samples, increases with grafting time. The increase in Fe at% for the latter part of the grafting process (2-4 h) is slower than the earlier part (0-2 h). The faster grafting rate at lower grafting time can be attributed to the larger number of available grafting site at the start of the grafting process. As the surface is being grafted with ferrocenyl groups, the number of available grafting site decreases, thus the rate of grafting becomes slower. The values of Fe at% are also less than 2%, which is within the atomic percent of an ethyl-linked Fc monolayer.

Tables 3.4 and 3.5 also show that the O at% of the samples are large. The large O at% could be attributed to the presence of silicon oxide on the sample's surface. Due to the mismatch between the size of the ethyl-linked Fc structure and the Si(111) spacing, not all the topmost Si atoms can be grafted with ferrocenyl groups. The absence of Si-C bonds would result to the formation of silicon oxide.

The grafted film was composed of neutral ferrocenyl groups. Figure 3.8 shows the Fe 2p spectra of the diethyl-prepared sample. The peaks at 708.0 and 720.9 eV binding energies correspond to Fe(II) $2p_{3/2}$ and Fe (II) $2p_{1/2}$, respectively. The presence of these large peaks indicates that the dominant oxidation state of Fe is +2, which correspond to presence of neutral ferrocenyl. Meanwhile, the small peaks on their higher binding energy side are associated with the presence of oxidized ferrocenyl.

The diethyl ether-prepared sample has lumps of materials on its surface. Figure 3.9a shows the step-like structure of the hydrogenated Si surface. This serves as the condition of the Si surface before the grafting process. Figure 3.9b shows the surface

topology after grafting. The image shows the presence of hump structures. Diethyl ether may have reacted with the hydrogenated surface and/or light, in which its by-product might have been deposited on the grafted surface (Figure 3.9c). This is compatible with the measured thicknesses of the diethyl ether-prepared samples, which are greater than the typical value of around 2 nm (Tables 3.4 and 3.5). These higher-than-expected values can be attributed to the lumps of deposited materials on the grafted surface.

The cyclic voltammogram (CV) of the sample shows the presence of anodic and cathodic peaks (Figure 3.10a). This signifies that the ferrocenyl groups are electrically connected with the Si surface. Figure 3.10b shows that the plots of scan rate with peak current density are linear. This signifies that the redox reactions are confined within the grafted surface. Likewise, the differences between the cathodic and anodic peaks are small, which is within the range of 0.014-0.021V (Table 3.6). These small differences indicate that the oxidation-reduction process does not involved diffusion of redox species. The deposited materials on the surface of the sample might have been redox-inert material that it does not significantly distort the CV curves.

3.3.2. Dibutyl ethyl-prepared samples

Table 3.7. XPS quantitative analytical data, ellipsometric thickness and C/Fe ratio of dibutyl ether-prepared samples on n-type substrate

Grafting Time (h)	**Fe (at%)**	**O (at%)**	**C (at%)**	**Si (at%)**	**Thickness (nm)**	**C/Fe**
0	0.00	4.24	6.42	89.34	---	---
0.5	1.48	6.63	18.39	83.44	1.93	12.4
1	1.42	9.69	15.99	72.91	1.84	11.3
2	1.35	8.73	16.44	73.48	1.94	12.2
4	1.05	12.26	20.64	78.68	2.59	19.7

Table 3.8. XPS quantitative analytical data, ellipsometric thickness and C/Fe ratio of dibutyl ether-prepared samples on p-type substrate

Grafting Time (h)	**Fe (at%)**	**O (at%)**	**C (at%)**	**Si (at%)**	**Thickness (nm)**	**C/Fe**
0	0.00	4.26	4.06	91.68	---	---
0.5	1.18	11.81	17.50	69.51	1.93	14.8
1	1.45	8.36	17.95	72.24	1.79	12.4
2	1.21	11.65	17.20	69.94	1.93	14.2
4	1.03	13.31	16.26	69.40	1.90	15.8

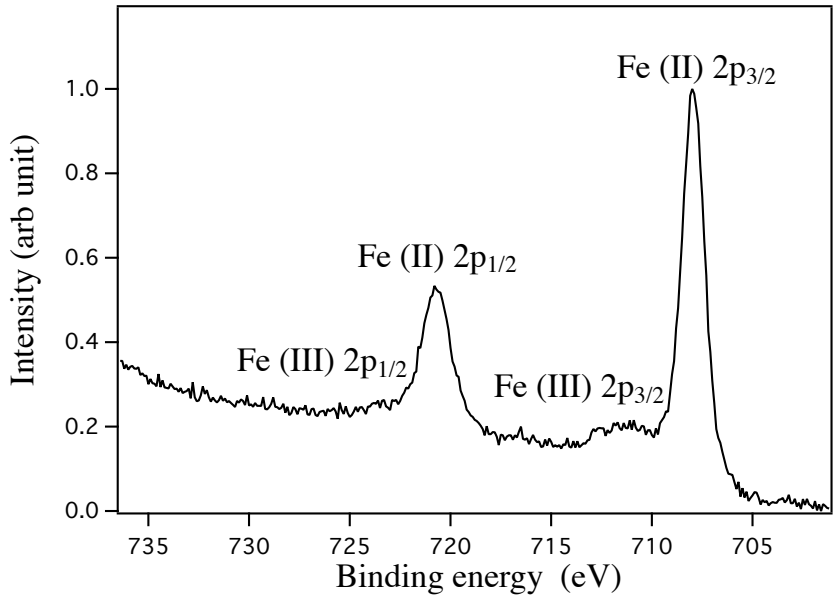

Figure 3.11. Fe 2p spectra of sample irradiated with 400 mW·cm^{-2} visible light in the vinylferrocene-dibutyl ether solution.

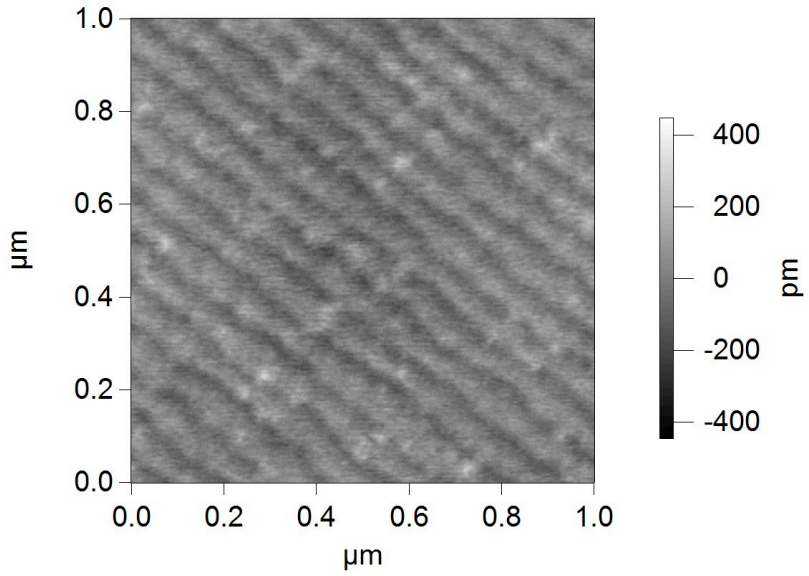

Figure 3.12. AFM topographical image of samples irradiated with 400 mW·cm^{-2} visible light in the vinylferrocene-dibutyl ether solution.

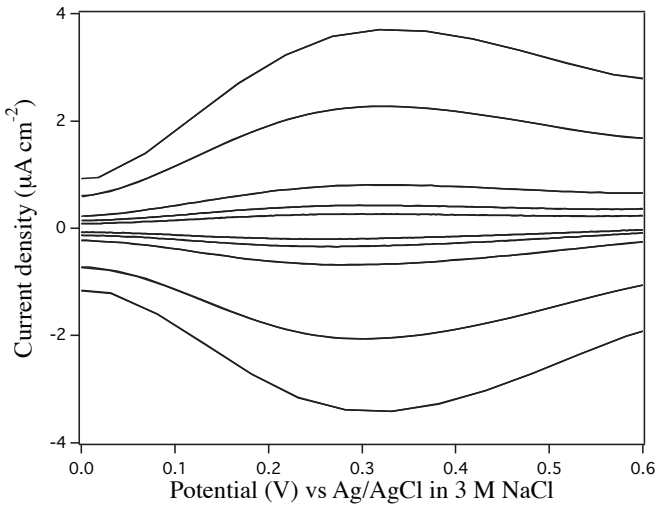

(a)

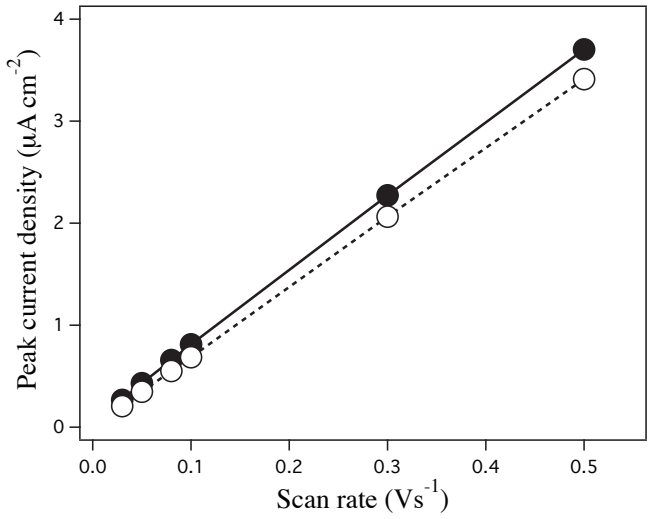

(b)

Figure 3.13. (a) Cyclic Voltammmograms of dibutyl ether- prepared vinylferrocene-terminated Si(111) on p-type substrate (scan rates are 500, 300, 100, 80, 50, 30 mV/s), and (b) its the corresponding graph of scan rate vs. peak current density (anodic current density: closed circle and solid line, anodic current density: open circle and dashed line).

Table 3.9. Parameters of cyclic voltammmograms of dibutyl ether- prepared vinylferrocene- terminated Si(111) on p-type substrate. (I_{pa} = anodic peak current density, E_{pa} = anodic peak potential, I_{pc} = cathodic peak current density, E_{pc} = cathodic peak potential)

Scan rate (V/s)	I_{pa} ($\mu A /cm^2$)	E_{pa} (V)	I_{pc} ($\mu A /cm^2$)	E_{pc} (V)
0.5	3.70	0.318	3.41	0.332
0.3	2.27	0.311	2.06	0.299
0.1	0.81	0.304	0.69	0.286
0.08	0.66	0.307	0.55	0.269
0.05	0.43	0.297	0.35	0.253
0.03	0.27	0.298	0.21	0.256

Scan rate (V/s)	$\lvert E_{pa}-E_{pc} \rvert$ (V)
0.5	0.014
0.3	0.012
0.1	0.018
0.08	0.038
0.05	0.044
0.03	0.042

The samples that were photochemically prepared in dibutyl ether- vinylferrocene solution yielded a monolayer of neutral ferrocenyl film that is electrically attached with the silicon surface and has an atomically flat surface.

Tables 3.7 and 3.8 show the Fe at%, the O at%, the C at%, the Si at%, the ellipsometric thickness and the C/Fe ratio of the dibutyl ether-prepared samples with n-type and p-type substrates, respectively. (The "zero grafting time" samples are Si-H samples, that undergone the same post-cleaning treatment as the dibutyl ether-prepared sample.) For n-type substrate, the highest Fe at% was attained at 0.5 h. Meanwhile, for p-type substrate, the highest Fe at% was attained at 1 h. After attaining their optimum values, the Fe at% decreases with grafting time. In such, the photogenerated charges might have degrading effect on the grafted structures. The Fe at% of the samples are within the typical values of ethyl-linked Fc-terminated Si. At their optimum grafting times, the C/Fe ratio for both the grafted n-type and the grafted p-type substrates is 12.4, which is near the ideal value of 12. The dibutyl ether might have prevented the transfer of charges from the Si surface to the active portion of VFc molecules, thus polymerization is prevented.

Figure 3.11 shows the Fe 2p spectra of the dibutyl-ether prepared sample. Similar to that of diethyl ether-prepared sample, the dominant oxidation state of Fe is +2. This indicates that the grafted structures are mainly composed of neutral ferrocenyl groups. Figure 3.12 shows the AFM image of the sample. The image shows stair-like structure, which is similar that of a Si-H (Figure 1.4 in Chapter 1). The perseverance of the stair-like structure of Si-H indicates that the grafted surface also has an atomically flat structure, similar to that of a Si-H surface.

Figure 3.13a shows the cyclic voltammogram (CV) of the dibutyl ether-prepared

sample. The presence of anodic and cathodic peaks signifies that the ferroncenyl groups are electrically connected with the Si surface. Figure 3.13b shows that the graph of scan rate vs peak current density is linear. This indicates that the oxidation-reduction reactions are confined within the grafted surface. Likewise, the differences between the anodic and cathodic peaks are small, ranging from 0.012-0.042 V (Table 3.9). These small differences signify that the redox process does not involved diffusion of redox species.

3.4. Summary and Conclusion

Photochemical grafting of vinylferrocene molecules were grafted on Si(111) surface using tetrahydrofuran, dietyl ether or dibutyl ether. In the preparation, a hydrogen-terminated Si(111) was immersed in solvent-vinylferrocene solution and was illuminated with visible light. Table 3.10 summarizes the characteristics of samples that were prepared in different media.

Table 3.10. Characteristics of samples that were prepared in different media

Solvent	Sample's Characteristics
Tetrahydrofuran	Produces degraded, oxidized, polymerized grafted structures on Si(111)
Diethyl Ether	Produces neutral ferrocenyl monolayer that is electrically connected with the Si surface but it has lumps of deposited materials on it
Dibutyl Ether	Produces neutral ferrocenyl monolayer that is electrically connected with the Si surface and has an atomically flat surface.

The use of diethyl ether or dibutyl ether enabled the production of ethyl-linked Fc-terminated Si, while the use of THF resulted to the polymerization of the grafted molecules. Diethyl ether and dibutyl ether might have prevented the transfer of charges from the Si surface to the active portion of VFc molecules that is needed for polymerization. On the other hand, the diethyl ether-prepared sample has lumps of deposited materials on it, however, these materials are not electrochemically active. Among the three media, the best in terms of easiness of preparation and quality of the grafted sample would be the use of diethyl ether. Dibutyl ether has low volatility, thus there is no need to place solvent reservoir to compensate for the loss liquid during the photochemical preparation. The dibutyl ether-prepared sample has good electrochemical properties and surface topography.

References:

1. S. R. Amy, D.J. Michalak, Y.J. Chabal, L. Wielunski, P.T. Hurley, N.S. Lewis: *J. Phys. Chem. C*. **2007.** 111. 13053.
2. C.D. Bain, G. M. Whitesides: J. Am. Chem. Soc. (1989) 111, 7164.
3. A. Bansal, X. Li, S.I. Yi, W.H. Weinberg, N.S. Lewis: *J. Phys. Chem. B*. **2001.** 105. 10266.
4. R.K. Bohn, A. Haaland: *J. Organometal. Chem*. **1966.** 5. 470.
5. R. Boukherroub, S. Morin, F. Bensebaa, D.D.M. Wayner: *Langmuir*. **1999.** 15. 3831.
6. R. Boukherroub: *Current Opinion in Solid State and Materials Science*. **2005.** 9. 66.
7. J.M. Buriak: *Chemical Reviews*. **2002.** 102. 1271.
8. X. Chen, R. Ferrigno, J. Yang, G.M. Whitesides: Langmuir (2002) 18, 7009.
9. S. Ciampi, P. K. Eggers, G. Le Saux, M. James, J. B. Harper, J. J. Goodin: *Langmuir.* **2009.** 25. 2530.
10. S. Ciampi, G. Le Saux, J. B. Harper, J. J. Gooding: *Electroanalysis* **2008.** 20. 1513.
11. R.L. Cicero, M.R. Linford, C.E.D. Chidsey: *Langmuir.* **2000.** 16. 5688.
12. M. Cossi, M. F. Iozzi, A. G. Marrani, T. Lavecchia, P. Galloni, R. Zanoni, F. Decker: *J. Phys. Chem. B* **2006.** 110. 22961.
13. E. A. Dalchiele, A. Aurora, G. Bernardini, F. Cattaruzza, A. Flamini, P. Pallavicini, R. Zanoni, F. Decker: J. *Electroanal. Chem*. **2005.** 579. 133.
14. A.L. Eckermann, D.J. Feld, J.A. Shaw, T.J. Meade: *Coordination Chemistry Reviews*. **2010.** 254. 1769.
15. B. Fabre: *Acc. Chem. Res*. **2010.** 43. 1509.
16. S. Fellah, R. Boukherroub, F. Ozanam, J.-N. Chazalviel: *Langmuir.* **2004.** 20. 6359.

17. S. Fellah, A. Teyssot, F. Ozanam, J.-N. Chazalviel, J. Vigneron, A. Etcheberry: *Langmuir.* **2002.** 18. 5851.

18. A. Fidelis, F. Ozanam, J.-N. Chazalviel: *Surface Science*. **2000.** 444. L7.

19. J.P. Flokers, P.E. Laibinis, G.M. Whitesides: Langmuir (1992) 8, 1330.

20. F. Frederix, K. Bonroy, W. Laureyn, G. Reekmans, A. Campitelli, W. Dehaen, G. Maes: Langmuir (2003) 19, 4351.

21. D. Hobara, S. Imabayashi, T. Kakiuchi: Nanoletters (2002) 2, 1021.

22. R. Hunger, R. Fritsche, B. Jaeckel, W. Jaegermann, L.J. Webb, N.S. Lewis: *Phys. Rev. B*. **2005.** 72. 045317.

23. R. Hunger, R. Fritsche, B. Jaeckel, L.J. Webb, W. Jaegermann, N.S. Lewis: *Surface Science*. **2007.** 601. 2896.

24. P.E. Laibinis, R.G. Nuzzo, G.M. Whitesides: J. Phys. Chem. (1992) 96, 5097.

25. Q. Li, G. Mathur, M. Homsi, S. Surthi, V. Misra, V. Malinovskii, K.-H. Schweikart, L. Yu, J. S. Lindsey, Z. Liu, R. B. Dabke, A. Yasseri, D. F. Bocian, W. G. Kuhr: *Appl. Phys. Lett*. **2002.** 81. 1494.

26. Q. Li, S. Surthi, G. Mathur, S. Gowda, V. Misra, T. A. Sorenson, R. C. Tenent, W. G. Kuhr, S. Tamaru, J. S. Lindsey, Z. Liu, D. F. Bocian: *Appl. Phys. Lett*. **2003.** 83. 198.

27. M. R. Linford, C.E.D. Chidsey: *J. Am. Chem. Soc*. **1993.** 115. 12631.

28. M.R. Linford, P. Fenter, P.M. Eisenberger, C.E.D. Chidsey: *J. Am. Chem. Soc*. **1995.** 117. 3145.

29. M. Lu, T. He, and J. M. Tour, *Chem. Mater.* **2008.** 20. 7352.

30. A. G. Marrani, F. Cattaruzza, F. Decker, P. Galloni, R. Zanoni: *Superlattices and Microstructures*. **2009.** 46. 40.

31. T. Miyadera, A. Koma, T. Shimada: *Surface Science*. **2003.** 526. 177.

32. D.A. Offord, C. M. John, M.R. Linford, J.H. Griffin: Langmuir (1994) 10, 883.

33. R. Okada, T. Miyadera, T. Shimada, A. Koma, K. Ueno, K. Saiki: *Surface Science*. **2004.** 552. 46.

34. E. Ostuni, B.A. Grzybowski, M. Mrksich, C.S. Roberts, G.M. Whitesides: Langmuir (2003) 19. 1861.

35. K. M. Roth, A. A. Yasseri, Z. Liu, R. B. Dabke, V. Malinovskii, K.-H. Schweikart, L. Yu, H. Tiznado, F. Zaera, J. S. Lindsey, W. G. Kuhr, D. F. Bocian: *J. Am. Chem. Soc*. **2003.** 125. 505.

36. H. Sano, M. Zhao, D. Kasahara, K. Murase, T. Ichii, H. Sugimura: *Journal of Colloid and Interface Science*. **2011.** 361. 259.

37. K. Shimazu, T. Kawaguchi, T. Isomura: J. Am. Chem. Soc. (2002) 124, 652.

38. A. B. Sieval, A.L. Demirel, J.W.M. Nissink, M.R. Linford, J.H. van der Maas, W.H. de Jeu, H. Zuilhof, E.J.R. Sudholter: *Langmuir.* **1998.** 14. 1759.

39. A.B. Sieval, R. Opitz, H.P.A. Maas, M.G. Schoeman, G. Meijer, F.J. Vergeldt, H. Zuilhof, E.J.R. Sudholter: *Langmuir.* **2000.** 16. 10359.

40. S.J. Stranick, A.N. Parikh, Y.-T. Tao, D.L. Allara, P.S. Weiss: J. Phys. Chem. (1994) 98. 7636.

41. Q.-Y. Sun, L.C.P.M. de Smet, B. van Lagen, M. Giesbers, P.C. Thune, J. van Engelenburg, F.A. de Wolf, H. Zuilhof, E.J.R. Sudholter: *J. Am. Chem. Soc*. **2005.** 127. 2514.

42. S. Takakusagi, T. Miyasaka, K. Uosaki: *J. of Electroanalytical Chemistry.* **2007.** 599. 344.

43. K. Tamada, M. Hara, H. Sasabe, W. Knoll: Langmuir (1997) 13, 1558.

44. Y. Tong, E. Tyrode, M. Osawa, N. Yoshida, T. Watanabe, A. Nakajima, S. Ye: Langmuir (2011) 27, 5420.

45. L. Touahir, P. Allongue, D. Aureau, R. Boukherroub, J.-N. Chazalviel, E. Galopin, A.C. Gouget-Laemmel, C.H. de Villeneuve, A. Moraillon, J. Niedziolka-Jonsson, F. Ozanam, J.S. Andresa, S. Sam, I. Solomon, S. Szunerits: *Bioelectrochemistry*. **2010.** 80. 17.

46. I. Waluyo, H. Ogasawara, M. Kawai, A. Nilsson, T. Yamada: *J. Phys. Chem. C*. **2010.** 114. 19004.

47. L.J. Webb, N.S. Lewis: *J. Phys. Chem. B*. **2003.** 107. 5404

48. L. J. Webb, S. Rivillon, D.J. Michalak, Y.J. Chabal, N.S. Lewis: *J. Phys. Chem. B*. **2006.** 110. 7349.

49. T. Yamada, M. Kawai, A. Wawro, S. Suto, A. Kasuya, *A. J. of Chem. Phys*. **2004.** 121. 10660.

50. H. Yu, L.J. Webb, R.S. Ries, S.D. Solares, W.A. Goddard, J.R. Heath, N.S. Lewis: *J. Phys. Chem. B*. **2005.** 109. 671.

51. H. Yu, L.J. Webb, J.R. Heath, N.S. Lewis: *Appl. Phys. Lett*. **2006.** 88. 252111.

Chapter 4
Role of Surface Charges on the Grafting of Vinylferrocene Molecules on Si surface

4.1. Introduction

The preparations of grafted organic molecules on silicon surface using alkenes or olefins as precursor molecules have been cited in literature (Buriak, 2002; Cicero et. al. 2000; Coletti et. al., 2006; Eves et. al. 2004; Kruse, et. al. 2002; Langner, et. al. 2005; Linford et. al. 1995; Lopinsky et. al. 2000; Sano et. al. 2008; Sieval et. al. 1998; Steward and Buriak, 2001; Sun et. al., 2005; Wang et. al. 2010; Zhong and Bernasek, 2011). It was previously proposed (Sano, et. al., 2011) that the grafting of VFc molecules on Si surface could arise when its carbon-carbon double bond approached the Si-H bond. In such event, they could form four-membered transition state that can lead to the formation of Si-C bonds. In photochemical preparation, illumination of the Si surface produces excitons. For n-type substrate, excitons dissociate into free carriers, with holes going on the Si surface. Surface holes can facilitate meeting between the nucleophilic alkene molecules and silicon atoms to form Si-C bonds. The case would be different for p-type substrate in which electrons go to the Si surface, instead of holes. The presence of negative charges on the Si surface would not be favorable to the attacked of nucleophilic alkene molecules. Model explaining the role of negative surface charges on alkene grafting is still not clear.

This report will give new insight about the role of surface charges on the grafting of alkene molecules. In this insight, surface charges are agents that facilitate the meeting of the VFc molecules and the Si-H bonds. In such, Si surface charges (electrons or holes)

produce electric field that can induce polarization of VFc molecules. The polarization of VFc molecules can lead to its attraction on the hydrogenated Si surface. The charges are not limited to those induced by illumination but could also included those tunneled charges from the bulk substrate. Tunneling of charges can occur in the dark, thus, we will also show that grafting of VFc molecules is also possible in the dark, without the aid of external agents (e.g., external bias, elevated temperature, radical initiator).

4.2 Methodology

Table 4.1. Kinds of silicon wafer that were used in the experiment

Notations	Sample	Characteristics
n-low Si	Phosphorus-doped Si with resistivity of 1-10 Ω cm	n-type, high resistivity, low dopant concentration
n-high Si	Phosphorus-doped Si with resistivity of 0.001-0.004 Ω cm	n-type, low resistivity, high dopant concentration
p-low Si	Boron-doped Si with resistivity of 1-30 Ω cm	p-type, high resistivity, low dopant concentration
p-high Si	Boron-doped Si with resistivity of 0.001-0.004 Ω cm	p-type, low resistivity, high dopant concentration

Table 4.1 shows the four types of substrates that were used. The experimental method that was done was similar with that presented in Chapter 3.2. For high-doped substrate, the hydrogen-terminated process specified in Chapter 2.2.1 was done. Note that we did not use substrate with high dopant concentration in Chapter 3.

4.3. Results and Discussion

4.3.1. Vinylferrocene molecules under electric field

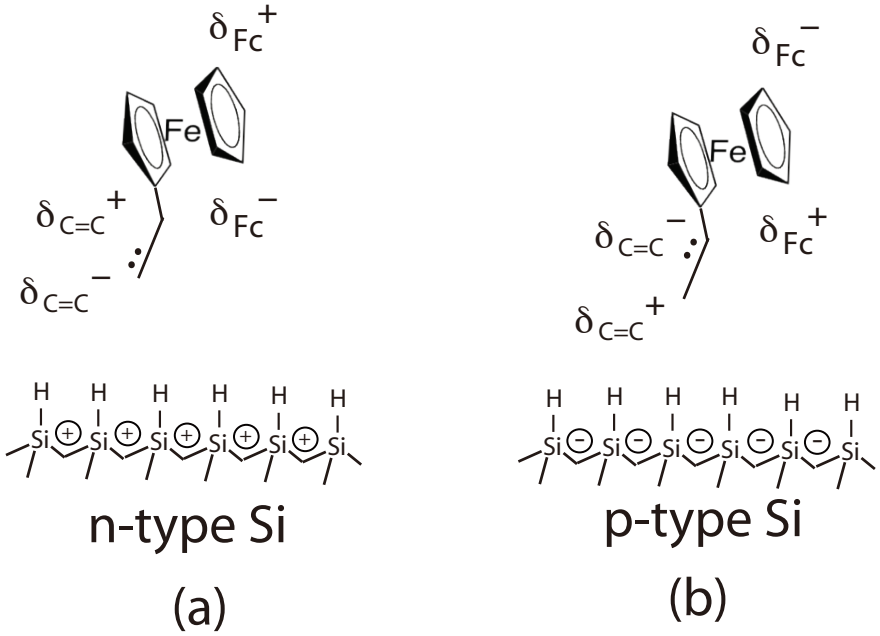

Figure 4.1. Polarization of VFc molecule due to the photogenerated charges on (a) n-type Si substrate and (b) p-type Si substrate.

At very short distance, the electric field produced by a solitary charge in vacuum is very strong (e.g. at 10 au or 0.529 nm, the electric field is about 0.01 au or 5.14 x 10^9 V/m). Thus, a pool of charges on the Si surface can create a very large electric field with a very short distance from the Si surface. This large amount of electric field could possibly be used to polarize alkene molecule (Amos and Crispin, 1975; Waite and Papadopoulos, 1991; Hush and Williams, 1970; Shigeta et. al., 1999) to create dipole moment that would result to its attraction on the Si surface.

The VFc molecules can undergoes polarization in the presence of electric field. The electric polarizability (α) of VFc molecules is 196 au (Waite and Papadopoulos, 1991).

(To note, 1 au ≈ 0.148 176 x 10-^{24} esu ≈ 0.164867 X 10^{-40} C^2 m^2 J^{-1}.) Polarizability is a measure of the amount of dipole moment that was induced by an electric field (Dewar and Stewart, 1984). When a molecule is polarized, the electron density profile redistribute and create a dipole moment. Electric polarizability describes the change on the electron density distribution in the presence of an electric field (Fuentealba and Reyes, 1993). It can also be viewed as the looseness of binding of electrons (Davies, 1952).

Figure 4.1 highlights two areas of polarization, they are the (1) Fc head and (2) the carbon double bond (C=C) direction. The terms "δ_{Fc}^{+}" and "δ_{Fc}^{-}" signify Fc head's positive and negative dipoles, respectively while the term "$\delta_{C=C}^{+}$" and "$\delta_{C=C}^{-}$" in Figure 4.1 signify the positive and negative dipoles in the C=C direction, respectively. Amos and Crispin (1975) calculated the polarizability of the localized orbitals in ethylene molecule (e.g. parallel to the CH bond) and shows that it is more polarizable at the C=C direction. This is expected since π bond is loosely bound to the molecule thus its effect on polarizability is greater than that of σ bonds. It is also worth mentioning that similar to C=C double bonds, the longitudinal polarizability of C=O and C=S double bonds is also greater than its transverse polarizability (Denbigh, 1940).

Figure 4.1 also shows two dots that represent the polarized π bond electrons (zwitterionic state) of the ethylene body. In Figure 4.1a, the π bond electrons are attracted to the positively charged surface while in Figure 4.1b, the π bond electrons are repelled farther to the negatively charged surface. In ethylene molecule, the existence of dipole moment is associated with the localization of the two electrons on one side of the molecule (Zijlstra et. al., 1996). Zwitterionic character of alkenes has been cited in literature (Brooks and Schaefer, 1979; Morais et. al., 1991; Schilling and Hilinski, 1988; Schuddeboom et. al.,

1993; Trinquier and Malrieu, 1980).

In our proposed model, we will assumed that the grafting medium is non-polar or has low polarity. Grafting medium can be (a) polar (Figure 4.2a) or (b) non-polar (Figure 4.2b). In the previous chapter, we used tetrahydrofuran, diethyl ether and dibutyl ether, as grafting media. Tetrahydrofuran has relatively high polarity compare with diethyl ether and dibutyl ether. For simplicity, we can consider, THF as polar while the other two ethers as non-polar.

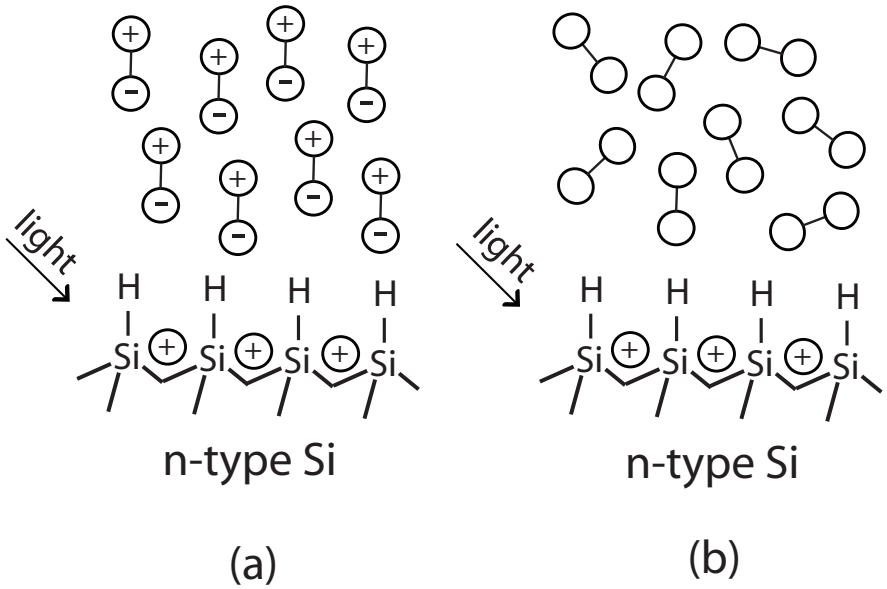

Figure 4.2. Two kinds of grafting media: (a) polar medium and (b) non-polar medium

Illumination with visible light induces surface charges. Similar to any other charges, these photogenerated surface charges create electric field. Electric field has the capability to align the dipole moment of the polar molecules as shown in Figure 4.2a. Because of the presence of aligned dipole moments in polar medium, pockets of electric field are scattered throughout the grafting medium. This scenario would be different for the

case of non-polar medium (Figure 4.2b), wherein no dipole moment will align and the sufficiently large electric field is found near the Si surface. Since this chapter will focus on the use of dibutyl ether (non-polar) as grafting medium, we will assumed that the source of electric field, which is responsible for the polarization of ethylene-like body of VFc molecule, are the charges on the Si surface, and not on the grafting medium.

For both the illuminated n-type and p-type Si substrates, the configuration of the polarized VFc molecule can led to its attraction to the charged Si surface. For the case of n-type Si, the positively charged surface can induce dipole in which the negative side is facing the positively charged Si surface (Figure 4.1a). This configuration could eventually lead to its attraction on the Si surface. For the case of p-type Si, the negatively charged surface can induce a dipole in which the positive side is facing the negatively charged Si surface (Figure 4.1b). This configuration could also lead to its attraction on the Si surface. At the surface, the VFc molecules can interact with the hydrogenated Si to form Si-C bonds. Thus, the presence of illumination-induced surface charges can led to a fast grafting process.

Figure 4.3 shows the Fe atomic percent (Fe at%) vs. grafting time of samples with n-type and p-type substrates that undergone photochemical grafting process and those that are grafted in the dark. The value of Fe at% is proportional to the amount of grafted ferrocenyl groups on the Si surface. At grafting time of 30 min, the samples that underwent photochemical grafting have Fe at% of 1.48% (n Si) and 1.18% (p Si). These values are very much higher than that of the sample that was prepared on the dark, which has Fe at% of 0.2% (n Si) and 0.0% (p Si). These values show that illumination with visible light greatly enhanced the grafting process.

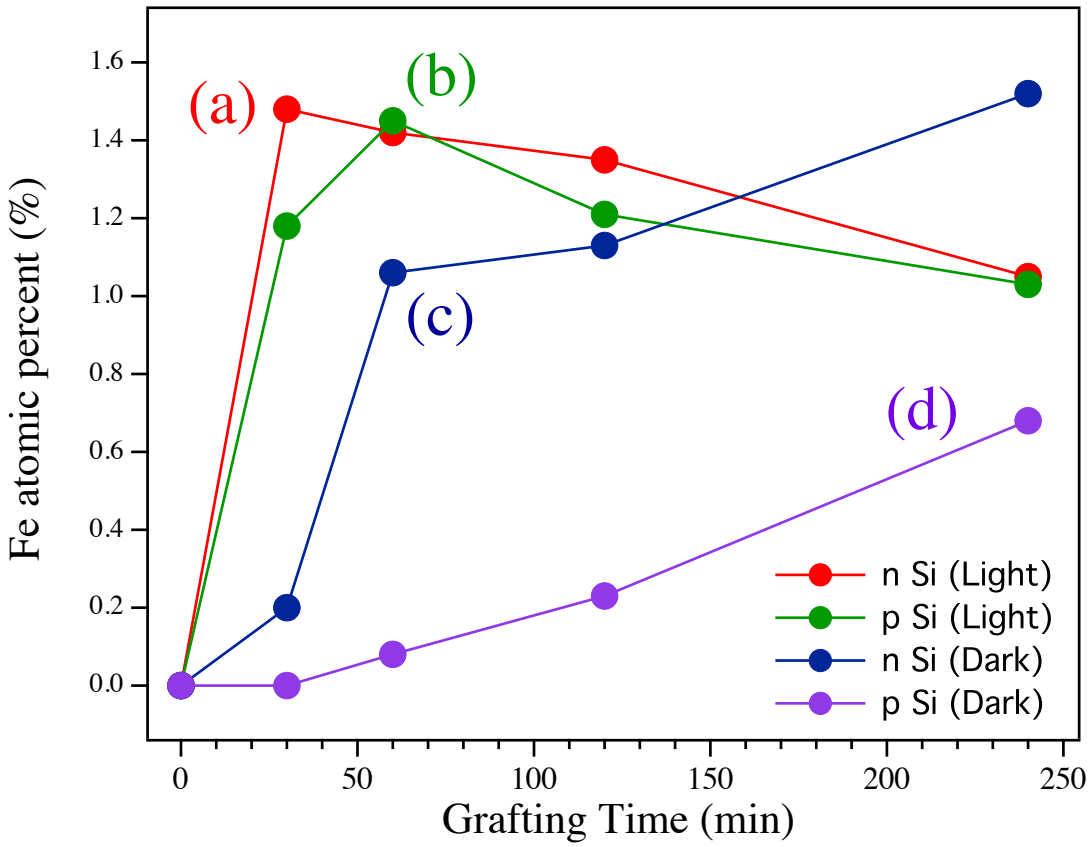

Figure 4.3. Fe atomic percent vs. grafting time of the following type of samples: (a) n-low Si-H samples that were illuminated with 400 mW• cm^{-2} visible light (n Si (light)), (b) p-low Si-H samples that were illuminated with 400 mW• cm^{-2} visible light (p Si (Light)), (c) n-low Si-H samples that were placed in the dark (n Si (dark)), and (d) p-low Si-H samples that were placed in the dark (p Si (dark)).

Figures 4.3a, 4.3b show that the highest Fe at% of the samples with p Si happens on longer grafting time of 60 min (Fe at% = 1.45%), compare with those of n Si, which is 30 min (1.48%). The presence of photogenerated holes is advantageous than the presence of photogenerated electrons since the π electrons of nucleophilic alkene molecules is

attracted to the surface. Meanwhile, the presence of photogenerated negative charges on the p-type Si surface might have contributed addition burden to the grafting process since they tend to repel away the π electrons. (It is important to note that the entire VFc molecule is still attracted to the Si surface.) This repulsion might have contributed to a slower grafting process on p Si surfaces compare to n Si.

Figures 4.3a, 4.3b also show that after reaching the highest Fe at%, their values slowly decrease. The decrease in the Fe at% might be attributed to the amount of grafted ferrocenyl groups that has been detached because of the continuous presence of photogenerated charges. The electric field created by the surface charges might have continuously polarizing the Fc head. The continuous pulling of the Fc head towards the Si surface might have resulted to the detachment of some of immobilized structures on the Si surface.

4.3.2. Effects of Si Substrate on Grafting

The nature of the Si substrate can affect the grafting process by influencing the availability of charges on the hydrogenated surface. The transport of charges from the bulk of the Si substrate to its surface is highly influenced by its energy band structure. Figure 1.5 (chapter 1) shows the energy band diagram of n Si-H and p Si-H samples at the dark and having zero external bias. The Si conduction (E_C) and valence (E_V) bands bend, creating a depletion layer and semiconductor barrier. The creation of semiconductor barrier can hinder the transfer of charges from bulk silicon out to its surface. Some possible ways in order for charges to go at the Si surface includes the following: (1) by placing external voltage, (2) by illumination of the surface and (3) by tunneling. The first two items were

discussed in Chapter 2 in relation to the methyl grafting process. This report will just tackle on item 2 (illumination of the surface) and item 3 (tunneling).

Table 4.2. XPS quantitative analytical data of hydrogen-terminated Si(111) that underwent photochemical preparation using 400 mW・cm^{-2} illumination.

Doping level	Grafting Time (min)	Fe (at%)	O (at. %)	C (at. %)	Si (at. %)
n-low Si	30	1.48	6.63	18.39	83.44
n-high Si	30	0.88	15.51	13.40	70.21
p-low Si	60	1.45	8.36	17.95	72.24
p-high Si	60	0.77	15.96	16.63	66.64

As discussed earlier, illumination of visible light can induced the production of surface charges. The amount of photogenerated charges on the Si surface can be affected by the width of depletion layer. The electric field in this layer split the electron-hole pairs, which one kind of charge will go to the Si surface. Substrate with thinner layer has fewer region wherein splitting will occur, thus would mean less denser surface charges. A less dense surface charge makes the grafting process slower. The Si substrate's dopant concentration affects the width of the depletion layer. The substrate with high dopant concentration or low resistivity will have thinner depletion layer than those with low dopant concentration. Table 4.2 shows the XPS quantitative analytical data of Si-H that underwent photochemical preparation using 400 mW・cm^{-2} illumination. The 30 min (n Si) and 60 min (p Si) in the second column correspond to the grafting time wherein the Fe at%

of samples with low-doped substrates are the highest. For both n Si and p Si, the samples with high dopant concentration have lower Fe at% indicating a slower grafting process. For sample using n-type Si, substrate with low dopant concentration has Fe at% of 1.48% while that of high dopant concentration has only 0.88%. Meanwhile for sample with p-type Si, substrate with low dopant concentration has Fe at% of 1.45% while that of high dopant concentration has only 0.77%.

Figures 4.3c and 4.3d shows that it is possible to graft vinylferrocene molecules onto the Si surface even in the dark without the aid of external agents (e.g., external bias, elevated temperature, radical initiator). However, the VFc grafting process in the dark is slower than under visible light illumination. In the dark and in the absence of external voltage, the electrons of n Si-H or the holes of p Si-H have probability to tunnel through the potential barrier and go to the surface to participate in the grafting process. The probability in which charges can tunnel across the semiconductor barrier can be influenced by (1) the height of the semiconductor barrier and (2) the width of the depletion region.

The height of the semiconductor barrier affects the probability of charge tunneling. Charges have higher probability to tunnel at barrier with shorter height than with taller height. The barrier height of n Si-H is less than those of p Si-H (Table 1.1 in Chapter 1). For example in the work of Maldonado et. al. (2007), the barrier height of n Si-H is 0.17 eV while that of p Si-H is 0.82 eV. Thus, the probability for holes in the bulk of p Si has lower probability to tunnel on the depletion region than for electrons in the bulk of n Si to do the same. This offers an explanation for the very slow rate of VFc grafting on p Si-H sample in the dark, compare to that of n Si-H (Figures 4.3c, 4.3d). For example, at 30 min grafting time, sample with n-type substrate has Fe at% of 0.2% while that of p-type has not

detected any significant amount of Fe atoms, thus the Fe at% is still 0%. When the grafting time is increase to 60 min, the Fe at% of sample with n-type substrate dramatically increases to 1.06%, while that of p-type substrate only increase to 0.08%.

Charges would have higher probability of tunneling on sample with shorter depletion region than that with longer depletion region. Si substrate with higher dopant concentration has shorter depletion width than substrate with lower dopant concentration. Thus, for a given span of time, sample with higher dopant concentration would have more tunneled charges on the Si surface than sample with lower dopant concentration. With this, VFc grafting in the dark would be much faster on sample with high dopant concentration than with those with low dopant concentration. Table 4.3 shows the XPS quantitative analytical data of Si-H that that was immersed in VFc- dibutyl ether solution in the dark. The table shows that for both samples with n-type and p-type substrates, grafting on substrate with high dopant concentration is faster than those of with low dopant concentration. For n-type substrate, substrate with high dopant concentration has Fe at% of 0.40% while that of low dopant concentration has only 0.20%. Meanwhile for p-type substrate, substrate with high dopant concentration has Fe at% of 0.21% while that of low dopant concentration has only 0.08%.

Table 4.3. XPS quantitative analytical data of hydrogen-terminated Si(111) that was immersed in VFc- dibutyl ether solution in the dark.

Doping level	Grafting Time (min)	Fe (at%)	O (at. %)	C (at. %)	Si (at. %)
n-low Si	30	0.20	8.17	7.56	84.07
n-high Si	30	0.40	18.26	10.13	71.21
p-low Si	60	0.08	7.84	9.76	82.32
p-high Si	60	0.21	14.27	11.42	74.1

It is important to note, that the trend for the effect of dopant concentration is different for the case of photochemical preparation and the case of grafting in the dark method. The difference in trend is attributed with the difference on how the width of the depletion layer affects the movement of charges to the Si surface. A thinner depletion region (high dopant concentration) has limited vicinity wherein the splitting of photogenerated electron-hole pairs occur, thus this translate to a lower amount of photogenerated charges on the Si surface that could participate in grafting. The case would be different when grafting is done in the dark, wherein making the depletion layer thinner would be favorable for charge tunneling, thus grafting is enhanced.

4.4. Summary and Conclusion

We are successful in grafting ferrocenyl groups on Si(111) surface on both n-type and p-type surface using photochemical preparation. The success was attributed to presence of photogenerated charges on the Si surface. In such, the surface charges create

electric field that has capability to polarized VFc molecules. When polarize, the dipole moment of the VFc molecules align with the electric field. The orientation of its dipole moment can led to its attraction towards the hydrogenated Si surface. When attracted near the surface, the VFc molecules can react with the hydrogenated Si to form Si-C bonds. The surface charges are not limited to charges caused by illumination, but could also include tunneled charges from the bulk substrate that could happen in the dark. We are also successful in grafting vinylferrocene molecules on Si surface in the dark. However, grafting in the dark is very slow compare to those under illumination. The density of surface charges, which is crucial to the grafting process, is influenced by the nature of the band bending of the Si (e.g. width of the depletion region), which in turn can be affected by the nature of the substrate (e.g. dopant concentration). Under illumination, the grafting rate improved with the use of substrate with low dopant concentration while in the dark, it improved with the use of substrate with high dopant concentration and n-type substrate.

References

1. A.T. Amos, R.J. Crispin: *J. Chem. Phys*. **1975.** 63. 1890.
2. B.R. Brooks, H.F. Schaefer: Journal of the American Chemical Society. **1979.** 101. 307.
3. J.M. Buriak: *Chemical Reviews*. **2002.** 102. 1271.
4. R.L. Cicero, M.R. Linford, C. E. D. Chidsey: *Langmuir.* **2000.** 16. 5688.
5. C. Coletti, A. Marrone, G. Giorgi, A. Sgamellotti, G. Cerofolini, N. Re: *Langmuir.* **2006.** 22. 9949.
6. P.L. Davies: *Trans. Faraday Soc*. **1952.** 48. 789.
7. K.G. Denbigh: *Trans. Faraday Soc*. **1940.** 36. 936.
8. M.J.S. Dewar, J.J.P. Stewart: *Chemical Physics Letters*. **1984.** 111. 416.
9. B.J. Eves, Q.-Y. Sun, G.P. Lopinski, H. Zuilhof: *J. Am. Chem. Soc*. **2004**. 126. 14318.
10. P. Fuentealba, O. Reyes: *Journal of Molecular Structure*. **1993.** 282. 65.
11. N.S. Hush, M.L. Williams: *Chemical Physics Letters*. **1970.** 6. 163.
12. P. Kruse, E.R. Johnson, G.A. DiLabio, R. A. Wolkow: Nanoletters. **2002.** 2. 807.
13. A. Langner, A. Panarello, S. Rivillon, O. Vassylyev, J.G. Khinast, Y. J. Chabal: *J. Am. Chem Soc*. **2005.** 127. 12798.
14. M.R. Linford, P. Fenter, P.M. Eisenberger, C.E.D. Chidsey: *J. Am. Chem Soc*. **1995.** 117, 3145.
15. G. P. Lopinski, D. D. M. Wayner, R. A. Wolkow: *Nature*. **2000.** 406. 48.
16. S. Maldonado, K. E. Plass, D. Knapp, N.S. Lewis: *J. Phys. Chem. C*. **2007.** 111. 17690.
17. J. Morais, J. Ma, M.B. Zimmt: *The Journal of Physical Chemistry.* **1991.** 95. 3885.

18. H. Sano, H. Maeda, S. Matsuoka, K.-H. Lee, K. Murase, H. Sugimura: *Japanese Journal of Applied Physics*. **2008.** 47. 5659.

19. H. Sano, M. Zhao, D. Kasahara, K. Murase, T. Ichii, H. Sugimura: *Journal of Colloid and Interface Science*. **2011.** 361. 259.

20. C.L. Schilling, E.F. Hilinski: *J. Am. Chem. Soc*. **1988.** 110. 2296.

21. W. Schuddeboom, S.A. Jonker, J.M. Warman, M.P. de Haas, M.J.W. Vermeulen, W. F. Jager, B. de Lange, B.L. Feringa, R.W. Fessenden: *J. Am. Chem. Soc*. **1993.** 115. 3286.

22. Y. Shigeta, S. Yamada, H. Nagao, M. Nakano, K. Ohta, K. Yamaguchi: *Synthetic Metals*. **1999.** 101. 513.

23. A. B. Sieval, A. L. Demirel, J. W. M. Nissink, M. R. Linford, J. H. van der Maas, W. H. de Jeu, H. Zuilhof, and E. J. R. Sudholyer: *Langmuir.* **1998.** 14. 1759.

24. M.P. Stewart, J.M. Buriak: *J. Am. Chem. Soc*. **2001.** 123. 7821.

25. Q.-Y. Sun, L.C. P. M. de Smet, B. van Lagen, M. Giesbers, P. C. Thune, J. van Engelenburg, F. A. de Wolf, H. Zuilhof, E. J. R. Sudholter: *J. Am. Chem. Soc*. **2005.** 127. 2514.

26. G. Trinquier, J-P. Malrieu: *Chemical Physics Letters*. **1980.** 72. 328.

27. J. Waite, M.G. Papadopoulos: *J. Phys. Chem*. **1991.** 95. 5426.

28. X. Wang, R.E. Ruther, J.A. Streifer, R. J. Hamers: *J. Am. Chem. Soc*. **2010.** 132. 4048.

29. Y. L. Zhong, S.L. Bernasek: *Langmuir.* **2011.** 27. 1796.

30. R.W.J. Zijlstra, P.Th. van Duijnen, A.H. de Vries: *Chemical Physics*. **1996.** 204. 439.

Chapter 5
Electrochemical Characteristics of Immobilized Ferrocenyl Group on Si Surface

5.1. Introduction

Ferrocene-containing molecules on semiconductor or semiconductor's oxide surface (Si-Fc) have been topic of different reports (Ciampi, 2008, Ciampi, 2009, Cossi, 2006, Dalchiele, 2005, Decker, 2006, Fabre, 2010, Fabre, 2006, Gowda, 2007, Li, 2002, Li, 2003, Lu, 2008, Marrani, 2008, Marrani, 2009, Roth, 2003, Sano, 2011, Zanoni, 2005, Zanoni, 2008). They are eyed for memory devices (Fabre, 2010, Li 2002, Li 2003, Roth 2003). The Fe atom in ferrocene (Fc) has two stable and reversible oxidation states and has potential to act as memory elements. Its two oxidation states could correspond to the memory bit "0" and "1". Its oxidation state can increase from +2 to +3 upon the introduction of potential and could return back to +2 when it is removed.

The electrochemical characteristics of Fc-terminated Si (Si-Fc) depend on the type of substrate (whether n-type or p-type). Cyclic voltammograms (CV) of samples with n-type substrates (n Si-Fc) shows peaks only when performed under illumination (Dalchiele, et. al. 2005, Gowda, et. al 2007, Fabre, 2010, Sano et al 2011). The case would be different for samples with p-type substrate (p Si-Fc), which show CV peaks with or without illumination (Dalchiele, et. al. 2005, Gowda, et. al. 2007, Fabre, 2010, Sano et. al 2011). Sano, et. al. (2011) presented a model to explained such phenomenon (Figures 5.1 and 5.2).

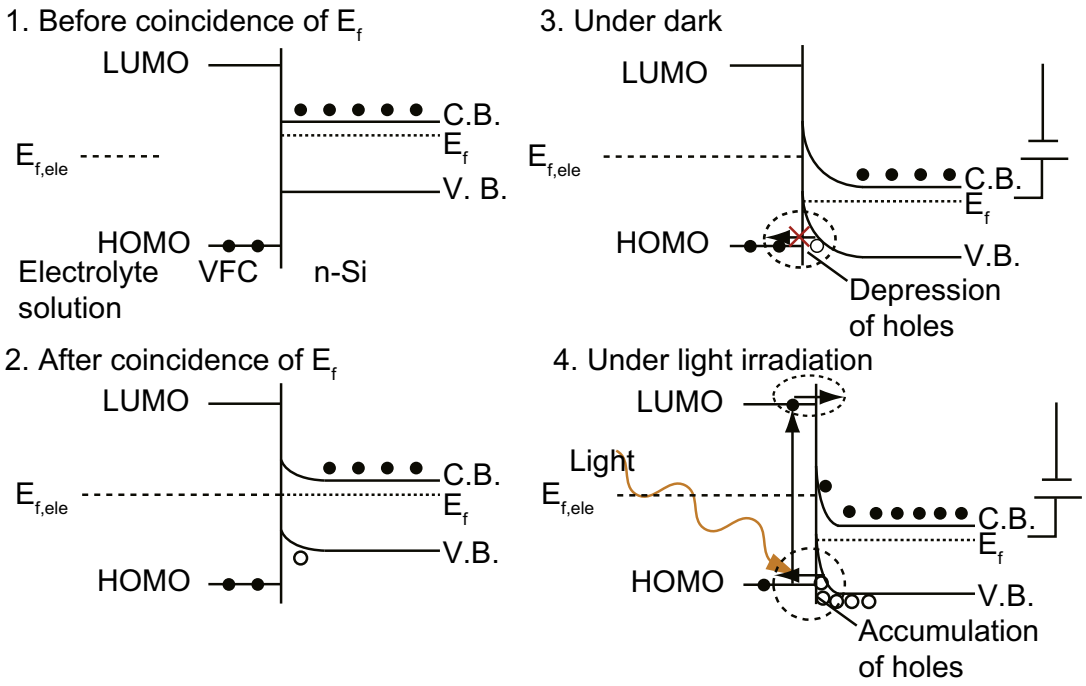

Figure 5.1. Energy diagram of Si-VFc sample on n-type substrate (Illustration taken from: Sano, et. al. 2011)

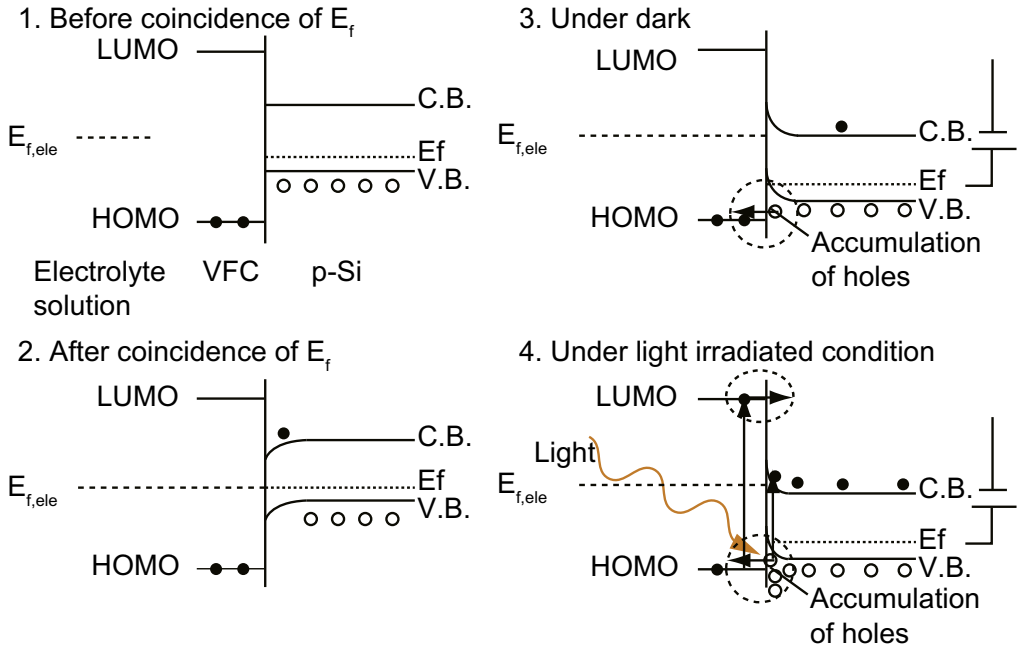

Figure 5.2. Energy diagram of Si-VFc sample on p-type substrate (Illustration taken from:

Sano, et. al. 2011)

This chapter will further analyze the electrochemical characteristics of Si-Fc sample on n-type substrate in the presence of illumination. This chapter intends to present a model that will explain the behavior of CV peak position with respect to illumination intensity. In such, the CV peak position of an n Si-Fc sample shifts to lower potential with the increase in illumination intensity until it saturates.

5.2. Methodology

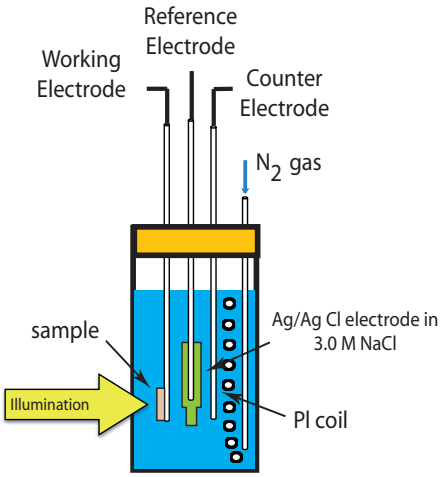

Figure 5.3. Cyclic voltammetry measurements set-up

The experimental method in producing the samples is similar to that of dibutyl ether-prepared sample that was presented in Chapter 3.2. The cyclic voltammetry measurements were done using a three-electrode setup that is connected to an electrochemical analyzer at room temperature (Figure 5.3). A 0.1 M $HClO_4$ solution serves as the electrolyte. The sample serves as the working electrode while a platinum coil serves

as the counter electrode. An Ag/AgCl electrode, which was immersed in 3.0 M NaCl, serves as the reference electrode.

5.3. Results and Discussion

5.3.1. Position of CV peak potential

The position of the anodic peak potential could be viewed as the total potential needed so that the holes from the valence band of Si can be used to increase the redox potential of the grafted film. This total potential could be composed of many individual potential (e.g. redox potential of the Fc moeity, and potential needed for the holes to start to travel to the VFc film). We could assumed for simplicity that only the potential needed to move from the Si substrate to the VFc film due to the band bending in depletion layer is the only kind of potential that can be affected by the application of external bias. With this, all other potential are considered to be independent of applied bias, thus could be considered constant.

The anodic peak can be correlated with the flat band potential. The flat band potential is the turning point between the depletion condition and accumulation condition (Figure 5.4). At potential below the flat band condition, the Si bands are still in depletion condition, thus the holes are still hindered to move to the Fc layer. At potential above the flat band condition, holes can move toward the Fc layer to increase the Fe oxidation state to +3. The flat band potential, being the onset potential for the hole transfer from the bulk Si to the Fc layer, could correlate to the position of the anodic peak. When the potential is brought below the flat band potential (from a potential higher than the flat band potential),

the holes can dissipate down from the Fc moieties, as dictated by its volatile nature. The dissipation of holes from the Fc moieties would bring back its oxidation potential to +2. This condition could be reflected as cathodic peak in CV measurements.

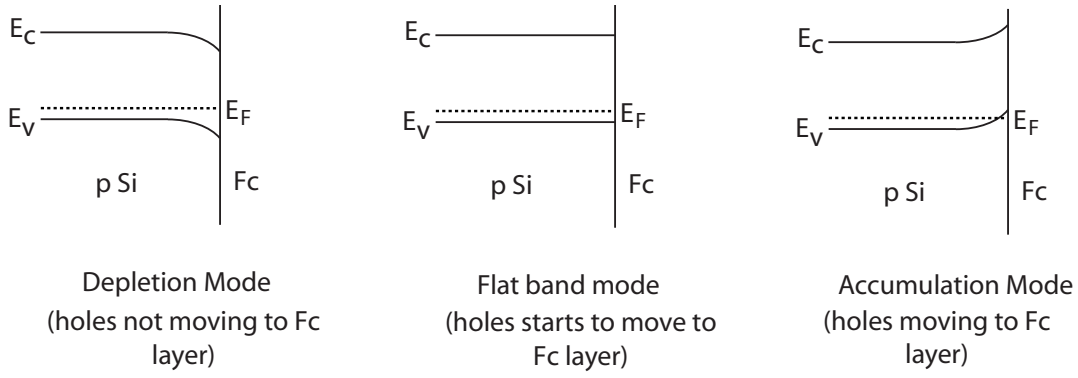

Figure 5.4. Energy band diagrams of Si-Fc sample having different modes

5.3.2. Effects of Illumination on the Electrochemical Characteristics of Ferrocene on Semiconductor Surface

Figure 5.5 shows the shift in the position of CV peaks to lower potential with the increase in illumination intensity. This shift was attributed to lowering of potential needed to start the transport of holes to the Fc layer to be able to increase its oxidation state to +3. Such shift is reflective of the change in Si band bending due to illumination. The details of this matter are the focus of this section.

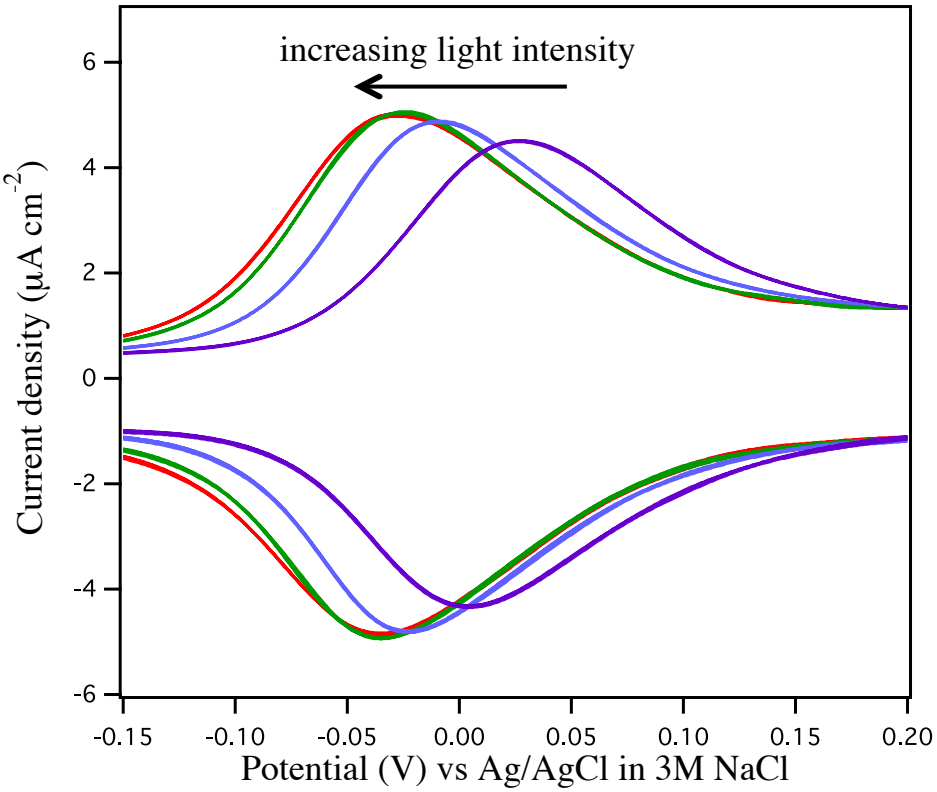

Figure 5.5. Cyclic Voltammmograms of the n Si-Fc sample. The voltammograms were measured at room temperature under 5 (violet), 10 (blue), 20 (green), and 30 (red) mW/cm^2 illumination intensities at scan rate of 0.5 V/s.

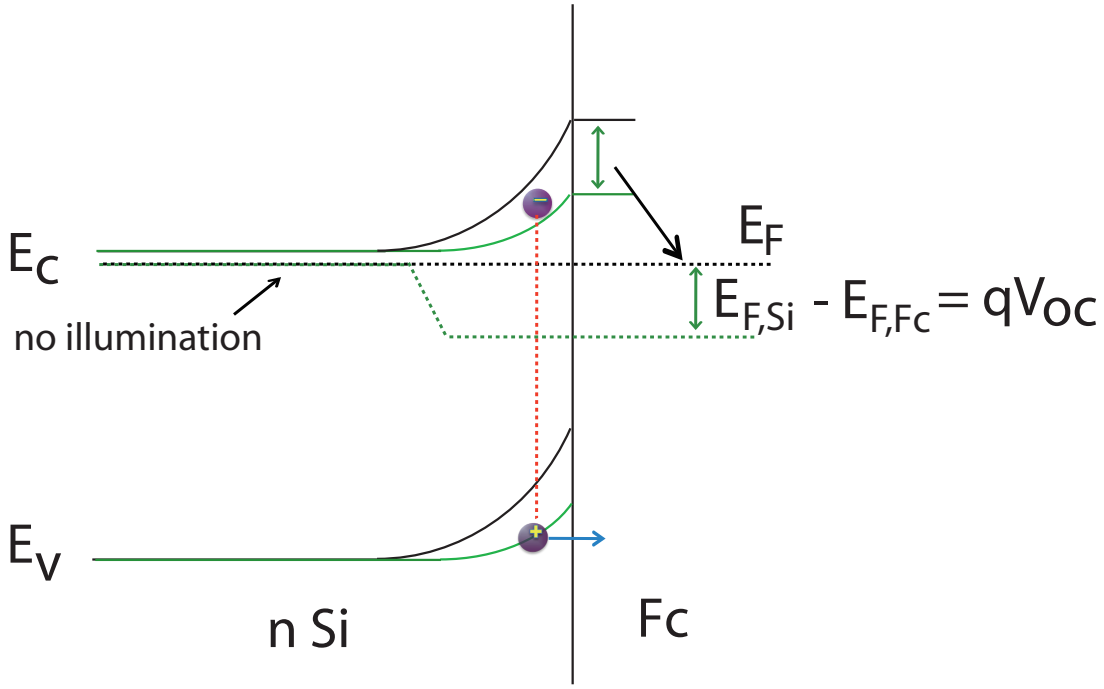

Figure 5.6. Band diagram of n Si-Fc sample in the dark (black line) and under illumination (green line). The sample is not connected to an external bias. ($E_{F,Si}$ is the Fermi energy of Si, $E_{F,Fc}$ is the Fermi energy of the grafted substrate and electrode system, q is the net charge on the surface)

Figure 5.6 shows the energy band diagram of Si-Fc with n-type substrates (with zero external bias) that is placed in the dark (black line) and under illumination (green line). At the dark (with no external bias), the Fermi energy (E_F) of the bulk Si and the Fc layer are equal. The built-in potential (V_{bi}) describes the amount of the Si band bending at this condition. The presence of illumination produces electron-hole pairs, in which the holes could go to the Si surface and into the Fc layer to increase its oxidation state. The presence of holes on the surface can change the potential of the surface (similar to a solar cell). The maximum voltage it can attain is called the open circuit voltage (V_{oc}). The voltage on its

surface would cause changes in their Fermi energies as shown in Figure 5.6. The difference in their Fermi energies would be equal to the energy of the photo-induced surface voltage (open circuit voltage).

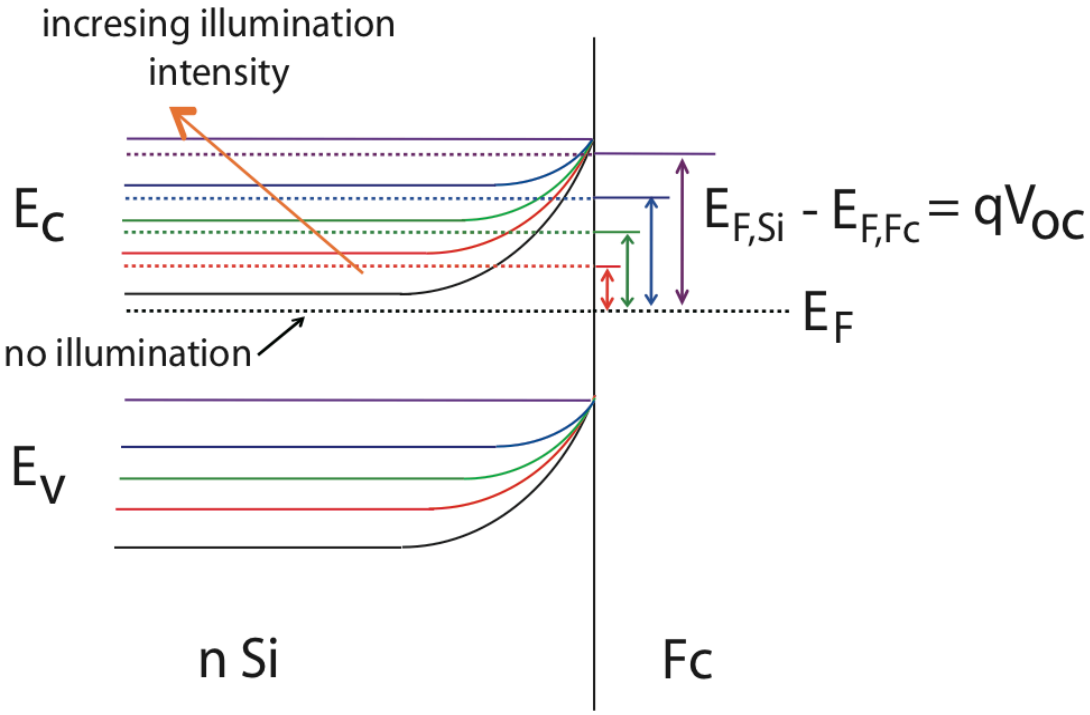

Figure 5.7. Band diagram of n Si-Fc sample, which is illuminated at different intensities. The sample is not connected to an external bias. The energy band diagram is in relative energy position for the purposes of comparing the effect of different illumination intensities. The Fermi energy level at the bulk Si is also simplified into a straight line. ($E_{F,Si}$ is the Fermi energy of Si, $E_{F,Fc}$ is the Fermi energy of the grafted substrate and electrode system, q is the net charge on the surface)

Figure 5.7 shows the energy band diagram of Si-Fc sample with n-type substrate (zero external bias), which is illuminated at different intensities. Note that the energy band diagram is in relative energy position for the purposes of comparing the effect of different illumination intensities. In addition, the Fermi energy level at the bulk Si is also simplified into a straight line. Increase in the illumination intensity triggers the production of more photogenerated holes, which could increase the open circuit voltage (V_{oc}) of the sample. The shift in the position of the anodic peak to lower potential with the increase in illumination intensity can be attributed to the increase in the open circuit voltage (V_{oc}). The increase in illumination reduces the total potential needed for the Fc redox reaction to occur, since it already supplies some of the needed potential (in terms of the open circuit voltage). However, as illumination intensity further increase, the band bending further reduces and can approached the flat band mode. At flat band mode, there is no more depletion region wherein the electron-hole pairs can split to produce photogenerated holes. With this condition, the open circuit voltage cannot further increase, thus there would no more further shift in anodic peak position to lower potential.

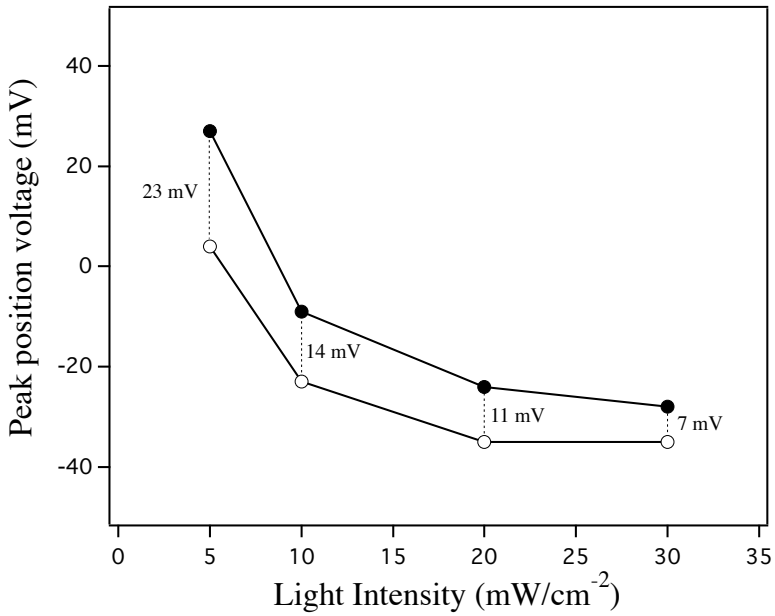

Figure 5.8. Graph of anodic (solid line and filled symbol) and cathodic (dashed line and open symbol) peak potential as a function of illumination intensity at scan rate of 0.5 V/s.

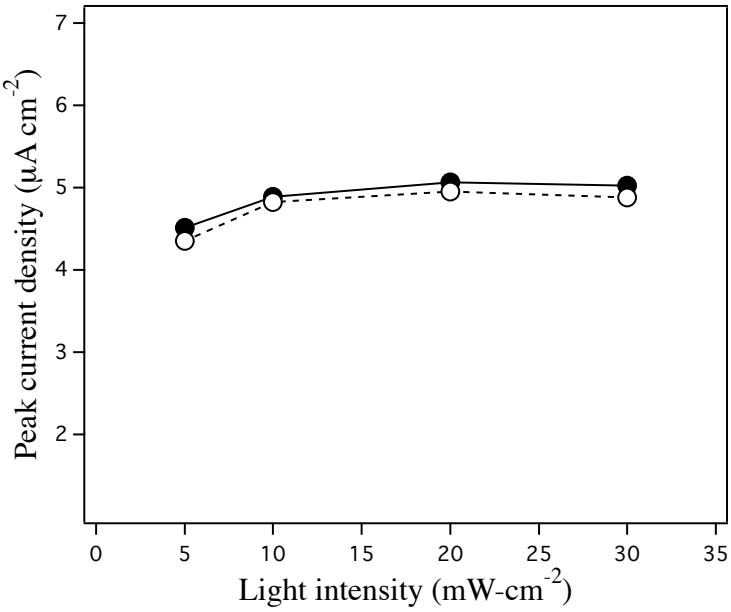

Figure 5.9. Graph of anodic (solid line and filled symbol) and cathodic (dashed line and open symbol) peak current density as a function of illumination intensity at scan rate of 0.5 V/s.

Figure 5.8 shows the experimental plots of CV peaks position with illumination intensity. The plot shows the shift of CV peak to lower potential with the increase in illumination intensities until the shift tends to saturate. The trend of the plots is compatible with our analysis earlier about the relation of CV peak with illumination intensity. Figure 5.8 also shows that the difference between the positions of the anodic and the cathodic peaks decreases with increase in light intensity. This may reflect that at high illumination intensity when current density is large, the effect of other redox reactions tends to become negligible. On another matter, Figure 5.9 shows that the peak current density tends to saturate at high value with illumination intensity. This may indicate that the production of photogenerate holes, which are essential with the redox reaction, is the rate-limiting step.

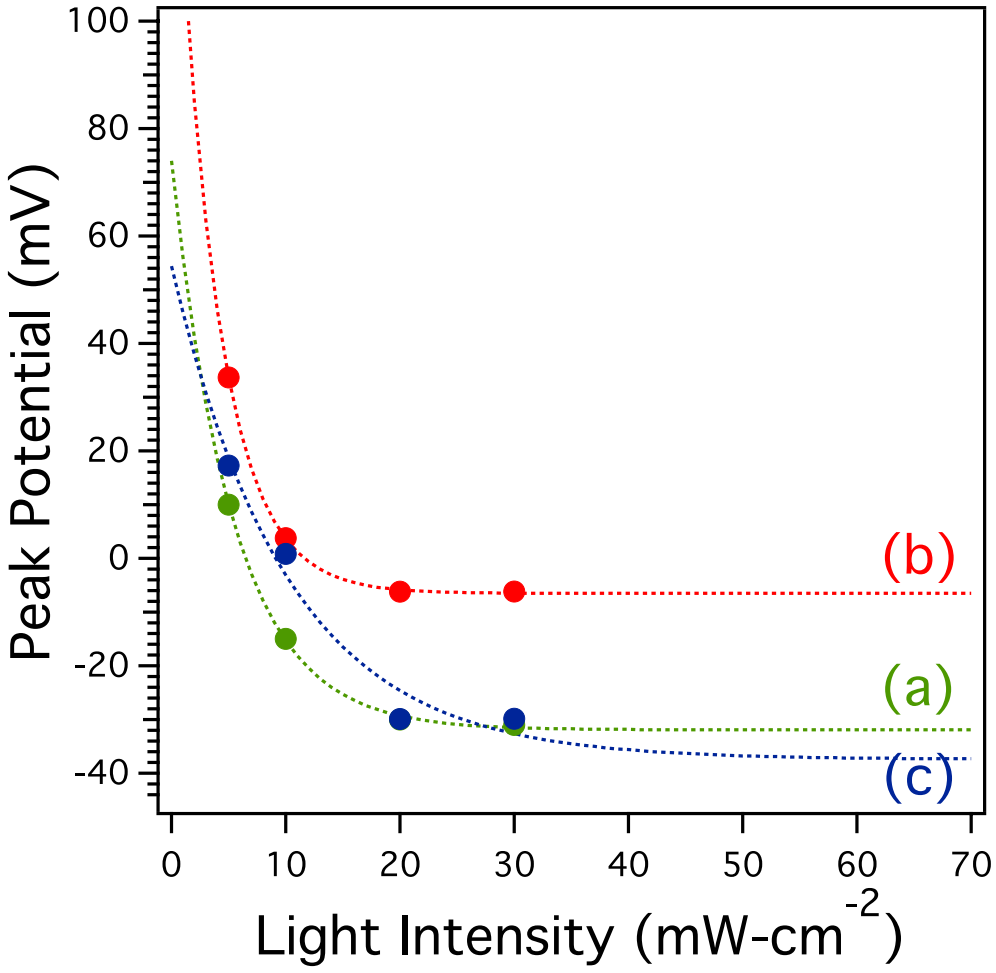

Figure 5.10. Light intensity vs. anodic peak potential (scan rate of 0.1 V/s) of the following n Si-Fc samples: (a) Dibutyl ether-prepared sample that was grafted under visible light illumination (green), (b) Dibutyl ether-prepared sample that was grafted in the dark (red), and (c) Diethyl ether-prepared sample that was grafted under visible light illumination (blue). The dashed line represents the trend of the graph and was interpolated down to zero light intensity (just for simplicity), wherein CV peak don't really exist.

Table 5.1. Estimate value of (1) projected and hypothetical anodic peak position at zero intensity ($E_{pa}(0)$), (2) projected anodic peak position at very high light intensity ($E_{pa}(\infty)$), (3) $E_{pa}(0)$ - $E_{pa}(\infty)$ and (4) projected light intensity when the value of E_{pa} saturates (L_{sat}) of the different Si-Fc samples using n-type substrate.

	Sample	$E_{pa}(0)$* (V)	$E_{pa}(\infty)$* (V)	$E_{pa}(0)$-$E_{pa}(\infty)$ (V)	L_s (mW/cm^2)
A	Dibutyl ether-prepared (illumination)	0.0740	-0.0319	0.1059	30
B	Dibutyl ether-prepared (dark)	0.1518	-0.0065	0.1583	30
C	Diethyl ether-prepared (illumination)	0.0544	-0.0374	0.0918	50

*V vs. Ag/AgCl in 3M NaCl

Figure 5.10. show the graph of light intensity vs. cathodic peak potential (scan rate of 0.1 V/s) of the following n Si-Fc samples: (a) Dibutyl ether-prepared sample that was grafted under visible light illumination, (b) Dibutyl ether-prepared sample that was grafted in the dark, and (c) Dibutyl ether-prepared sample that was grafted under visible light illumination. The dashed line represents the trend of the graph and was interpolated down to zero light intensity, wherein CV peak don't really exist. The data were fitted using

the equation:

$$E_{pa} = E_i + A * \exp\left(\frac{-(L - L_i)}{\tau}\right) \quad \text{equation 1}$$

where E_i, A, L_i and τ are fitting parameter constant while the variable terms are the anodic peak position (E_{pa}) and light intensity (L). The best-fitted curve was predicted using Igor Pro. 6.21. Equation 1 incorporates both (1) the seemingly linear behavior of the open circuit voltage (which we assumed to coincide with the anodic peak position) with light intensity as seen in different literature (Cowan, et. al., 2010, Li, et. al., 2012) and (2) its saturation at high light intensity. The linear behavior of Equation 1 at low light intensity, L (relative to the term $(L-L_i)/\tau$) is seen when its form is expanded to its series form:

$$E_{pa} = E_i - A\left(\frac{(L - L_i)}{\tau}\right) + \frac{A}{2}\left(\frac{(L - L_i)}{\tau}\right)^2 + \ldots \quad \text{equation 2}$$

The difference between the hypothetical value of E_{pa} at zero light intensity (E_{pa} (0)), and the projected value of E_{pa} at very high light intensity ($E_{pa}(\infty)$) reflects the extend of the built-in potential (or the band bending at equilibrium condition):

$$V_{bi} \propto E_{pc}(0) - E_{pc}(\infty) \quad \text{equation 3}$$

Table 5.1 summarized the characteristics of the graphs in Figure 5.10. The table presents three types of samples; they are (a) Dibutyl ether-prepared sample that was grafted under visible light illumination (green), (b) Dibutyl ether-prepared sample that was grafted in the dark (red), and (c) Diethyl ether-prepared sample that was grafted under visible light illumination (blue).

The values of E_{pa} saturate for the two dibutyl ether-prepared samples (grafted with light (sample A) and grafted in the dark (sample B)) are estimated to saturate at lower light intensity (L_s= 30 mW/cm^2) than the diethyl ether-prepared sample (C) (L_s = 50 mW/cm^2). This could be explained by the fact that diethyl ether-prepared sample has lumps of materials deposited on it (Figure 3.9 in Chapter 3), which might act as light blockage, thus the effective light hitting the Si surface is lesser. The graph of the two samples, which is grafted in the presence of illumination (samples A and C), might look different but the values of their $E_{pa}(0)$ - $E_{pa}(\infty)$ are close to each other and greatly differ with the sample grafted in the dark (sample B). Since we have associated this parameter with the built-in potential (band bending at equilibrium condition), it seems that the built-in potential of samples prepared using visible light illumination is significantly different with that prepared in the dark. Further verifications and analysis are still needed to justify this claim.

5.4. Summary and Conclusion

The effects of illumination on the electrochemical characteristics of ferrocene group on n-type Si surface were modeled and experimentally determined. Experimentally, the increase in illumination intensity during cyclic voltammetry measurements shifts the position of anodic and cathodic peaks to lower potential until it saturates. This shift was attributed (Figure 5.11) to the surface voltage (open circuit voltage) that was produced during illumination, which lowers the potential needed to start the transport of holes to the Fc layer to be able to increase the Fe oxidation state to +3. However, further increase in the illumination intensity could decrease the Si band bending until it became flat. When the Si energy band is already flat, there would be no more depletion region that could further split

the electron-hole pairs to produce further photogenerated holes. With this condition, there could be no further increase in surface voltage, thus the positions of the CV peaks cannot further shift to lower potential.

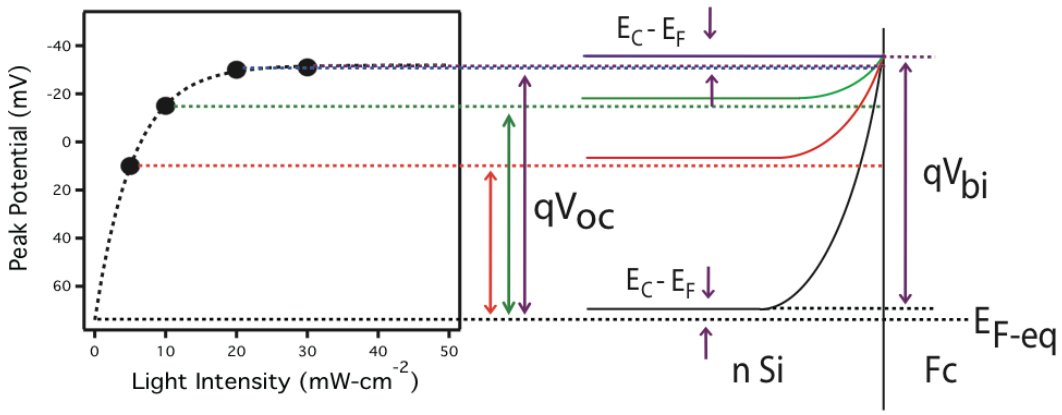

Figure 5.11. Relation between the position of anodic peak potential and Si band bending when the illumination intensity is changed.

References

1. S. Ciampi, P. K. Eggers, G. Le Saux, M. James, J. B. Harper, J. J. Goodin: *Langmuir.* **2009.** 25. 2530.
2. S. Ciampi, G. Le Saux, J. B. Harper, J. J. Gooding: *Electroanalysis* **2008.** 20. 1513.
3. M. Cossi, M. F. Iozzi, A. G. Marrani, T. Lavecchia, P. Galloni, R. Zanoni, F. Decker: *J. Phys. Chem. B* **2006.** 110. 22961.
4. S.R. Cowan, A. Roy, A.J. Heeger: *Physical Review B*. **2010.** 82. 245207.
5. E. A. Dalchiele, A. Aurora, G. Bernardini, F. Cattaruzza, A. Flamini, P. Pallavicini, R. Zanoni, F. Decker: J. *Electroanal. Chem*. **2005.** 579. 133.
6. F. Decker, F. Cattaruzza, C. Coluzza, A. Flamini, A. G. Marrani, R. Zanoni, E.A. Dalchiele: J. Phys. Chem B **2006.** 110. 7374.
7. B. Fabre: *Acc. Chem. Res*. **2010.** 43. 1509.
8. B. Fabre, F. Hauquier: *J. Phys. Chem. B*. **2006.** 110. 6848.
9. S. Gowda, G. Mathur, V. Misra: *Applied Physics Letters*. **2007.** 90. 142113.
10. L. Li, J.H. Kwon, J. Jang: *Organic Electronics*. **2012.** 13. 230.
11. Q. Li, G. Mathur, M. Homsi, S. Surthi, V. Misra, V. Malinovskii, K.-H. Schweikart, L. Yu, J. S. Lindsey, Z. Liu, R. B. Dabke, A. Yasseri, D. F. Bocian, W. G. Kuhr: *Appl. Phys. Lett*. **2002.** 81. 1494.
12. Q. Li, S. Surthi, G. Mathur, S. Gowda, V. Misra, T. A. Sorenson, R. C. Tenent, W. G. Kuhr, S. Tamaru, J. S. Lindsey, Z. Liu, D. F. Bocian: *Appl. Phys. Lett*. **2003.** 83. 198.
13. M. Lu, T. He, J.M. Tour: *Chem. Mater.* **2008.** 20. 7352.
14. A.G. Marrani, E.A. Dalchiele, R. Zanoni, F. Decker, F. Cattaruzza, D. Bonifazi, M. Prato: *Electrochimica Acta*. **2008.** 53. 3903.

15. A. G. Marrani, F. Cattaruzza, F. Decker, P. Galloni, R. Zanoni: *Superlattices and Microstructures*. **2009.** 46. 40.

16. K. M. Roth, A. A. Yasseri, Z. Liu, R. B. Dabke, V. Malinovskii, K.-H. Schweikart, L. Yu, H. Tiznado, F. Zaera, J. S. Lindsey, W. G. Kuhr, D. F. Bocian: *J. Am. Chem. Soc*. **2003.** 125. 505.

17. H. Sano, M. Zhao, D. Kasahara, K. Murase, T. Ichii, H. Sugimura: *Journal of Colloid and Interface Science*. **2011.** 361. 259.

18. R. Zanoni, F. Cattaruzza, C. Coluzza, E.A. Dalchiele, F. Decker, G. Di Santo, A. Flamini, L. Funari, A.G. Marrani: *Surface Science*. **2005.** 575. 260.

19. R. Zanoni, M. Cossi, M.F. Iozzi, F. Cattaruzza, E.A. Dalchiele, F. Decker, A.G. Marrani, M. Valori: *Superlattices and Microstructures*. **2008.** 44. 542.

Chapter 5
Summary and Conclusions

This study has successfully grafted methyl and ferrocenyl groups on Si(111) surface using photochemical preparations. The outcome organic assemblies are alkyl groups (-CH_3 and –C_2H_4Fc) that are covalently bonded with the Si surface.

This study has explored two different processes in which alkyl structures could be grafted on the Si surface using visible light illumination. One process involves the use of organomagnesium halide (Grignard reagent) while the other involves the use of 1-alkene (vinylferrocene) molecules. The way in which visible light interacts with the two types of the precursor molecules to induce grafting process were modeled to be different. In the use of Grignard reagent, the photogenerated holes induce the oxidative decomposition of Grignard reagent, which releases the alkyl molecules that is needed for grafting. On the other hand, in the use of 1-alkene molecules, the photogenerated holes facilitate the reaction between the hydrogenated surface and vinylferrocene in nucleophilic fashion.

This study explore on the two possible functions of grafted molecules on semiconductor surface. In such, we have shown that the grafted -CH_3 group can make Si surface chemically inert, in terms of resisting silicon oxide formation. Meanwhile, we have shown that the grafted –C_2H_4Fc group have good electrochemical characteristics (e.g. small different in cathodic and anodic peak positions) in terms of its potential application in memory devices.

The preparation of methyl-terminated Si(111) was successfully done using a photochemical grafting technique. The ATR-FTIR spectrum of the sample shows the

presence of high intensity peak at around 1255 cm^{-1}, which is attributed to the presence of Si-CH_3 umbrella mode. This peak confirms the presence of methyl groups, which are oriented perpendicular to the Si(111) surface. The methylated Si surface had atomically flat structure, is hydrophobic and has lower electron affinity compare to the bulk Si. The grafting process improves with the use of sample with low dopant concentration and high illumination intensity.

The photochemical grafting of vinylferrocene molecule on Si(111) surface was successfully been employed. The use of diethyl ether or dibutyl ether as grafting medium enabled the production of monolayer-thick molecular layer, however, the use of tetrahydrofuran leads to the polymerization of the grafted substance. The samples, which were prepared using diethyl ether, has lumps of deposited materials on it, however, these materials are not electrochemical active. The use of dibutyl ether stands the best in terms of easiness of preparation and quality of the grafted sample. Dibutyl ether has low volatility, thus very easy to manage during the preparation and the produces samples with good electrochemical properties and surface topography.

The photochemical preparation of ferrocene-terminated Si(111) with n-type and p-type substrate was successfully been employed. The success was attributed to presence of photogenerated charges on the Si surface. The photogenerated charges create electric field, which polarized the vinylferrocene molecules for it to be attracted on the Si surface. When attracted near the surface, the vinylferocene molecules can react with hydrogenated Si to form Si-C bonds. The kind of charges that can led to the attraction of vinylferrocene molecules to the Si surface are not limited to the charges caused by illumination, but could also include tunneled charges from the bulk substrate that could happen in the dark. We are

also successful in grafting vinylferrocene molecules on Si surface in the dark. However, the process in the dark is very slow compare to those prepared under illumination. The density of surface charges, which is crucial to the grafting rate, is influenced by the band bending characteristics of Si (e.g. width of the depletion region), which in turn can be affected by the nature of the substrate (e.g. dopant concentration). Under illumination, the grafting rate becomes faster with the use of substrate with low dopant concentration while in the dark, it improved with the use of substrate with high dopant concentration and n-type substrate.

The electrochemical characteristics of ferrocene group on n-type Si surface and the effect of illumination were modeled and experimentally determined. Experimentally, the anodic and cathodic peaks shift to lower potential when the illumination intensity during cyclic voltammetry measurements was increased. However, this shift saturates at high illumination intensity. The shift of the peaks to lower potential was attributed to the illumination-induced surface voltage (open circuit voltage). This surface voltage lowers the potential needed to start the transport of holes to the Fc layer to be able to increase the Fe oxidation state to +3. However, further increase in the intensity of illumination reduces the band bending until it became flat. When the Si energy bands are flat, there would be no more depletion region that could further split the electron-hole pairs to produced further photogenerated holes. With this situation, the surface voltage (open circuit voltage) will not further increase, thus, the cyclic voltammogram peaks cannot further shifts to lower potential.

Acknowledgements

I would like to express my deepest gratitude to Prof. Hiroyuki SUGIMURA (Department of Materials Science and Engineering, Kyoto University) for giving me opportunity to become a doctoral student in Kyoto University. I sincerely appreciate and value your guidance, advices and support that you have given me. Words are insufficient to describe how grateful I am to be part of your laboratory.

I would like to thank Prof. Akira SAKAI (Department of Materials Science and Engineering, Kyoto University) and Prof. Kuniaki MURASE (Department of Materials Science and Engineering, Kyoto University) for giving your valuable time reviewing my thesis (Department of Materials Science and Engineering, Kyoto University).

I would like to give my deep appreciation to Prof. Kuniaki MURASE (Department of Materials Science and Engineering, Kyoto University) and Prof. Takashi ICHII (Department of Materials Science and Engineering, Kyoto University). I value all the advices and support that you have given me. You are a great help in pursuing my research.

I would like to thank Mr. Yutaka SONOBASHI and Akiko YASUI for all the assistance you have given me. I appreciate and value all the help you have given me.

I would also like to thank the members of Prof. SUGIMURA's research group for all the help and patience you have given me. You are a great help in almost every aspect of my life in the laboratory.

Finally, I would like to thank my family for your endless support and unconditional love.